2.1 GENERAL NOTATION

A complete summary and definition of all notation used in the Datcom is given in this section. The summary is divided into upper and lower case English, upper and lower case Greek, derivatives, and abbreviations. In all cases a general alphabetical listing is used. Throughout the Datcom units are in pounds, feet, seconds, and degrees unless otherwise specified.

A. ENGLISH SYMBOLS

SYMBOL	DEFINITION	SECTIONS
A	aspect ratio of surface, based on total planform, $\frac{b^2}{S}$	Several
A', A''	aspect ratios of forward and aft surfaces, respectively	4.5.1.1 7.4.1.1 7.4.4.1
$\bar{A}$	transonic aspect-ratio similarity parameter, $A\left(\frac{t}{c}\right)^{1/3}$	4.1.4.2
A_D	duct aspect ratio, $\frac{d_e}{c}$	9.3 9.3.1 9.3.2 9.3.3
A_H	aspect ratio of auxiliary horizontal surface, aft tail or canard, $\frac{b_H^2}{S_H}$	Several
A_{H_e}	aspect ratio of exposed horizontal tail	6.2.1.2
$A_H e_H$	effective aspect ratio of horizontal stabilizer	4.5.3.2
A_I	inlet duct area for jet engine	4.6 4.6.1 4.6.3
A_{U_e}	aspect ratio of exposed lower vertical panel	Several
$(A)_V$	geometric aspect ratio of isolated vertical panel, with span and area of panel measured to body center line	Several
A_{V_e}	aspect ratio of exposed upper vertical panel	Several
$(A)_{V(B)}$	aspect ratio of vertical panel in presence of body	Several

SYMBOL	DEFINITION	SECTIONS
$(A)_{V(HB)}$	vertical-panel aspect ratio in presence of horizontal tail and body	Several
A_W	aspect ratio of wing	Several
A_{bw}	aspect ratio of the basic wing	Several
A_e	aspect ratio of exposed (panels joined together) surface, $\frac{b_e^2}{S_e}$	Several
A'_e, A''_e	aspect ratios of forward and aft exposed surfaces, respectively	4.4.1 4.5.1.1 4.5.1.2 7.4.1.1
A_{eff}	1. effective aspect ratio of surface as determined by tip flow separation	4.4.1 5.3.1.1 5.6.1.1
	2. effective aspect ratio of the vertical panel	Several
A'_{eff}	effective aspect ratio of forward surface as determined by tip flow separation	4.5.1.1
$(A_e)_i$	aspect ratio of exposed inboard panels of wing	4.3.2.2
A_f	aspect ratio of flap or control surface, $\frac{b_f^2}{S_f}$	6.1.6.1 6.1.6.2 6.2.1.1
A_g	aspect ratio of glove of a double-delta or a cranked wing	4.1.3.2 5.1.2.1
A_i	1. aspect ratio of that portion of main surface immersed in propeller slipstream, $\frac{b_i}{c_i}$	4.6 4.6.1
	2. aspect ratio of planform formed by the two inboard panels of wing	Several
A_o	aspect ratio of planform formed by the two outboard panels of wing	4.1.5.1 4.1.5.2
A'_o	aspect ratio of planform formed by the two constructed outboard panels of wing	4.1.4.2 4.3.2.2 5.1.2.1
A_s	aspect ratio of a particular spanwise wing section	6.1.5.1
A_t	1. aspect ratio of wing based on total wing area, including flap extension	6.1.4.1 6.1.4.2
	2. aspect ratio of total wing based on extended wing chord, using the particular section value for the chord	6.1.5.1
A_1, A_2	aspect ratio of constructed panels of non-straight-tapered wings	4.1.3.2
a	1. difference in lift-curve slope, or $(C_{L_\alpha}$ at $M_{fb}) - (C_{L_\alpha}$ at $M_a)$	4.1.3.2
	2. $\frac{\tan \Lambda_{HL}}{\beta}$	6.1.6.1

SYMBOL	DEFINITION	SECTIONS
b_e	total span of exposed surface	Several
b'_e, b''_e	total spans of exposed forward and aft surfaces, respectively	7.4.1.1
$(b_e)_i$, $(b)_e$	total span of exposed inboard panels of wing	4.3.2.2 4.3.3.1
b_{eff}	effective surface span	4.7 4.7.1 4.4.1
b'_{eff}	effective forward-surface span	4.5.1.1 7.4.1.1
b_f	total span of flaps or control surfaces, measured normal to the plane of symmetry	Several
b'_f	effective span for increment in load due to flaps	4.7 4.7.1
b_g	span of glove of double-delta and cranked wings	4.1.3.2 5.1.2.1
b_i	1. span of planform formed by two inboard panels	2.2.2 4.1.4.2 4.1.5.1 5.1.2.1
	2. total span of a given portion of main surface immersed in propeller slipstream, $2\sqrt{R_p^2 - (z_s + z_w)^2}$	4.6 4.6.1 4.6.3
b_{kk}	parameter in span-loading calculation	6.1.7
b_{max}	minor semiaxis of body cross section	4.2.3.1
b_o	span of planform formed by joining two outboard panels of wing	Several
b'_o	span of planform formed by joining two constructed outboard panels of wing	4.1.4.2 4.3.2.2 5.1.2.1
b_p	propeller blade width at any propeller span station	4.6 4.6.1
b_s	span of spoiler, on one wing panel	6.2.1.1 6.2.2.1
b_{slat}	total span of slats	6.1.4.3
b_v	span of the wing-tip vortices at a given longitudinal station behind a lifting surface	4.4.1 4.5.1.1 7.4.4.1

SYMBOL	DEFINITION	SECTIONS
b'_v, b''_v	vortex spans at the forward and aft surfaces, respectively	Several
b_{vn}	parameter in span-loading calculation	6.1.7
b_{vv}	parameter in span-loading calculation	6.1.7
$b_{v_{ru}}$	span of completely rolled up wing-tip vortices (at distances far downstream from lifting surface)	4.4.1 7.4.4.1
b_1, b_2	span of constructed panels of non-straight-tapered wings	4.1.3.2
b_1, b_2, b_3	vertical span of a given region as defined in Sketch (b) in Section 5.3.1.1	5.3.1.1 5.3.1.2
$b'_{.25,\ .50,\ \ldots}$	propeller blade chord at $\frac{r}{R} = 0.25, 0.50, \ldots$	9.1 9.1.1 9.1.3
$b/(2\ell)$, $\frac{b_w}{2\ell}$	wing slenderness parameter	Several
C	1. thickness correction factor for supersonic wing lift	4.1.3.3 4.1.3.4
	2. roll-moment-of-inertia correction factor for solid component	8.2
$(C_{LE})_{bw}$	leading-edge effect of basic wing on normal-force-curve slope	4.1.3.2
$(C_{LE})_g$	leading-edge effect of glove on normal-force-curve slope	4.1.3.2 4.1.3.4
C_a, C_b, C_c	wing parameters measured to plane of symmetry (see Figure 8.1-22)	8.1
C_0, C_1, ... C_{18}	regression coefficients as a function of Mach number	4.3.2.1
C_1, C_2	1. empirical taper-ratio constants	Several
	2. empirical constants that determine propeller downwash gradients	4.6 4.6.1 4.6.4
	3. Mach-number functions that determine thickness correction factors to supersonic flat-plate aerodynamic derivatives, $C_1 = \frac{2}{\sqrt{M^2 - 1}}$ $C_2 = \frac{(\gamma + 1) M^4 - 4 (M^2 - 1)}{2 (M^2 - 1)^2}$	Several
C_3	1. taper-ratio correction factor for wing aerodynamic center	4.1.4.3
	2. maximum lift-correction factor at transonic speeds	4.1.3.4

SYMBOL.	DEFINITION	SECTIONS
c	1. transonic wing lift-curve slope at M_{fb}	4.1.3.2
	2. chord of airfoil section	Several
	3. duct chord	9.3 9.3.1 9.3.2 9.3.3
	4. nozzle discharge coefficient	6.3.2
c'	1. effective chord of airfoil with deflected extensible-type flap (see Figures 6.1.1.1-44, -45, -46, -48, -51, and 6.1.5.1-60)	Several
	2. airfoil chord measured perpendicular to the wing quarter-chord line	6.1.6.1 6.1.6.2
$\bar{c}$, $\bar{c}_W$	wing mean aerodynamic chord	Several
$\bar{c}'$	mean aerodynamic chord of the wing segment affected by the leading-edge device (see Sketch (h), Section 6.1.5.1)	6.1.5.1
$\bar{c}'$, $\bar{c}''$	mean aerodynamic chords of forward and aft surfaces, respectively	Several
c_B	chord at break span station	2.2.2 4.1.3.2 4.1.3.3
$\bar{c}_H$	mean aerodynamic chord of auxiliary horizontal surface, aft tail or canard	4.4.1 4.6 4.6.1 7.4.2.2
$\bar{c}_{H_e}$	mean aerodynamic chord of exposed horizontal-tail panel	4.5.3.1
c'_{LE}	airfoil chord with only leading-edge device extended	6.1.2.1 6.1.5.1
c_V	vertical tail chord at the distance z_H above body center line (see Figure 5.3.1.1-22b)	Several
$\bar{c}_{V_e}$	mean aerodynamic chord of exposed vertical-tail panel	4.5.3.1
$\bar{c}_{W_e}$	mean aerodynamic chord of exposed wing	4.5.3.1
c_a	hypothetical airfoil chord including trailing-edge flap extension and subtracting leading-edge flap extension	6.1.2.1 6.1.5.1
c'_a	extended wing chord due to complete forward-flap extension (see Figures 6.1.1.1-45, -46)	6.1.1.1
$\bar{c}_{\text{area not immersed}}$	mean aerodynamic chord of the wing area not immersed in the slipstream	4.6 4.6.3
c_{av}	average chord of airfoil	6.1.5.1
c_b	balance chord of a control or flap surface	6.1.3.1 6.1.3.2 6.1.6.1 6.1.6.2
c'_b	balance chord of control or flap surface measured perpendicular to the wing quarter-chord line	6.1.6.1

SYMBOL	DEFINITION	SECTIONS
c_{b_t}	chord of tab balance	6.1.3.1 6.1.3.2 6.1.3.3 6.1.3.4
c_{bw}	chord of basic wing	4.1.5.1 4.3.3.1
$\bar{c}_c$	mean aerodynamic chord of a particular control surface	6.3.4
$c_{c.p.}$	wing chord at spanwise center-of-pressure location	6.1.5.1
$\bar{c}_e$	1. mean aerodynamic chord of exposed panel	Several
	2. mean aerodynamic chord of elevator	6.3.4
$\bar{c}_e'$, $\bar{c}_e''$	mean aerodynamic chords of exposed forward and aft surfaces, respectively	7.4.1.1 7.4.1.2 7.4.4.1 7.4.4.2
c_f	flap or control chord measured parallel to plane of symmetry	Several
c_f'	flap or control chord measured perpendicular to the wing quarter-chord line	6.1.6.1
$\bar{c}_f$	mean flap chord	6.1.7
c_{f_i}	chord of a particular segment of a flap of n segments	6.1.2.1 6.1.5.1
$c_{f_{inc}}$	incompressible turbulent flat-plate skin-friction coefficient	4.2.3.1
$c_{f_{LE}}$	chord of the leading-edge flap	6.1.2.1 6.1.5.1
c_{f_r}	root chord of flap or control surface measured parallel to plane of symmetry	6.1.6.1
c_{f_t}	tip chord of flap or control surface measured parallel to plane of symmetry	6.1.6.1
c_{f_1}, c_{f_2}, c_{f_3}	effective chords of combined flap segments as defined by the principle of superposition, shown in Sketch (g), Section 6.1.2.1	6.1.2.1
$c_{f_{\perp LE}}$	chord of leading-edge flap perpendicular to leading edge of airfoil	6.1.5.1
c_i	average chord of that portion of wing immersed in propeller slipstream	4.6 4.6.1 4.6.3
$\bar{c}_i$	mean aerodynamic chord of inboard panel of wing	4.1.5.1 4.1.5.2
$(\bar{c}_i)_e$, $(\bar{c}_o)_e$	mean aerodynamic chords of exposed inboard and outboard panels, respectively, of wing	4.3.3.1
$\bar{c}_{i_H}$	mean aerodynamic chord of that portion of auxiliary surface immersed in propeller slipstream	4.6.3
$\bar{c}_o$	mean aerodynamic chord of outboard panel of wing	4.1.5.1 4.1.5.2 4.3.3.1
$\bar{c}_{P_e}$	mean aerodynamic chord of exposed tail panel	4.5.3.1
c_r	surface root chord	Several

SYMBOL	DEFINITION	SECTIONS
c_r', c_r''	root chords of forward and aft surfaces, respectively	4.5.2.1 7.4.1.1
c_{r_B}	root chord of basic triangular wing (see Sketch (a), Section 7.1.1.1)	5.1.3.1 7.1.1.1 7.1.4.2
$c_{r_{bw}}$	root chord of basic wing of double-delta and cranked wings	4.1.5.1 4.3.3.1 5.1.2.1
c_{r_E}	root chord of trailing edge extension of double-delta and cranked wings	4.1.3.2
c_{r_e}	root chord of exposed surface	Several
c_{r_e}', c_{r_e}''	root chords of exposed forward and aft surfaces, respectively	4.5.1.2 7.4.1.1
$(c_{r_e})_H$	root chord of exposed horizontal surface	5.3.1.2
$(c_{r_e})_i$	root chord of exposed inboard panels of wing	4.3.2.2
c_{r_f}	root chord of control surface	6.1.5.1
c_{r_g}	root chord of glove of double-delta and cranked wings	4.1.3.2 5.1.2.1
c_{r_H}	root chord of horizontal stabilizer	8.1
c_{r_i}	root chord of inboard panel of wing	4.1.4.2 4.1.5.1 4.3.2.2
$(c_{r_i})_e$	root chord of inboard panel (exposed) of wing	4.3.3.1
c_{r_o}	root chord of outboard panel of wing	4.1.4.2 4.1.5.1 4.3.3.1
c_{r_o}'	root chord of constructed outboard panel of wing	4.1.4.2 4.3.2.2
c_{r_V}	root chord of vertical stabilizer (at fuselage)	8.1
c_{r_W}	root chord of wing	Several
c_{r_1}, c_{r_2}	root chords of constructed panel of non-straight-tapered wings	4.1.3.2
c_s	chord of spoiler	6.2.1.1 6.2.2.1
c_t	1. tip chord of surface	Several
	2. chord of tab, aft of hinge line	6.1.3.1 6.1.3.2 6.1.3.3 6.1.3.4
$\bar{c}_{tc}$	mean aerodynamic chord of control tab	6.3.4
$(c_{t_e})_i$	tip chord of exposed inboard panels of wing	4.3.2.2

SYMBOL	DEFINITION	SECTIONS
c_{t_H}	tip chord of horizontal stabilizer	8.1
c_{t_i}	tip chord of inboard panel of wing	4.1.4.2 4.3.3.1
c_{t_o}	tip chord of outboard panel of wing	4.1.4.2 4.3.2.2
c_{t_V}	tip chord of vertical stabilizer	8.1
c_{t_W}	tip chord of wing	4.1.3.2 5.1.2.1
$c_{\delta\delta}$	extended wing chord due to deflection of leading-edge and trailing-edge flaps (see Sketch (f), Section 6.1.2.1)	6.1.2.1 6.1.5.1
$(c')_{\eta_i}, (c')_{\eta_o}$	effective chords of airfoil with deflected extensible-type flap, at the inboard and outboard edge, respectively, of the flap	6.1.5.1
c_1, c_2	chords of forward and aft flaps, respectively, of a double-slotted flap	6.1.1.1
c_1, c_2, c_3	intersecting flap chord segments that approximate the mean-camber-line distribution of the flap components (see Sketch (e), Section 6.1.2.1)	6.1.2.1 6.1.5.1
$\Delta c_1, \Delta c_2, \Delta c_4, \Delta c_6$	terms analogous to section lift coefficients used in calculating section pitching moments	6.1.2.1 6.1.5.1
$\Delta c_{5_1}, \Delta c_{5_2}, \Delta c_{5_i}$	terms analogous to section lift coefficients for the first, second, and i^{th} trailing-edge flap segments, respectively	6.1.2.1 6.1.5.1
c_1'	flap chord of the forward-flap segment; i.e., for a broken trailing edge the forward-flap segment is extended to form a complete airfoil (see Figure 6.1.1.1-46)	6.1.1.1
$(\bar{c}/4)_V$	the quarter-chord point of the MAC of the vertical panel extending to body center line	Several
$(\bar{c}/2)_{V_e}$	50-percent-chord point of the MAC of exposed vertical panel	5.3.2.1 5.3.3.1
$(\bar{c}/4)_W$	the quarter-chord point of the MAC of the total wing	Several
D	1. total drag	2.1 4.7
	2. empirical factor used in calculating wing lift at high angles of attack	4.1.3.3
	3. diameter of a hemisphere	8.2
	4. propeller diameter	Several
	5. drag force	4.1.3
D'	base diameter of spherical-segment shell	8.2
D_o	body diameter	4.6.4
D_1'	nozzle-exit diameter	4.6.4
d	1. maximum fuselage diameter	Several
	2. $\frac{\tan \Lambda_{TE}}{\beta}$	6.1.6.1

SYMBOL	DEFINITION	SECTIONS
	3. average maximum diameter of fuselage	8.1
	4. outside diameter of a hollow cylindrical element	8.2
	5. equivalent-cylinder diameter for a hemisphere	8.2
	6. base diameter of a spherical nose segment or given frustum	4.2.2.1 4.2.3.1 7.2.1.1 7.2.1.2
	7. average body diameter at the exposed wing root	Several
	8. maximum diameter of forebody or afterbody	4.2.3.1
	9. 2/3 root chord of basic triangular wing	7.1.1.1 7.1.1.2 7.1.4.2
	10. maximum body height at wing-body intersection	5.2.1.1
d', d''	body diameters at the midchord points of the MAC of the forward and aft surfaces, respectively	4.4.1 4.5.1.1 4.5.1.2 7.4.1.1
d_{CB}	duct center-body diameter at exit plane	9.3 9.3.1 9.3.2 9.3.3
d_H	average fuselage width in region of horizontal tail	6.2.1.2
d_{LE}	diameter of leading edge	6.3.1 6.3.2
d_a	diameter at forward end of missile component	8.2
d_b	1. base diameter of body	Several
	2. diameter at aft end of missile component	8.2
	3. base diameter of jet nozzle	4.6.4
$(d_b)_{equiv}$	equivalent base diameter of a non-body-of-revolution configuration	4.2.3.1
d_{cyl}	diameter of cylinder	4.2.1.2 4.2.2.1
d_e	1. average maximum diameter of engine	8.1
	2. exit diameter of duct or nozzle	Several
d_{equiv}	equivalent diameter of a non-body-of-revolution configuration	4.2.1.2 4.2.3.1
$(d_{equiv})_{av}$	average equivalent diameter of non-body-of-revolution configuration	5.2.2.1
d_j	diameter of nozzle exit	4.6.4
d_{max}	maximum diameter of body	4.3.3.1 4.5.3.1

SYMBOL	DEFINITION	SECTIONS
d_n	base diameter of one of n segments of a body	4.2.3.1
d_o	1. base diameter of a spherically blunted body nose	4.2.3.1
	2. theoretical effect of blowing on lift derivative	6.1.4.1
d_p	diameter of ducted propeller	9.3 9.3.1
d_s	diameter of sphere for spherically blunted body noses	Several
d_t	width of nozzle throat	6.3.2
d_0	inside diameter of a hollow cylindrical element	8.2
d_1	upstream pressure interaction length	6.3.1
d_2	downstream interaction length	6.3.1
d_3	distance from reference line to point of intersection of two lines tangent to pressure curve (see Sketch (d), Page 6.3.1-9)	6.3.1
$d_1, d_2, d_3 \ldots$	diameter at aft end of given body segment	Several
$\frac{d}{b}$	ratio of maximum body width to wing span	4.3.2.1
E	empirical constant used in calculating wing lift at high angles of attack	4.1.3.3 4.1.3.4
$E''(\beta C)$	elliptical integral factors of the stability derivative	Several
e	1. Oswald (span) efficiency factor for induced drag	Several
	2. value of error	Several
e^*	induced span efficiency factor (inviscid)	4.1.5.2
e_H	Oswald (span) efficiency factor for induced drag of horizontal stabilizer	4.5.3.2
F	1. general force	4.1.3 8.1
	2. resultant force	4.7 9.2
F_c	1. control force	6.3.2
	2. control-column force (pull force positive)	6.3.4
F_{j_0}	vacuum thrust	6.3.2
F_p	rudder-pedal force (push on left pedal positive)	6.3.4
F_s	elevator stick force (pull force positive)	6.3.4
F_x	1. propeller-wing combination negative-drag force	9.2
	2. duct negative-drag force	9.3

SYMBOL	DEFINITION	SECTIONS
$F_w(\lvert y_{i,o} \rvert)$, $F_w(Y_{i,o})$, $F_{w,o}$	functions used to determine w	4.4.1
$F_1(N)$, $F_2(N)$, $F_3(N)$, $F_4(N)$, $F_5(N)$, $F_6(N)$, $F_7(N)$, $F_8(N)$, $F_9(N)$, $F_{11}(N)$	F(N) factors of the stability derivative	Several
F/T	thrust-recovery factor	9.2 9.2.1 9.2.3
f	1. fineness ratio of body	Several
	2. inflow factor of propeller	4.6 4.6.1
f_A	fineness ratio of body minus the nose	Several
f_C	fineness ratio of cylindrical segment of body	4.2.3.2
f_N	1. fineness ratio of body nose	Several
	2. fineness ratio of body nose and forebody	4.3.2.2
f_{N_o}	fineness ratio of spherically blunted cone extended to cone apex	4.2.3.1
f_b	fineness ratio of boattail	4.2.2.1
$(f)_{equiv}$	equivalent fineness ratio (see Equation 4.3.2.1-d)	4.3.2.2
f_f, $(f)_{forebody}$	fineness ratio of body forebody (see Sketch (a), Section 4.3.2.1)	4.3.2.2
f_{fus}	fineness ratio of fuselage	4.3.3.1
f_n, $(f)_{nose}$	fineness ratio of nose	4.3.2.2
G_c	main-control-surface stick gearing	6.3.4
$G_{c_{max}}$	maximum control-surface stick gearing	6.3.4
$G_{e_{max}}$	maximum elevator stick gearing	6.3.4
G_k, G_n, G_v	span-loading coefficients at spanwise stations k, n, and v, respectively	6.1.7
G_{tc}	control-tab stick gearing	6.3.4
$G(\beta C)$	elliptical integral factors of the stability derivative	7.1.1.1 7.1.1.2 7.1.4.1 7.1.4.2
$\frac{G}{\delta}$	subsonic spanwise loading coefficient	6.1.5.1 6.1.7
$\Delta \frac{G}{\delta}$	increment in spanwise loading coefficient	6.1.5.1

SYMBOL	DEFINITION	SECTIONS
$\left(\frac{G}{\delta}\right)_v$	spanwise-loading coefficient at spanwise station v	6.1.7
$\left(\frac{G}{\delta}\right)_{\eta_i}, \left(\frac{G}{\delta}\right)_{\eta_o}$	spanwise loading coefficient at inboard and outboard ends, respectively, of a flap	6.1.5.1
g	$\frac{\tan \Lambda_{LE}}{\beta}$	6.1.6.1
g', g''	distances parallel to the plane of symmetry from panel apex to the forward end of the MAC of forward and aft panels, respectively	4.5.2.1
H	height of the quarter-chord point of the MAC of the wing above the ground plane	4.7 4.7.1 4.7.4
H_c	hinge moment of main control surface	6.3.4
H_H	height of the quarter-chord point of the MAC of the auxiliary horizontal surface above the ground plane	4.7 4.7.1
H_{tc}	hinge moment of control tab	6.3.4
h	1. average height of fuselage at the wing root chord	5.2.2.1 5.2.3.1 5.6.2.1 5.6.3.1
	2. downward displacement of trailing-vortex sheet from z = 0 plane (in this application z = 0 is chosen at the quarter-chord point of the MAC of the forward surface)	4.4.1 7.4.4.1
	3. altitude	4.6 4.6.1
	4. maximum height of sonic line above surface (effective jet height)	6.3.2
	5. average height above the ground of the quarter-chord point of wing chord of 75-percent semispan and the three-quarter-chord point of the wing root chord (see sketch on Figure 4.7.1-14)	4.7 4.7.1
h_H	height of aft-surface MAC quarter-chord point above or below the forward-surface root chord, measured in plane of symmetry normal to extended-forward-surface root chord, positive for the aft-surface MAC above the plane of the root chord	Several
$h_{c_r/4}$	height of the quarter-chord point of the wing root chord above the ground	4.7 4.7.1
h_d	distance of deflector lip below surface of wing, perpendicular to wing chord plane	6.2.1.1
h_s	1. distance of spoiler lip above surface of wing, measured from and normal to the airfoil mean line	6.1.1.1 6.2.1.1 6.2.2.1
	2. maximum height of separated boundary layer above the surface	6.3.2
h_v	distance of wing vortex above horizontal tail at tail center of pressure, measured normal to body axis	4.4.1

SYMBOL	DEFINITION	SECTIONS
h_1, h_2	fuselage depths as defined in Figure 5.2.3.1-8	5.2.3.1 5.6.3.1
$\frac{h}{d}$	ratio of maximum canopy height measured from body centerline to body height at the point of maximum canopy height	4.3.2.1
I	moment of inertia (see Figure 8.1-22)	8.1
I_{oy}	moment of inertia about centroidal axis of section	8.1
I_{oy}, I_{ox}, I_{oz}	pitching, rolling, and yawing moments of inertia, respectively, about the centroidal axis of the body	8.1
I_{sp}	jet vacuum specific impulse	6.3.2
$I_{v_{B(H)}}$	vortex interference factor for a lifting surface mounted on the body center line	6.2.1.2
$I_{v_{B(W)}}$	interference factor for effect of body vortex on horizontal panel	4.3.1.3 4.3.1.4
$I_{v_{B(W')}}, I_{v_{B(W'')}}$	interference factors for effects of body vortex on fore and aft panels, respectively	4.5.1.2
$I_{v_{W'(W'')}}$	interference factor for effect of forward panel vortex on aft panel	4.4.1 4.5.1.1 4.5.1.2 7.4.1.1
I_{xx}, I_{yy}, I_{zz}	moments of inertia of the vehicle about x-x axis, y-y axis, and z-z axis, respectively	8.2
$I_{xx}', I_{yy}', I_{zz}'$	moments of inertia of body component about x-x axis, y-y axis, and z-z axis, respectively	8.2
I_y, I_x, I_z	pitching, rolling, and yawing moments of inertia, respectively, about a remote axis	8.1
1	a particular segment of a trailing-edge flap of n segments	6.1.2.1 6.1.5.1
i', i''	angles of incidence of forward and aft surfaces, respectively	4.5.1.2 4.6.1 7.4.1.1
i_H	incidence of auxiliary horizontal surface, aft tail or canard, positive nose up	4.6 4.6.1 4.6.3 4.7.1
i_T	incidence of thrust axis, positive nose up	4.6 4.6.1 4.6.4
i_W	incidence of main surface, positive nose up	Several
Δi_v	total body vortices interference factor	5.3.1.2 5.6.1.2
i_{v_1}, i_{v_2}	body vortex interference factors	5.3.1.2 5.6.1.2

SYMBOL	DEFINITION	SECTIONS
J	1. empirical factor for estimating the lift of wings at high angles of attack	4.1.3.3 4.5.1.2
	2. ducted-propeller advance ratio, $\frac{V_\infty}{nd_p}$	9.3 9.3.1 9.3.2 9.3.3
	3. propeller advance ratio, $\frac{V_\infty}{nD}$	9.1 9.1.1 9.1.3 9.2
	4. jet momentum at the wing trailing edge, $m_j V_j$	6.1.1.1 6.1.4.1
J'	modified advance ratio, $J \cos \alpha$	9.1 9.1.1 9.1.3
J_{0_P}	advance ratio at zero power	9.1 9.1.3
J_{0_T}	advance ratio at zero thrust	9.1 9.1.1 9.1.3
j	one section of a wing of n sections having constant sweep angles within its boundary	4.1.3.2
K	1. factor used to estimate the maximum lift increment of a surface due to propeller power effects	4.6 4.6.2
	2. ratio of rolling-moment coefficient of a spoiler-slot-deflector to that of a plain spoiler	6.2.1.1
	3. parameter accounting for effective wing thickness	4.7 4.7.1
	4. factor accounting for the lift carry-over due to flap deflection on wing sections adjacent to flaps at subsonic speeds	6.1.5.1
	5. factor used to estimate the pitching effectiveness of trailing-edge flaps at transonic speeds	6.1.5.1
	6. surface-element pressure-coefficient constant	4.2.1.2 4.2.2.2
	7. apparent-mass factor	Several
	8. upstream amplification factor (control force normal to the surface normalized with respect to vacuum thrust of sonic nozzle)	6.3.2
	9. pitching-moment-of-inertia correction factor for solid component	8.2
	10. drag-due-to-lift factor	4.1.5.2
	11. ratio of extended wing chord, including extensions of both leading-edge and trailing-edge flaps, to retracted wing chord, $K = c_{\delta\delta}/c$	6.1.2.1
	12. theoretical correction factor for finite aspect-ratio effects on $c_{\ell_{\delta_f}}$, as defined in Equation 6.1.5.1-p	6.1.5.1

SYMBOL	DEFINITION	SECTIONS
	13. constant factor for a given sharp-nosed airfoil section	4.1.5.1 4.3.3.1
	14. empirical correlation factor corresponding to lift-interference factor K_L	4.1.3.2
	15. empirical correlation factor depending upon planform geometry	6.2.2.1
	16. ratio of yawing-moment coefficient of spoiler-slot-deflector to that of a plain spoiler	6.2.2.1
	17. dimensionless correction factor used to extrapolate the potential-flow values to high lift coefficients	7.1.2.1 7.1.2.3
	18. number of propellers	9.2 9.2.1 9.2.3
K'	1. effective apparent-mass factor	Several
	2. flap-span factor	6.1.7
	3. empirical correction factor to section lift increment for nonlinear effects at high flap deflections	Several
K_A	wing-aspect-ratio factor	4.4.1 6.2.1.2
$K_{B(W)}$	ratio of the lift of the body in the presence of the wing to that of the wing alone	Several
K_D	propeller drag factor	4.6 4.6.4
K_H	1. factor accounting for relative size of horizontal and vertical tails	Several
	2. horizontal-tail-location factor	4.4.1 6.2.1.2
$K_{H(B)}$	apparent-mass factor of the horizontal tail in the presence of the body	Several
K_L	1. lift-interference factor for normal-force-curve slope	4.1.3.2 5.1.2.1
	2. pitch-moment-of-inertia correction factor for liquid mass	8.2
K_{M_Γ}	compressibility correction to the dihedral effect used in estimating C_{l_β}	5.1.2.1 5.2.2.1 5.6.2.1
K_{M_Λ}	compressibility correction to the sweep contribution used in estimating C_{l_β}	5.1.2.1 5.2.2.1 5.6.2.1
$K_{M_{\Lambda_i}}, K_{M_{\Lambda'_o}}$	compressibility correction to sweep contribution used in estimating C_{l_β} for constructed inboard and outboard panels, respectively, of a composite wing	5.1.2.1

SYMBOL	DEFINITION	SECTIONS
K_N	1. ratio of body-nose lift to that of wing alone	4.3.1.2 4.3.1.3 4.3.1.4 4.5.1.2
	2. propeller normal-force factor	4.6 4.6.1
	3. correlation factor for pressure drag of ogive noses	4.2.3.1 4.3.3.1 4.5.3.1
	4. empirical factor related to sideslip derivative C_{n_β} for body and wing-body interference	5.2.3.1 5.6.3.1
K_{R_ℓ}	empirical Reynolds-number factor	5.2.3.1
$K_{V(B)}$	apparent-mass factor of the upper vertical panel in the presence of the body	Several
$K_{V(BHU)}$	apparent-mass factor of the upper vertical panel in the presence of the body, horizontal tail, and lower vertical panel	Several
$K_{V(BU)}$	apparent-mass factor of the upper vertical panel in the presence of the body and lower vertical panel	Several
$K_{V(BW)}$	apparent-mass factor of the upper vertical panel in the presence of the body and wing	5.3.1.1
$K_{V(BWH)}$	apparent-mass factor of the upper vertical panel in the presence of the body, wing, and horizontal tail	Several
$K_{W(B)}$	1. ratio of the lift of the wing in the presence of the body to that of the wing alone	Several
	2. apparent-mass factor of the wing in the presence of the body	Several
$K_{(WB)}$	ratio of the lift of the wing-body combination to that of the wing alone	4.3.1.2 7.3.1.1 7.3.1.2 7.3.4.2
K'_N, $K_{W(B)}{}'$, $K_{B(W)}{}'$	appropriate wing-body interference factors for the forward surface	Several
$K_{W(B)}{}''$, $K_{B(W)}{}''$	appropriate wing-body interference factors for the aft surface	Several
K_b	factor used in estimating the lift effectiveness of flaps and control surfaces at subsonic speeds	6.1.4.1 6.1.4.2 6.1.5.1 6.1.7
K_{b_k}, $K_{b_{k-1}}$	values of the span factor for outboard and inboard ends, respectively, of the k^{th} wing section	6.1.5.1
$(K_b)_{\eta_i}$, $(K_b)_{\eta_o}$	value of K_b due to a flap extending from the plane of symmetry to the inboard and outboard span stations, respectively, of the actual flap	6.1.4.1 6.1.4.2
K_f	factor used in estimating the body contribution to wing-body C_{l_β}	5.2.2.1 5.6.2.1
K_i	factor used to estimate the body contribution to wing-body C_{Y_β}	5.2.1.1 5.6.1.1
K_m	empirical nonlinear pitching-moment factor	4.1.4.3

SYMBOL	DEFINITION	SECTIONS
K_n	1. factor used to estimate the body contribution to wing-body C_{n_β}	5.2.3.1
	2. Knudsen number	4.2.3.1
K_o	upstream amplification factor of normal sonic nozzle	6.3.2
K_p	1. potential-flow lift parameter	4.2.1.2
	2. conversion factor for a partial-span flap on a sweptback wing	6.1.5.1
$(K_p)_{\eta_i}, (K_p)_{\eta_o}$	value of K_p due to a flap extending from the plane of symmetry to the inboard and outboard span stations, respectively, of the actual flap	6.1.5.1
K_t	hypersonic similarity parameter, $M\frac{t}{c}$, for a wing	4.1.5.1
K_v	viscous-flow lift parameter	4.2.1.2
K_α	factor accounting for the effect of control-surface span in the estimation of the parameter C_{h_α}	6.1.6.1
K_δ	factor accounting for the effect of control-surface span in the estimation of the parameter C_{h_δ}	6.1.6.2
K_θ	pressure-surface slope integral	4.2.1.2 4.2.2.2
K_Λ	1. empirically derived correction factor accounting for the effects of the wing planform	6.1.4.3
	2. flap-span factor	6.1.5.1
$(K_\Lambda)_{\eta_i}, (K_\Lambda)_{\eta_o}$	value of K_Λ due to a flap extending from the plane of symmetry to the inboard and outboard span stations, respectively, of the actual flap	6.1.5.1
K_λ	wing-taper-ratio factor	4.4.1 6.2.1.2
K_{ϕ_U}	cross-coupling interference factor of lower vertical surface	5.3.1.2 5.6.1.2
K_{ϕ_V}	cross-coupling interference factor of upper vertical surface	5.3.1.2 5.6.1.2
K_1	factor accounting for the effect of nacelles and fuselage on wing lift due to power effects	4.6 4.6.1
K_1, K_2, K_3	Mach-number functions used in determining supersonic flap pitching effectiveness	6.1.5.1
$K_1, K_2, K_3, \ldots$	empirical factors used in calculating moments of inertia	8.1
$K_1, K_2, \ldots K_{12}$	geometric and Mach-number parameters used in supersonic hinge-moment-derivation calculations (Page 6.1.6.1-7)	6.1.6.1
$K(A_t, C'_J)$	correction factor for blown flaps as a function of jet momentum and aspect ratio	6.1.4.2
k	1. surface-roughness height	Several
	2. factor used in estimating supersonic parameter C_{h_α}	6.1.6.1
	3. the number of the wing section, numbered from fuselage center line outboard	6.1.5.1

SYMBOL	DEFINITION	SECTIONS
	4. empirical factor used in estimating sideslip derivative C_{Y_β}	Several
	5. spanwise station, $\frac{m+1}{2}$	6.1.7
	6. factor used in determining the a.c. location of wing-lift carryover on the body, d/b	4.3.2.2
	7. tab spring effectiveness	6.3.4
$k_{B(H)}$, $k_{H(B)}$	tail-body interference factors	6.2.1.2
$k_{B(W)}$	ratio of lift-curve slope of body in presence of wing to that of wing alone, fuselage at zero angle of attack and wing incidence varying	4.2.1.1 4.3.1.2 4.3.1.3
$k_{W(B)}$	ratio of lift-curve slope of wing in presence of body to that of wing alone, fuselage at zero angle of attack and wing incidence varying	4.3.1.2 4.3.1.3
$k_{W(B)}'$, $k_{B(W)}'$, $k_{W(B)}''$, $k_{B(W)}''$	wing-body interference factors for the forward and aft panels, respectively	4.5.1.2
k_t	airfoil-theory thickness factor	6.1.1.1 6.1.1.2 6.1.4.1
k_1, k_2, k_3	empirical factors used in determining the maximum lift increment due to flap deflection	6.1.1.3 6.1.4.3
$(k_2 - k_1)$	apparent mass factor used in determining the subsonic lift and moment of bodies	Several
$k(\alpha)$	angle-of-attack correction to the horizontal-tail-body interference coefficient	5.2.1.2 5.3.1.2
L	1. general lift force	4.1.2 4.7
	2. equivalent-cylinder length for a hemisphere	8.2
	3. duct lift force, $L = C_L q_\infty S_D$	9.3 9.3.1 9.3.2
	4. airfoil-thickness-location parameter	4.1.5.1 4.3.3.1 4.5.3.1 7.4.2.2
	5. reference length	6.3.1
	6. distance of nozzle from plate leading edge	6.3.2
$L_{.75}$	left-blade position at 3/4-radius point	9.1 9.1.3
$\frac{L}{L_o} - 1$	parameter accounting for effect of image bound vortex on lift	4.7 4.7.1
$(LER)_i$, $(LER)_o$	leading-edge radius of the inboard and outboard panels, respectively, of a wing	4.1.5.2
$\frac{LER}{\bar{c}}$	ratio of leading-edge radius to mean aerodynamic chord taken at the mean aerodynamic chord	4.3.2.1

SYMBOL	DEFINITION	SECTIONS
ℓ	1. reference length	Several
	2. over-all length from wing apex to most aft point on the trailing edge	2.2.2 4.1.3.2 4.1.5.2 4.3.3.2
	3. control-surface linkage arm (see Sketch (f), Section 6.3.4)	6.3.4
ℓ''	distance parallel to longitudinal axis between quarter-chord point of MAC of total forward panel and quarter-chord point of MAC of total aft horizontal panel	Several
ℓ_A	1. length of body minus nose	Several
	2. length of afterbody (see Sketch (a), Section 4.3.3.2)	4.3.2.1 4.3.3.2
	3. length of the boattail segment of a jet nozzle	4.6.4
ℓ_B	1. total length of body	Several
	2. total length of body used as reference length in place of $\bar{c}$	7.2.1.1 7.2.1.2 7.2.2.1 7.2.2.2
	3. length of ogive-cylinder or cone-cylinder segment of body	4.2.2.1
ℓ_C	length of cylindrical segment of a body	4.2.1.1 4.2.1.2 4.2.3.1 4.2.3.2
ℓ_E	length of nozzle past afterbody	4.6.4
ℓ_F	length of flare	4.2.3.2
ℓ_H	1. longitudinal distance from quarter-chord point of the MAC of main surface to quarter-chord point of the MAC of the auxiliary horizontal surface, positive for auxiliary surface behind main surface	Several
	2. distance to the center of pressure of a horizontal stabilizer, measured parallel to the body center line, from the moment reference center	5.6.3.1
	3. distance from the moment reference center to the center of pressure of a horizontal-tail interference side force, measured parallel to the body center line	5.3.3.2 5.6.3.2
ℓ_N	1. length of body nose	Several
	2. length of body nose and forebody	4.3.2.1 4.3.2.2 4.3.3.2
ℓ_{N_o}	length of spherically blunted cone extended to cone apex	4.2.3.1
ℓ_U	distance to the center of pressure of the lower vertical stabilizer (ventral) measured parallel to the body center line, from the moment reference center	Several
ℓ_V	distance to the center of pressure of the upper vertical stabilizer, measured parallel to the body center line, from the moment reference center	Several
$\bar{\ell}_{W(B)}$	distance to center of pressure of the wing-induced body side force measured from the body nose, defined by Equations 5.2.3.2-c, -d	5.2.3.2
ℓ_a, ℓ_b	longitudinal distances from Z-axis to beginning and end stations of body component, respectively	8.2
ℓ_b	length of boattail	4.2.2.1
$\ell_{c.g.}$	longitudinal distance from beginning station of body component to the center of gravity of the component	8.2

SYMBOL	DEFINITION	SECTIONS
ℓ_e	length of engine including propeller	8.1
ℓ_{eff}	distance measured parallel to the forward-surface root chord, between the effective-forward-surface tip quarter-chord point and the aft-surface MAC quarter-chord point	4.4.1 4.5.1.1 7.4.4.1
ℓ_{equiv}	length of equivalent body nose, $f_{equiv}\, d$	4.3.2.2
ℓ_f	1. longitudinal distance from nose of body to midpoint of wing tip	5.2.2.1 5.6.2.1
	2. length of body forebody	4.3.2.2
	3. length of control	6.3.1
ℓ_{f_i}	free interaction length	6.3.1
ℓ_h	distance from intersection of wing trailing edge with fuselage and the quarter-chord point of the MAC of the horizontal tail	4.2.2.1
ℓ_n	1. longitudinal distance from nose of body to exposed root chord of the wing	5.2.2.1 5.2.3.2
	2. length of body nose	4.3.2.2
ℓ_p	1. length of nacelle structure	8.1
	2. distance to the center of pressure of a panel in the empennage, measured parallel to the center line, from the moment reference center	Several
ℓ_s	separation length	6.3.1
ℓ_t	control-tab linkage arm (see Sketch (f), Section 6.3.4)	6.3.4
ℓ_x	distance from moment center to a transverse element, positive where element is forward of moment center	4.2.2.2
ℓ_0	distance from apex of forward-body theoretical cone to face of forward-body segment (see sketch, Page 7.2.1.1-5)	7.2.1.1 7.2.1.2
ℓ_1, ℓ_2	control-surface linkage arms (see Sketch (f), Section 6.3.4)	6.3.4
$\ell_1, \ell_2, \ell_3, \ldots$	length of a given segment of a body	Several
ℓ_2	distance measured parallel to the forward-surface root chord, between the forward-surface root-chord aft end and the aft-surface MAC quarter-chord point	4.4.1 4.5.1.1 7.4.4.1
ℓ_3	distance measured parallel to the plane of symmetry, between the forward-surface MAC forward end and the root-chord aft end	4.4.1 4.5.1.1 7.4.4.1
M	1. Mach number	Several
	2. moment	2.1
	3. length of molecular mean tree path for rarefied gas	4.2.3.1
	4. duct pitching moment, $M = C_m\, q_\infty\, S_D\, c$	9.3 9.3.1

SYMBOL	DEFINITION	SECTIONS
ΔM	Mach-number increment	4.1.3.2
$(MAC)_{V_e}$	mean aerodynamic chord of exposed upper vertical panel	5.3.2.1
$M_{C_{D_{w_{peak}}}}{}_{\Lambda_{c/4} = n}$	Mach number for maximum wave-drag increment for swept wing with $\Lambda_{c/4} = n$	4.1.5.1 4.3.3.1 4.5.3.1
$M_{\Delta C_{D_{peak}}}$	Mach number for maximum wave-drag increment	4.1.5.1 4.3.3.1 4.5.3.1
$M_{\left(\frac{\partial C_D}{\partial M}\right)_{C_L = \text{const}} = 0.10}$	Mach number at which the numerical value of the slope of the curve of C_D vs M is 0.10	4.1.5.1
M_D	Mach number for drag divergence	4.1.5.1 4.2.3.1 4.3.3.1 4.5.3.1
$M_{D_{\Lambda_{c/4} = n}}$	Mach number for drag divergence for swept wing with $\Lambda_{c/4} = n$	4.1.5.1 4.3.3.1 4.5.3.1
M_I	initial drag-rise Mach number	4.5.3.1
M_N	Mach number determining if leading edge of wing is supersonic	4.1.5.1
M_a	1. Mach number used in estimating transonic lift-curve slope (see Page 4.1.3.2-13), $M_{fb} + .07$	4.1.3.2
	2. moment-area of a control surface about its hinge axis	6.1.6.1
M_b	Mach number used in estimating transonic lift-curve slope (see Page 4.1.3.2-13), $M_{fb} + .14$	4.1.3.2
M_c	1. Mach number normal to a circular cylinder in steady cross-flow, $M_\infty \sin \alpha$	4.2.1.2 4.2.2.2 4.2.3.2 4.3.3.2
	2. Mach number normal to a circular cylinder in steady cross-flow, $M_\infty \sin \alpha'$	5.2.1.2 5.3.1.2
	3. control-surface moment	6.3.4
M_{cr}	critical Mach number	7.1.1.2
M_e	nozzle-exit Mach number	6.3.2
M_{fb}	force-break Mach number	4.1.3.2 4.1.4.2 5.2.2.1 7.1.1.2
$(M_{fb})_\Lambda$	sweep correction for transonic force-break Mach number	4.1.3.2 4.1.4.2

SYMBOL	DEFINITION	SECTIONS
$(M_{fb})_{\Lambda=0}$	transonic force-break Mach number for zero sweep	4.1.3.2 4.1.4.2
M_o	slope of leading edge	4.4.1
M_p	propeller pitching moment	9.3.1
M_{tc}	tab-surface moment	6.3.4
M_α	local Mach number upstream of interaction	6.3.1
M_1	local Mach number	6.3.2
M_1'	Mach number at nozzle exit	4.6.4
M_∞	free-stream Mach number	Several
$M_\perp$	upstream Mach number normal to the leading edge of the wing	4.1.3.3
$(M_\perp)_{\alpha=0}$	upstream Mach number normal to the leading edge of wing at zero angle of attack	4.1.3.3
m	1. number of spanwise stations on full-span wing	6.1.7
	2. mass	8.1
	3. slope of lifting line	4.4.1
m, n	nondimensional chordwise stations in terms of c	2.2.2
$\dot{m}$	nozzle mass-flow rate	6.3.2
m_i	duct internal mass flow	9.3 9.3.1
m_j	mass-flow rate of gas efflux (per section)	6.1.1.1
N	1. normal force	4.1.3
	2. propeller normal force	9.1
	3. ducted-propeller normal force	9.3 9.3.1
N_I	normal force acting at inlet of jet engine due to inclination of inlet to oncoming flow	4.6
N_p	propeller normal force	4.6 9.3.1
n	1. chordwise distance from the wing apex to the pitching-moment reference center measured in root chords, positive for reference center aft of apex	4.1.4 4.1.4.2 4.1.4.3
	2. chordwise distance from wing apex to moment reference center measured in wing mean aerodynamic chords, positive aft	4.7 4.7.3

SYMBOL	DEFINITION	SECTIONS
	3. number of engines	4.6 4.6.1
	4. nondimensional coordinate used in integration of wing-root and wing-tip conical pressures	6.1.6.1
	5. value of sweep angle	4.1.5.1
	6. distance from the face of a given body segment to the desired moment reference axis of the configuration	4.2.2.1 7.2.1.1 7.2.1.2
	7. spanwise station along wing	6.1.7
	8. propeller rotational speed, r.p.s.	9.1 9.3 9.3.1
	9. number of segments of trailing-edge flap	6.1.2.1 6.1.5.1
n'	load factor	4.6 4.6.4 6.3.4
n_i	distance of the desired moment reference center behind the forward face of any given body segment, positive for reference center aft of forward face	4.2.2.1
n_1, n_2	value of i at left- and right-hand wing tips of a swept wing, left and right as viewed from trailing edge to leading edge	4.4.1
P	pressure	6.3.1
P'	ratio of local pressure coefficient to two-dimensional pressure coefficient	6.1.6.1
P_P	plateau pressure	6.3.1
P_e	nozzle-exit pressure	6.3.2
P_o	pressure upstream of separation	6.3.1
P_s	separation pressure	6.3.1
P_α	local pressure upstream of interaction	6.3.1
P_{0_j}	jet plenum pressure	6.3.2
P_1	local pressure	6.3.2
P_2	1. pressure peak value	6.3.1
	2. plateau pressure	6.3.2
P_2'	upstream over-all pressure	6.3.2
P_3	pressure immediately downstream of a transverse jet	6.3.2
P_4	downstream over-all pressure	6.3.2

SYMBOL	DEFINITION	SECTIONS
P_∞	free-stream pressure	6.3.1 6.3.2
p	1. static pressure	Several
	2. cross-section perimeter	4.2.3.1
	3. planform-shape parameter, $S/(b\ell)$	2.2.2 4.1.3.2 4.1.5.2 4.3.3.2
	4. angular velocity in roll	Several
	5. total number of wing sections	6.1.5.1
Δp	static-pressure increment from ambient, $p - p_\infty$	4.6 4.6.1
P_{T_e}	total pressure at jet exit	4.6.1
p_b	base pressure	4.6.4
p_j	jet total pressure	4.6.4
p'_o	internal jet pressure	4.6.4
p_∞	free-stream ambient pressure	4.6.1 4.6.4
q	1. dynamic pressure	Several
	2. angular velocity in pitch	Several
q''	slipstream dynamic pressure	9.2
q_H	average dynamic pressure at an aft horizontal tail	Several
q_V	dynamic pressure at a vertical tail	7.4.2.1 7.4.2.2 7.4.2.3 8.1.2
q_p	average dynamic pressure acting on an aft panel	4.5.3.1
q_s	dynamic pressure in propeller slipstream	4.6
q_l	local dynamic pressure	6.3.2
q_∞	free-stream dynamic pressure	Several
q/p_t, $(q/p_t)_{ref}$	dynamic-pressure ratio for Prandtl-Meyer expansion	4.4.1
q/q_∞	average dynamic-pressure ratio	Several

SYMBOL	DEFINITION	SECTIONS
$\frac{q'}{q_\infty}$	average dynamic-pressure ratio acting on the forward surface	4.5.1.2
$\frac{q''}{q_\infty}$	average dynamic-pressure ratio acting on the aft surface	Several
$\frac{\Delta q}{q}$	dynamic-pressure-loss ratio for points not on the wake center line	4.4.1
$\frac{q_H}{q_\infty}$	effective dynamic-pressure ratio at horizontal tail	4.7 4.7.3
$\frac{\Delta q_H}{q_\infty}$	ratio of the change in dynamic pressure at the horizontal tail	4.6.3
$\frac{\Delta q_s}{q_\infty}$	ratio of the change from free-stream dynamic pressure to slipstream dynamic pressure to the free-stream dynamic pressure	4.6.1 4.6.3
$\left(\frac{\Delta q}{q}\right)_0$	dynamic-pressure-loss ratio at the wake center	4.4.1
R	1. Reynolds number	Several
	2. radial distance from thrust axis to centroid of incremental tail area	4.6.1
	3. reference radius of arbitrary body of revolution	4.2.1.2 4.2.2.2
	4. radius of hemisphere	8.2
	5. propeller radius	Several
	6. leading-edge-suction parameter defined as the ratio of the leading-edge suction actually attained to that theoretically possible	4.1.5.2 4.3.3.2
R'	leading-edge-suction parameter that accounts for the portion of the inboard panel submerged in the body	4.1.5.2
R_L	aerodynamic boost link ratio	6.3.4
$R_{L.S.}$	lifting-surface correlation factor	4.1.5.1 4.3.3.1 7.4.2.2
$(R_{L.S.})_H$	lifting-surface correlation factor of the horizontal-tail panel	4.5.3.1
$(R_{L.S.})_i$, $(R_{L.S.})_o$	lifting-surface correlation factor of the inboard panel and outboard panel, respectively, of the wing	4.3.3.1
$(R_{L.S.})_p$	lifting-surface correlation factor of the tail panel	4.5.3.1

SYMBOL	DEFINITION	SECTIONS
$(R_{L.S.})_V$	lifting-surface correlation factor of the vertical panel	4.5.3.1
$(R_{L.S.})_W$	lifting-surface correlation factor of the wing	4.5.3.1
R_{WB}	wing-body interference factor	4.3.3.1 4.5.3.1
R_b	base radius of body	4.6.4
R_{fus}	maximum fuselage radius forward of propeller plane	9.1 9.1.3
R_i, R_o	leading-edge suction parameter of inboard panel and outboard panel, respectively, of the wing	4.1.5.2
R_j	radius of jet exit	4.6 4.6.1
R'_j	radius of equivalent jet exit	4.6 4.6.1
R_ℓ	Reynolds number	Several
R_{ℓ_L}	Reynolds number based on length	6.3.2
$R_{\ell_{LER}}$	Reynolds number based on the leading-edge radius of the MAC	4.1.5.2 4.3.3.2
$\left(R_{\ell_{LER}}\right)_i$, $\left(R_{\ell_{LER}}\right)_o$	Reynolds numbers based on the leading-edge radius of the MAC of the inboard panel and outboard panel, respectively, of the wing	4.1.5.2
$R_{\ell_{MAC}}$, R_ℓ	Reynolds number based on the length of the mean aerodynamic chord	Several
$R_{\ell_{fus}}$	fuselage Reynolds number	4.3.3.1 4.5.3.1
R_{ℓ_s}	Reynolds number based on distance to the separation point	6.3.2
R_{ℓ_α}	local Reynolds number upstream of interaction	6.3.1 6.3.2
$R^*_{\ell_\alpha}$	reference Reynolds number upstream of interaction	6.3.1
$\left(R_{\ell_\alpha}\right)_{HL}$	Reynolds number at control hinge line, referred to local Reynolds number upstream of interaction	6.3.1

SYMBOL	DEFINITION	SECTIONS
$\left(R_{\ell_\alpha}\right)_{x_o}$	Reynolds number at the point of the beginning of interaction, referred to local Reynolds number upstream of interaction	6.3.1
$\left(R_{\ell_\alpha}\right)_{x_t}$	Reynolds number at transition point, referred to local Reynolds number upstream of interaction	6.3.1
R_{ℓ_∞}	free-stream Reynolds number	6.3.1 6.3.2
R_o	body radius	4.6.4
R_p	propeller radius	Several
R'_1	nozzle-exit radius	4.6.4
$R_{.75}$	right-blade position at 3/4-radius point	9.1 9.1.3
r	1. radius of base of body nose	4.3.1.3
	2. body radius at any station	Several
	3. radius of spherical nose segment	4.2.3.1
	4. body radius	4.3.1.2
	5. $\sqrt{1+\left(\frac{2h}{b}\right)^2}-\frac{2h}{b}$	4.7 4.7.1 4.7.4
	6. radius	8.1
	7. radial distance to propeller blade element	9.1 9.1.1 9.1.2 9.1.3
	8. angular velocity in yaw	Several
	9. average radius of body at vertical-tail exposed root chord	5.3.1.2
	10. average radius of body in the region of the horizontal tail	6.2.1.2
r'	nondimensional coordinate used in integrating wing-root and wing-tip conical pressures	6.1.6.1
r', r''	body radii at the midpoints of the exposed root chords of the forward and aft panels, respectively	4.1.5.2
$\bar{r}$	distance from the axis to the centroid of the total mass	8.1
$r_{LE_{bw}}$	leading-edge radius of basic wing	4.1.5.1 4.3.3.1
r_b	average radius of the body at the wing-body juncture	4.3.3.1
$(r)_{x_o}$	body radius at point where flow ceases to be potential	4.3.3.2

SYMBOL	DEFINITION	SECTIONS
r_1	1. radius of spherical body nose	4.2.1.1 7.2.1.1 7.2.1.2
	2. average body half-depth in the region of the tail panel(s), measured from center line	Several
r_2	average body half-width in the region of the tail panel(s), measured from center line	Several
$\frac{r}{b_W}$	ratio of body radius at exposed-wing-root quarter-chord point or midchord point of forward lifting surface to span of forward surface	4.3.1.3
$\frac{r'}{b'}$	ratio of body radius at root-quarter-chord point or midchord point of exposed forward lifting surface to span of forward surface	4.5.1.2
$\frac{r''}{b''}$	ratio of body radius at exposed-wing-root quarter-chord point at midchord point of aft lifting surface to span of aft surface	4.5.1.2
$(r_1/b)_U$	ratio of average body half-depth in the region of the lower vertical panel to span of lower vertical panel measured to body center line	Several
$(r_1/b)_V$	ratio of average body half-depth in region of the upper vertical panel to span of upper vertical panel measured to body center line	Several
$r_2 \Big/ \frac{b_H}{2}$	ratio of average body half-width in region of horizontal panel(s) to horizontal panel semispan	Several
S	1. cross-sectional reference area of the cylindrical portion of body	4.2.1.2 4.2.2.2
	2. cross-sectional area of body at any point x	4.3.3.1
	3. reference area	4.6 4.6.4 6.3.1
S, S_W	wing area	Several
S'	nose area of forebody or base area of afterbody	4.2.3.1
S', S''	gross planform areas of the forward and aft surfaces, respectively	Several
S_B	frontal area of body	Several
$(S_B)_{ref}$	body reference area	4.3.3.2 5.3.1.1
S_{B_S}	projected side area of body	5.2.1.2 5.2.3.1 5.6.3.1
S_D	duct planform area, $S_D = d_e c$	9.3 9.3.1 9.3.2 9.3.3

SYMBOL	DEFINITION	SECTIONS
S_E	area of trailing-edge extension of double-delta and cranked wings	4.1.3.2
S_H	area of auxiliary horizontal surface, aft tail or canard	Several
ΔS_H	incremental segments of horizontal-tail area	4.6.1
S_{H_e}	area of exposed horizontal-tail panel	4.5.3.1 6.2.1.2
S_{H_i}	area of portion of horizontal tail immersed in propeller slipstream	4.6.3
S_I	total surface area immersed in slipstream	4.6 4.6.4
S_J	streamwise basic wing area ahead of jet flap	6.1.5.1
S_L	area of a loaded region of wing in pressure-moment-area calculations	6.1.6.1
$S_{N_{ref}}$	base area of body nose, πr^2	Several
S_S	wetted or surface area of body excluding base area	Several
$(S_S)_e$	exposed wetted area of body (isolated body minus surface area covered by wing at wing-body juncture)	4.3.3.1 4.5.3.1
S_{U_e}	area of exposed lower vertical panel	Several
S_V	1. area of single vertical panel for configuration with twin vertical panels	5.3.1.1 5.6.1.1
	2. area of upper vertical panel measured to body center line	Several
S_{V_e}	area of exposed upper vertical panel	Several
S_W	wing area	Several
S_{W_e}	area of exposed wing	4.3.3.1 4.5.3.1
S_{W_f}	1. wing planform area including and directly forward of flap area (flap area not included) (see Section 2.2.2)	4.6 4.6.4 6.1.4.2 6.1.4.3
	2. flap-affected wing area, including increase in area due to flap extension	6.1.4.1 6.1.4.2 6.1.5.1
S_{W_i}	wing planform area including and directly forward of flap area immersed in propeller slipstream	4.6.4
S_b	body base area	Several
S_{bw}	area of basic wing	4.1.3.2 4.1.5.1 4.3.3.1 5.1.2.1

SYMBOL	DEFINITION	SECTIONS
$(S_{bw})_e$	area of exposed basic wing	4.3.3.1
S_c	main-control-surface area	6.3.4
S_e	1. area of exposed wing	Several
	2. area of elevator	6.3.4
	3. flow area at duct exit plane, $\frac{\pi d_e^2}{4}\left[1-\left(\frac{d_{CB}}{d_e}\right)^2\right]$	9.3.1
S'_e, S''_e	exposed planform areas of the forward and aft surfaces, respectively	Several
$(S_e)_i$	area of exposed inboard panel of wing	4.3.2.2
S_f	area of flap or control surface	6.1.4.1 6.1.5.1 6.2.1.1
S_g	area of glove of double-delta and cranked wings	4.1.3.2 5.1.2.1
S_i	1. total area of inboard panels of wing	Several
	2. area of portion of wing immersed in propeller slipstream, $b_i c_i$	Several
	3. primary-surface planform area forward of and including the flap area inside the primary-surface tip Mach cone (Figure 6.1.7-28b)	6.1.7
$(S_i)_e$, $(S_o)_e$	areas of exposed inboard and outboard panels, respectively, of wing	4.3.3.1
S_j	area of one section of wing of n sections	4.1.3.2 4.1.3.3
S_k	area of k^{th} wing segment with all flaps retracted	6.1.5.1
S_{ni}	primary-surface planform area forward of and including the flap area outside the primary-surface tip Mach cone (Figure 6.1.7-28b)	6.1.7
S_o	1. total area of outboard panels of wing	Several
	2. cross-sectional area at body station x_o	Several
S'_o	total area of constructed outboard panels of wing	4.1.4.2 4.3.2.2 5.1.2.1
S_p	1. body planform area	4.2.1.2 4.2.2.2 4.2.3.2 4.3.3.2
	2. propeller disk area, πR_p^2	Several
S_{ref}	reference area	Several

SYMBOL	DEFINITION	SECTIONS
S_t	total wing area, including increase in area due to flap extensions	6.1.4.1 6.1.4.2
S_{tc}	control-tab area	6.3.4
S_{wet}	wetted area	4.1.5.1 4.3.3.1 7.4.2.2
$(S_{wet})_e$	wetted area of exposed wing	4.3.3.1 4.5.3.1
$\left[(S_{wet})_H\right]_e$	wetted area of exposed horizontal-tail panel	4.5.3.1
$(S_{wet})_i, (S_{wet})_o$	wetted areas of inboard and outboard panels, respectively, of wing	4.1.5.1 4.3.3.1
$\left(S_{wet_i}\right)_e, \left(S_{wet_o}\right)_e$	wetted areas of exposed inboard and outboard panels, respectively, of wing	4.3.3.1
$\left[(S_{wet})_p\right]_e$	wetted area of exposed tail panel	4.5.3.1
$\left[(S_{wet})_V\right]_e$	wetted area of exposed vertical-tail panel	4.5.3.1
$\left[(S_{wet})_W\right]_e$	wetted area of exposed wing	4.5.3.1
S_x, $S(x)$	body cross-sectional area at any body station, πr^2	Several
S_1, S_2	area of constructed wing panels used to obtain wing lift-curve slope	4.1.3.2 5.1.2.1
S_1, S_2, S_3, . . .	areas on added vertical panel affected by Mach lines emanating from the intersection of exposed leading and trailing edges of all other panels with the body	Several
S_2, S_3	areas of constructed wing panels affected by jet flaps	6.1.5.1
S_{act}/S_{ext}	ratio of actual projected side area of fuselage to that of extended fuselage as determined by Mach lines emanating from leading and trailing edges of exposed root chord of the horizontal panel	Several
T	1. thrust per engine	Several
	2. temperature	6.3.1
	3. factor that accounts for the reduction in longitudinal velocity for wings of infinite span	4.7 4.7.1 4.7.4
	4. product of force and radius	8.1
	5. thrust per propeller or total thrust when used in thrust-recovery factor	9.1 9.1.2 9.2

SYMBOL	DEFINITION	SECTIONS
	6. ducted-propeller thrust	9.3 9.3.1
T_R	transition-strip indicator	4.3.2.1 4.3.3.2
T_{aw}	adiabatic wall temperature	6.3.1
T_c	1. thrust coefficient based on free-stream velocity and propeller disk area, $\frac{T}{q_\infty S_p}$	9.1 9.1.2 9.1.3
	2. propeller thrust coefficient based on free-stream velocity and wing area, $\frac{T}{q_\infty S}$	9.2 9.2.1 9.2.3
T_c'	thrust coefficient per engine, $\frac{2T}{\rho V_\infty^2 S_W}$	Several
T_c''	propeller thrust coefficient based on slipstream velocity and propeller disk area, $\frac{T}{q'' S_p}$	9.2 9.2.1 9.2.3
T_i	total internal axial thrust	9.3 9.3.1
T_{net}	ducted-propeller total net thrust, $(T_i - C_{D_e} q_\infty S_D)$	9.3 9.3.1
T_o	1. free-stream temperature	4.6.4
	2. hovering thrust	9.3.1
T_o'	internal jet temperature	4.6.4
T_p	propeller thrust	9.3.1
T_w	wall temperature	6.3.1
T_α	local temperature upstream of interaction	6.3.1
T_∞	free-stream temperature	6.3.1
t	airfoil maximum thickness	Several
t_c	thickness of control device at hinge line	6.1.3.1 6.1.3.2 6.1.6.1 6.1.6.2
$t_{c.p}$	nondimensional parameter used in calculating moment-arm parameter	6.1.6.1
$t/c, (t/c)_{av}$	average streamwise thickness ratio of lifting surface	Several
$\frac{t}{c'}$	airfoil thickness ratio, based on extended wing chord	6.1.1.1 6.1.1.2 6.1.4.1
$\left(\frac{t}{c}\right)'$	maximum airfoil thickness ratio measured normal to control-surface hinge line	6.1.6.1 6.1.6.2

SYMBOL	DEFINITION	SECTIONS
$\frac{t}{\bar{c}}$	wing thickness ratio at mean aerodynamic chord	4.3.2.1
$(t/c)_{bw}$	average thickness of the basic wing	4.3.3.1
$(t/c)_{eff}$	effective thickness ratio	4.1.5.1 4.3.3.1 4.5.3.1
$(t/c)_i$, $(t/c)_o$	average streamwise thickness ratios of inboard and outboard panels, respectively, of a lifting surface	4.1.5.1 4.3.3.1
$(t/c)_{max}$	maximum thickness ratio	4.1.3.4 4.5.3.1 4.7 4.7.1
$(t/c)_p$	thickness ratio of tail panel	4.5.3.1
V, V_∞	free-stream velocity	Several
$\overline{V}$	transonic velocity similarity parameter, $\frac{\beta^2}{\left(\frac{t}{c}\right)^{2/3}}$	4.1.4.2
V_B	total body volume	Several
V_N	volume of nose	7.3.1.1
V_T	vertical-tail indicator	4.3.2.1
V_e	1. duct exit velocity	9.3 9.3.1
	2. nozzle exit velocity	6.3.2
	3. equivalent airspeed	6.3.4
V_i	velocity increment of internal mass flow due to power	9.3 9.3.1
V_{i_o}	internal mass-flow velocity with power off	9.3
V_j	1. jet exit velocity	4.6 4.6.1
	2. velocity of gas efflux leaving the trailing edge of the airfoil	6.1.1.1
V'_j	equivalent jet-exit velocity	4.6 4.6.1
$\frac{V_e}{V_\infty}$	exit-velocity ratio	9.3 9.3.1 9.3.2 9.3.3
v	1. any spanwise station on wing	6.1.7
	2. induced-drag factor	4.1.5.2 4.3.3.2

SYMBOL	DEFINITION	SECTIONS
W	weight	4.6 4.6.4 6.3.4 8.2
W_H	weight of horizontal-stabilizer section	8.1
W_L	wing-location index	4.3.2.1
W_P	weight of power-plant section	8.1
W_V	weight of vertical stabilizer	8.1
W_W	weight of wing section including wing carry-through structure	8.1
W_e	weight of engine and propeller	8.1
W_f	weight of fuselage section	8.1
W_{fs}	weight of fuselage structure	8.1
w	1. average body width at the exposed-wing or exposed-tail root chord	5.2.2.1 5.6.2.1
	2. maximum body width	4.3.1.4 5.2.3.1 5.6.3.1
	3. factor used to determine the downwash gradient at a particular point in the flow field not close to the trailing edge of the wing	4.4.1
	4. weight per unit length of element	8.2
	5. induced drag factor	4.1.5.2 4.3.3.2
	6. local vertical disturbance velocity	7.1.1.2
w_a, w_b	weights per unit length at beginning and end stations of body component, respectively	8.2
X	axial force	4.1.3
$\overline{X}$	longitudinal distance of vehicle center of gravity from nose apex	8.2
x	1. distance along airfoil chord, origin at LE	2.2.1 2.2.2 6.1.2.1 6.3.1
	2. distance between the moment center and the a.c. of the lifting surface affected by downwash, positive when a.c. is ahead of moment center	4.5.1.1
	3. parameter accounting for effect of image trailing vortex on lift	4.7 4.7.1

SYMBOL	DEFINITION	SECTIONS
	4. distance of centroid of the area affected by jet power effects from moment reference center, positive for area forward of reference center	4.6.3
	5. distance of the local center of pressure aft of the quarter-chord of the MAC (see Equation 6.1.5.1-j)	6.1.5.1
	6. longitudinal distance from the nose to quarter-chord point of the MAC of the exposed wing panel	4.3.1.3
	7. any station along body	Several
	8. longitudinal distance measured from the wing-root trailing edge aft	4.4.1 7.4.1.1
	9. longitudinal coordinate measured forward from wing leading edge	9.1 9.1.3
	10. longitudinal distance from the body nose to midchord point of the MAC of exposed vertical panel	5.3.1.2 5.6.1.2
	11. distance of origin of moments from the 2/3 c_{r_B} point of the basic triangular wing, measured along the longitudinal axis, positive ahead of the 2/3 c_{r_B} point	5.1.3.1 7.1.1.1
	12. distance of origin of moments from the wing midchord point, measured along the longitudinal axis, positive ahead of midchord point	5.1.3.1
	13. distance of center of loading of a conical-flow region from control hinge axis measured normal to the hinge axis	6.1.6.1
	14. longitudinal distance measured from vertical-tail leading edge to projected quarter-chord of horizontal-tail MAC on to root chord (see sketch, Figure 5.3.1.1-22b)	5.3.1.1 7.4.2.1 7.4.2.2 7.4.2.3
	15. distance from body nose to quarter-chord point of the MAC of exposed horizontal tail in subsonic flow	6.2.1.2
	16. distance from body nose to midchord point of the MAC of exposed horizontal tail in supersonic flow	6.2.1.2
	17. distance from nose to center of pressure of given body segment	4.2.2.1
Δx	1. increment between successive longitudinal stations	4.2.3.2 4.3.3.1 6.1.7
	2. the chordwise distance from the quarter-chord point of the 75-percent-semispan chord to the three-quarter-chord point of the wing root chord, positive when the latter is aft of the former (see Figure 4.7.1-14)	4.7 4.7.1
	3. distance between forward and aft faces of given body segment	4.2.2.1
x'	stations measured from leading to trailing edge of airfoil surface	4.4.1
x', x''	longitudinal distances used in estimating wing pitching moment	4.5.2.1

SYMBOL	DEFINITION	SECTIONS
x', z'	corresponding point on the airfoil for a point x, z in the flow field	4.4.1
x''	location of quarter-chord point of MAC of total aft horizontal panel	7.4.1.1 7.4.1.2 7.4.4.1 7.4.4.2
$\bar{x}$	1. distance between a.c. and c.g., positive when c.g. is ahead of a.c.	Several
	2. longitudinal distance from axes origin to c.g. of component	8.2
	3. chordwise distance between duct moment reference center and installed duct center of pressure, positive for center of pressure ahead of moment reference center	9.3 9.3.2
x_H	distance between vehicle center of gravity and quarter-chord point of horizontal stabilizer MAC (see Figure 4.5.3.2-4)	4.5.3.2
x'_H	distance from jet wake origin to the quarter-chord point of the MAC of the horizontal tail, parallel to the thrust axis	4.6 4.6.1
x_{HL}	distance from nose of configuration to control hinge line	6.3.1
x_I	longitudinal distance between jet inlet and quarter-chord point of wing MAC	4.6 4.6.1 4.6.3
x_{LE}	longitudinal distance from aircraft reference-axis origin to leading edge of mean aerodynamic chord of wing segment affected by leading-edge device	6.1.5.1
$\bar{x}_{LE}$	chordwise distance from apex to leading edge of MAC	2.2.2
x_{MRP}	distance from the leading edge of MAC to the moment reference point, positive for the moment reference point aft of the leading edge of the MAC	6.1.5.1
x_R	point of reattachment pressure rise (see Sketch (a), Page 6.3.1-2)	6.3.1 6.3.2
x_W	longitudinal distance from aerodynamic center of that portion of wing immersed in propeller slipstream to moment-reference-center location, positive for a.c. forward of moment reference center.	4.6 4.6.3
x_a	center-of-lift location of incremental load due to flap deflection, measured positive aft from extended airfoil leading edge parallel to free stream	6.1.2.1
$x_{a.c.}$	1. distance between aerodynamic center and wing apex, parallel to the MAC,positive for a.c. aft of wing apex	Several
	2. airfoil-section a.c. position	4.1.2.2
	3. distance between aerodynamic center and airfoil leading edge, parallel to free stream, positive for aerodynamic center aft of leading edge	6.1.2.1
$\Delta x_{a.c.}$	shift in wing aerodynamic center at transonic speeds due to flow separation	4.1.4.2
$x'_{a.c.}$	aerodynamic center of the forward panel, referred to forward-panel apex	4.3.2.2
$x''_{a.c.}$	aerodynamic center of the aft panel, referred to aft-panel apex	4.5.2.1 4.5.2.1
$(x'_{a.c.})'_o$	aerodynamic center of the constructed outboard panel of the wing	4.3.2.2
$(x_{a.c.})_p$	distance between quarter-chord point of MAC of added panel and aerodynamic center of added panel. For supersonic case the distance between the mid-chord point of MAC and aerodynamic center	5.3.3.1 5.6.3.1

SYMBOL	DEFINITION	SECTIONS
$(x_{a.c.})_V$	distance between quarter-chord point of MAC of vertical panel and aerodynamic center of vertical panel	5.3.3.1
x_c	1. axial distance from vertex of body nose to centroid of body planform area	Several
	2. location of hinge line (for corner flow)	6.3.1
	3. fore and aft displacement of control column, positive forward	6.3.4
$x_{c_{max}}$	maximum displacement of control column, positive forward	6.3.4
$x_{centroid}$	distance of the centroid of area of a wing behind the wing apex, parallel to wing MAC and plane of symmetry	2.2.2
$x_{c.g.}$	1. distance between center of gravity and quarter-chord point of wing MAC, parallel to MAC, positive for c.g. aft of MAC	4.5.2.1 4.6 5.3.3.1 7.1.3.3
	2. distance from wing apex to center of gravity, parallel to MAC, positive for c.g. aft of wing apex	Several
$x_{c.p.}$	1. distance from wing apex to center of pressure, parallel to wing chord and plane of symmetry, positive for c.p. aft of wing apex	4.1.4 4.3.2.2
	2. distance from body nose to body center-of-pressure location, positive aft	4.2.2.1 5.2.3.2
	3. distance from airfoil leading edge to center of pressure of incremental load due to flaps, parallel to wing chord, positive for center of pressure aft of leading edge	6.1.2.1
	4. chordwise center-of-pressure location aft of the leading edge for a flapped wing section	6.1.5.1
	5. center-of-pressure location measured relative to the leading edge (two dimensional)	6.3.2
	6. chordwise distance from duct leading edge to center of pressure of unstalled duct, positive aft of duct leading edge	9.3 9.3.2
$x_{c.p._b}$	chordwise center-of-pressure location aft of the leading edge for the basic loading of a plain flap	6.1.5.1
$(x_{c.p.})_b$	center-of-pressure location of boattail, measured aft of the forward face of the boattail	4.2.2.1
$(x_{c.p.})_{\Delta C_N}$	distance of center of pressure of normal-force increment from moment reference point, negative aft	6.3.1
x_{c_V}	parameter accounting for relative positions of the horizontal and vertical tails	5.3.1.1
$(x_{\bar{c}/4})_V$	longitudinal distance between quarter-chord point of MAC of vertical panel and the forward end of its root chord	5.3.3.1
x_e	location of nozzle exit (see Sketch (a), Page 6.3.2-3)	6.3.2
x'_e	distance from jet exit to the quarter-chord point of the MAC of the horizontal tail, parallel to the thrust axis	4.6 4.6.1
x_f	1. distance from airfoil leading edge, parallel to free stream, where total lift increment due to flaps acts	6.1.2.1
	2. distance of the leading edge of the control root chord behind the wing axis of pitch	6.1.5.1
$\bar{x}_f$	longitudinal centroidal distance of fuselage from nose	8.1
$x_{f_1}, x_{f_2}, x_{f_i}$	center-of-lift location of incremental load due to deflection of first, second, and i^{th} flap segment, respectively, measured aft from airfoil leading edge parallel to free stream	6.1.2.1 6.1.5.1

SYMBOL	DEFINITION	SECTIONS
$x_{i(\alpha)}$	distance to center of pressure of wing-induced body side force from juncture of wing leading edge and body at angle of attack	5.2.3.2
$x_{i(\alpha = 0)}$	distance to center of pressure of wing-induced body side force from juncture of wing leading edge and body at zero angle of attack	5.2.3.2
x_j	distance from airfoil leading edge, parallel to free stream, where total lift increment due to jet efflux acts	6.1.2.1 6.1.5.1
x_j'	longitudinal distance from jet wake origin to jet exit, usually considered to be 4.6 times the orifice exhaust radius	4.6 4.6.1
Δx_k	longitudinal distance from moment reference center to chord for zero sweep, defined in x_m definition 4 below, for the k^{th} wing segment	6.1.5.1
x_m	1. longitudinal distance from the body nose to the chosen moment center, positive aft	Several
	2. chordwise distance from duct leading edge to moment reference center, positive aft of duct leading edge	9.3 9.3.2
	3. desired pitching-moment reference point measured positive aft from basic airfoil leading edge parallel to wing chord	6.1.2.1 6.1.5.1
	4. distance from wing leading edge to unique unswept reference line so that the ratio of x_m to local chord is constant for straight-tapered wings (see Sketch (K), Section 6.1.5.1)	6.1.5.1
x_o	1. body station where flow ceases to be of a potential nature	Several
	2. function of the slope of the lifting line (m), $\frac{mx}{b/2}$	4.4.1
	3. beginning of pressure interaction	6.3.1
x_p	1. longitudinal distance from intersection of propeller plane with thrust axis and the quarter-chord point of the MAC of the wing	4.6 4.6.1 4.6.3
	2. fore and aft displacement of right rudder pedal, positive forward	6.3.4
x_r	distance from forward end of root chord to intersection of control hinge line with root chord, parallel to wing root chord	6.1.6.1
Δx_r	distance from wing apex to desired moment reference center, measured positive aft	6.1.5.1
x_{ref}	desired pitching-moment reference point, measured positive aft from basic airfoil leading edge parallel to wing chord	6.1.2.1
x_s	1. longitudinal distance from model vertex to point of vortex separation	4.3.1.3 5.3.1.2 5.6.1.2 6.2.1.2
	2. distance from nose of airfoil to spoiler lip, parallel to wing chord (Figure 6.1.1.1-52b)	6.1.1.1 6.2.1.1 5.2.2.1
	3. point of separation pressure rise (see Sketch (a), Page 6.3.1-2)	6.3.1 6.3.2

SYMBOL	DEFINITION	SECTIONS
x_s'	distance from wing leading edge to spoiler hinge line (see Sketch (g), Page 6.2.1.1-6)	6.2.1.1
x_t	1. chordwise position of airfoil maximum thickness	2.2.1 4.1.5.1 4.3.3.1
	2. distance from forward end of tip chord to intersection of control hinge line with tip chord, parallel to root chord	6.1.6.1
	3. transition distance	6.3.1
$x_{(y_c)_{max}}$	chordwise position of maximum camber of airfoil	2.2.1
x_1	1. body station where $\frac{dS_x}{dx}$ first reaches its maximum negative value	Several
	2. distance from intersection of wing leading edge or trailing edge with fuselage and the center of pressure of given body segment (see Sketch (a))	4.2.2.1
$\bar{x}_1$	distance from intersection of wing leading edge with fuselage to forward face of body segment adjacent to the intersection (see Sketch (a))	4.2.2.1
x_1, x_2, x_3	distance parameters used to define section thickness-ratio factor for hexagonal airfoils	4.1.5.1 4.3.3.1
x_1, x_2, x_6	moment arms corresponding to section lift terms Δc_1, Δc_2, Δc_6, respectively	6.1.2.1 6.1.5.1
x_3	point of beginning of downstream pressure rise (see Sketch (a), Page 6.3.2-3)	6.3.2
x_4	point of peak downstream pressure rise (see Sketch (a), Page 6.3.2-3)	6.3.2
$x_{5_1}, x_{5_2}, (x_5)_i$	moment arms corresponding to section lift terms Δc_{5_1}, Δc_{5_2}, Δc_{5_i}, respectively, for the first, second and i^{th} flap segments, respectively	6.1.2.1 6.1.5.1
$\frac{x}{c_V}$	parameter accounting for relative positions of horizontal and vertical tails	5.3.1.1 5.6.1.1
$\frac{x_{a.c.}}{\bar{c}}$	distance of aerodynamic center of wing aft of wing apex, measured in mean aerodynamic chords, positive aft	4.1.4.3
$\frac{x_{a.c.}}{c_r}$	distance of aerodynamic center of wing aft of wing apex measured in root chords, positive aft	4.1.4.2 4.1.4.3 4.3.2.2

SYMBOL	DEFINITION	SECTIONS
$\frac{\Delta x_{a.c.}}{c_r}$	incremental a.c. location accounting for separation effects	4.1.4.2
$\left(\frac{x_{a.c.}}{c_r}\right)_{B(W)}$	value of parameter for body in presence of wing	4.3.2.2
$\left(\frac{x_{a.c.}}{c_r}\right)_{C_L=0}$	aerodynamic-center location at zero lift	4.1.4.3
$\left(\frac{x_{a.c.}}{c_r}\right)_i$	distance of a.c. location of inboard panel of wing aft of apex of inboard panel measured in its root chords	4.1.4.2
$\left(\frac{x_{a.c.}}{c_r}\right)_N$	value of parameter for body nose	4.3.2.2
$\left(\frac{x_{a.c.}}{c_r}\right)_o$	distance of a.c. location of outboard panel of wing aft of the apex of outboard panel, measured in its root chords	4.1.4.2
$\left(\frac{x_{a.c.}}{c_r}\right)'_o$	distance of a.c. location of constructed outboard panel of wing aft of the apex of the constructed outboard panel, measured in its root chords	4.1.4.2 4.3.2.2
$\left(\frac{x_{a.c.}}{c_r}\right)_{W(B)}$	value of parameter for wing in presence of body	4.3.2.2
$\frac{x'_{a.c.}}{c_{r_e}}$	distance of aerodynamic center of wing-body configuration from apex of exposed wing, measured in exposed-wing root chords	4.3.2.2
$\left(\frac{x'_{a.c.}}{c_{r_e}}\right)_{B(W)}$	distance of aerodynamic center of body in presence of the wing from apex of exposed wing, measured in exposed-wing root chords	4.3.2.2
$\left(\frac{x'_{a.c.}}{c_{r_e}}\right)_i$	distance of aerodynamic center of inboard panel of wing from apex of exposed wing, measured in its exposed-wing root chords	4.3.2.2
$\left(\frac{x'_{a.c.}}{c_{r_e}}\right)_N$	distance of aerodynamic center of body nose ahead of wing-body juncture from apex of exposed wing, measured in exposed-wing root chords	4.3.2.2

SYMBOL	DEFINITION	SECTIONS
$\left(\frac{X_{a.c.}}{c_{r_e}}\right)_W$	value of parameter for wing	4.3.2.2
$\left(\frac{X_{a.c.}}{c_{r_e}}\right)_{W(B)}$	distance of aerodynamic center of exposed wing in presence of the body from apex of exposed wing, measured in exposed-wing root chords	4.3.2.2
$\frac{X_{c.p.}}{c_{c.p.}}$	empirically derived chordwise center-of-pressure location of the incremental load due to surface deflection	6.1.5.1
$\left(\frac{X_{c.p.}}{c_{c.p.}}\right)_1$	empirically derived factor of $\frac{x_{c.p.}}{c_{c.p.}}$	6.1.5.1
$\frac{X_{c.p.}}{c_r}$	distance of wing center-of-pressure location, in wing root chords, measured positive aft of wing apex	4.1.4.3
$\left(\frac{X_{c.p.}}{c_r}\right)_{C_L=0}$	wing center-of-pressure location at zero lift	4.1.4.3
$\left(\frac{X_{c.p.}}{c_r}\right)_{C_{L_{max}}}$	wing center-of-pressure location at maximum lift	4.1.4.3
$\left(\frac{X_{c.p.}}{c_r}\right)_{ref}$	wing reference center-of-pressure location	4.1.4.3
$\left(\frac{X_{c.p.}}{c_r}\right)_1$	component of wing center-of-pressure location at maximum lift due to leading-edge sharpness	4.1.4.3
$\Delta\left(\frac{X_{c.p.}}{c_r}\right)_2$, $\Delta\left(\frac{X_{c.p.}}{c_r}\right)_3$, $\Delta\left(\frac{X_{c.p.}}{c_r}\right)_4$	increments of wing center-of-pressure location due to planform geometry	4.1.4.3

SYMBOL	DEFINITION	SECTIONS
$\left(\frac{x_{3D}}{x_{2D}}\right)_i$	ratio of center-of-lift location of a finite-aspect-ratio wing to center-of-lift location of an infinite-aspect-ratio wing for the incremental load due to deflection of the i^{th} trailing-edge flap segment	6.1.5.1
$\left(\frac{x_{3D}}{x_{2D}}\right)_j$	ratio of center-of-lift location of a finite-aspect-ratio wing to center-of-lift location of an infinite-aspect-ratio wing for the incremental load due to jet momentum acting at some angle to trailing-edge camber line	6.1.5.1
$\left(\frac{x_h}{c}\right)'$	distance of the hinge axis behind wing leading edge measured in plane normal to control hinge axis	6.1.6.1 6.1.6.2
Y_{90}, Y_{99}	airfoil ordinates at 90- and 99-percent chord, in percent chords	4.1.1.2 6.1.5.1 7.1.2.2
Y_{90}, Y_{100}	upper-surface ordinates of flap in retracted position at 90- and 100-percent chord, respectively, in fractions of the chord	6.1.1.1
y	1. airfoil ordinate at some value of x	2.2.1
	2. coordinate with origin at midspan of wing leading edge, perpendicular to plane of symmetry	4.4.1
	3. lateral coordinate measured positive to right of plane of symmetry	Several
Δy	1. difference between airfoil ordinate at 6% chord and ordinate at 0.15% chord	Several
	2. lateral distance from thrust axis of one propeller to blade element of another	9.1 9.1.3
	3. spanwise distance on constructed inboard panel = $1/2\ b_i$	4.1.4.2 4.3.2.2
y (x)	thickness distribution of airfoil	2.2.1
$\bar{y}$	lateral distance from axes origin to c.g. of component	8.2
y_B	spanwise location of break span station	2.2.2
$\bar{y}_H$	1. lateral center-of-pressure coordinate of the horizontal tail, measured from and normal to the longitudinal axis	6.2.1.2
	2. lateral centroidal distance of half horizontal stabilizer from aircraft plane of symmetry	8.1

SYMBOL	DEFINITION	SECTIONS
y_{MAC}	distance of the wing MAC from the plane of symmetry	2.2.2
y_T	spanwise distance from thrust axis to body center line	4.6 4.6.1
$\overline{y}_W$	lateral centroidal distance of half-wing from aircraft plane of symmetry	8.1
$y_{\bar{c}}$	lateral distance to wing mean aerodynamic chord from fuselage center line	6.1.4.2 6.1.5.1
$y'_{\bar{c}}$	lateral distance to mean aerodynamic chord of wing segment affected by the leading-edge device from fuselage center line	6.1.5.1
$y_c(x)$	camber-line distribution of airfoil	2.2.1
$(y_c)_{max}$	maximum ordinate of mean line of airfoil	2.2.1 4.3.2.1 4.3.3.2
y_i	spanwise distance from center line to inboard edge of flap or control surface	6.1.6.1 6.1.6.2 6.2.1.1 6.2.2.1
$y_{i,o}$	distance of inboard corners of horseshoe vortices from plane of symmetry	4.4.1
y_{max}	vertical distance from airfoil chord line to airfoil maximum upper-surface ordinate (see Sketch (a), Section 4.1.4.3)	4.1.4.3
y_o	1. distance of theoretical lateral vortex from plane of symmetry	Several
	2. spanwise distance from center line to outboard edge of flap or control surface	6.1.6.1 6.1.6.2 6.2.1.1 6.2.2.1
y_o, z_o	coordinate axes with origin at c.g. of component	8.2
$\frac{y_{v_1}}{b_v}, \frac{y_{v_2}}{b_v}$	body vortex lateral position at the vertical tail spans (defined by Equation 5.3.1.2-f)	5.3.1.2 5.6.1.2
$\Delta y_\perp$	value of Δy for chord perpendicular to wing leading edge, where Δy is defined above in 1.	Several

SYMBOL	DEFINITION	SECTIONS
Z	parameter used in determining horizontal stabilizer lift coefficient; defined by Equation 4.5.3.2-h	4.5.3.2
z	1. vertical distance between c.g. and quarter-chord point of wing MAC positive for MAC below c.g.	7.1.3.2
	2. vertical distance between c.g. and quarter-chord point of wing root chord, positive for quarter-chord point of root chord below c.g.	7.1.2.1 7.1.2.2 7.3.2.1 7.3.2.2
	3. vertical coordinate with origin at midspan of wing leading edge	4.4.1 4.5.1.1 4.5.1.2
	4. vertical distance from the vortex sheet to the point of interest (usually the quarter-chord point of the MAC of the horizontal tail)	4.4.1 7.4.1.1 7.4.4.1
	5. vertical distance of vertical-tail center-of-pressure location above or below moment-reference-center location	7.4.2.1 7.4.2.2 7.4.2.3
Δz	vertical distance between desired moment-reference-center-chord location and quarter-chord of MAC, positive for wing below desired location	6.1.5.1
z'	vertical distance of the horizontal tail below the body center line	6.2.1.2
z', z''	vertical distance between c.g. and quarter-chord point of forward and aft panel MAC's, respectively	4.5.2.1
$\bar{z}$	vertical distance from axes origin to c.g. of component	8.2
z_H	1. vertical distance between quarter-chord point of horizontal tail and X-axis, positive for tail below X-axis	Several
	2. distance measured normal to the longitudinal axis between the horizontal tail c.p. and the moment reference center, positive for c.p. above longitudinal axis	Several
	3. distance to c.p. of horizontal-tail-interference side force, measured from and normal to the longitudinal axis	5.3.3.2 5.6.3.2
	4. distance from quarter-chord point of wing MAC to quarter-chord point of horizontal-tail MAC, measured normal to longitudinal axis, positive for tail above wing	4.5.1.3
$z_{H_{eff}}$	vertical distance of center line of propeller slipstream from quarter-chord point of horizontal tail MAC (see Figure 4.6-13a), positive for slipstream above horizontal tail	4.6 4.6.3
z_{HL}	distance of hinge line measured from and normal to the X-axis, positive down	6.3.1
z_{H_T}	vertical distance from quarter-chord point of horizontal tail to propeller thrust axis; positive for quarter-chord point above thrust axis (see Figure 4.6-13a)	4.6 4.6.3
z_T	vertical distance from propeller thrust axis to coordinate origin, positive for thrust axis below origin (see Figure 4.6-13)	4.6 4.6.1 4.6.3
z_U	distance normal to the longitudinal axis between the lower-vertical-stabilizer (ventral) center of pressure and the moment reference center (normally negative)	5.3.3.2 5.6.2.1 5.6.3.2

SYMBOL	DEFINITION	SECTIONS
z_V	1. distance normal to the longitudinal axis between the upper-vertical-stabilizer center of pressure and the moment reference center (always positive)	Several
	2. vertical centroidal distance of vertical stabilizer from root chord (at fuselage)	8.1
z_W	1. vertical distance from the quarter-chord point of the wing MAC, to the coordinate origin, positive for wing below the origin (see Figure 4.6-13)	Several
	2. vertical distance from body center line to quarter-chord point of root chord, positive for quarter-chord point below center line	Several
	3. half-width of the wake at any position x	4.4.1 4.5.1.1 4.5.1.2 7.4.1.1
$z_{c.g.}$	vertical distance between c.g. and X-axis, positive for c.g. below X-axis	4.5.2.1 4.6
$\Delta z_{c.g.}$	vertical distance between c.g. and wing MAC quarter-chord, positive above quarter-chord	6.1.5.1
$(z_{c.p.})_{\Delta C_A}$	distance of center of pressure of axial-force increment from moment reference point, positive down	6.3.1
z_j'	distance from jet thrust axis to quarter-chord point of horizontal tail perpendicular to thrust axis, positive for quarter-chord point above thrust axis	4.6 4.6.1
z_o	vertical distance of theoretical vortex above reference plane	Several
z_p	distance normal to the longitudinal axis between the center of pressure of a vertical panel and the moment reference center, positive for the panel above the body	5.6.2.1
z_s	vertical distance from X-axis to propeller-slipstream center line at the quarter-chord of the wing MAC, positive for center line above X-axis (see Figure 4.6-13a)	4.6 4.6.1 4.6.3
$\left(\frac{2z}{b}\right)_{eff}$	effective value of height parameter relative to the displaced vortex	4.4.1
$\left(\frac{2z}{b'}\right)_{eff}$	value of parameter for forward panel	7.4.4.1
$\frac{z_H}{r_1}$	ratio of height of horizontal tail to average half-depth of body in region of horizontal tail (ratio is positive for tail below body center line)	5.3.1.1 5.6.1.1
$\frac{z_{v_1}}{b_V}, \frac{z_{v_2}}{b_V}$	body vortex vertical positions at the vertical tail spans; defined by Equation 5.3.1.2-f	5.3.1.2 5.6.1.2

B. GREEK SYMBOLS

SYMBOL	DEFINITION	SECTIONS
α	1. angle of attack, positive nose up	Several
	2. angular acceleration	8.1
	3. flow deflection angle	6.3.1
$\Delta\alpha$	1. angle-of-attack increment from incipient shock detachment to full detachment, $\alpha' - \alpha^*$	4.1.3.3
	2. change in wing angle of attack due to propeller upwash or downwash, $\frac{-\epsilon_p}{1+\frac{\partial \epsilon_u}{\partial \alpha}}$	4.6.1
	3. increment in angle of attack	4.7 4.7.1
α'	1. angle of attack at end of shock-detachment transition region	4.1.3.3
	2. angle of attack of forward panel	Several
	3. angle of inclination, $\sqrt{\alpha^2+\beta^2}$	Several
	4. an incidence angle defined as $\alpha' = \alpha$ for $0 \leq \alpha \leq 90^o$, and $\alpha' = 180^o - \alpha$ for $90^o \leq \alpha \leq 180^o$	4.2.1.2 4.2.2.2 4.2.3.2
α''	angle of attack of aft panel, $\alpha - \epsilon + i''$	4.1.5.2 4.5.1.2 4.5.2.1
$\bar{\alpha}$	transonic similarity parameter, $\frac{\alpha}{t/c}$	4.1.4.2
α^*	1. angle of attack at which section lift curve begins to deviate from linear variation	Several
	2. angle of attack at incipient shock detachment	4.1.3.3
$\alpha_{C_{L_{max}}}$	wing angle of attack at maximum lift coefficient	Several
$\Delta\alpha_{C_{L_{max}}}$	incremental value of parameter (see Figures 4.1.3.4-21b, -25b)	4.1.3.4
$\alpha'_{C_{L_{max}}}$	wing angle of attack of forward panel at maximum lift coefficient	7.4.4.1
$\left(\alpha_{C_{L_{max}}}\right)_{base}$	base value of parameter	4.1.3.3 4.1.3.4
$\left[\left(\alpha_{C_{L_{max}}}\right)_{base}\right]''_e$	subsonic angle of attack for $C_{L_{max}}$ of exposed aft panel	4.5.1.2

SYMBOL	DEFINITION	SECTIONS
$\left(\alpha_{C_{L_{max}}}\right)_e'$, $\left(\alpha_{C_{L_{max}}}\right)_e''$	angles of attack at maximum lift coefficients of exposed forward and aft panels, respectively	4.1.5.2
$\left(\Delta\alpha_{C_{L_{max}}}\right)_e'$	incremental value of parameter for exposed forward panel	4.5.1.2
$\left(\alpha_{C_{L_{max}}}\right)_W$	value of parameter for wing	4.3.1.4
$\left(\alpha_{C_{L_{max}}}\right)_{WB}$	value of parameter for wing-body combination	4.3.1.4 4.5.1.3
α_D	angle of attack between duct axis and free-stream direction	9.3 9.3.1 9.3.2 9.3.3
α_{FRP}	angle of attack for fuselage reference plane	4.3.1.3
$(\Delta\alpha)_G$	increment in angle of attack at a constant lift coefficient in the presence of the ground	4.7 4.7.1
α_H	angle of attack of horizontal tail or canard surface	4.6.3 4.7.1 6.3.4
$(\Delta\alpha_H)_G$	increment in angle of attack of the horizontal tail in the presence of the ground	4.7 4.7.1
α_L	local angle of attack for a particular spanwise wing section	6.1.5.1
α_T	angle of attack of thrust axis	4.6 4.6.1 4.6.3 4.6.4
α_V	angle of attack of vertical tail	6.3.4
α_W	angle of attack of wing	Several
$\Delta\alpha_W$	change in wing angle of attack ahead or behind the propellers	4.6.1
α_{WB}	wing-body angle of attack	4.5.3.2
α_{break}	angle of attack of wing at which the lift-curve slope becomes nonlinear	4.1.3.3
$\alpha_{c_{\ell_{max}}}$	section angle of attack at maximum lift coefficient	4.1.1 4.1.3.4 4.1.4.3 6.1.1
α_e	equivalent angle of attack for cambered wing	4.1.3.3
$(\alpha_e)_{C_{L_{max}}}$	equivalent angle of attack for cambered wing at maximum lift coefficient	4.1.3.3
α_i	angle of attack for section design lift coefficient	Several
α_{in}	inflow angle at propeller disk	9.1 9.1.3

SYMBOL	DEFINITION	SECTIONS
α_j	angle between jet thrust axis and local velocity at jet intake, $\alpha_T + \epsilon_u$	4.6 4.6.1 4.6.3
α_p	angle between propeller thrust axis and local velocity of propeller plane	4.6 4.6.1 4.6.4
α_s	angle of attack of surface to which main control surface is attached	6.3.4
$\Delta\alpha_s'$	change in section zero-lift angle of attack due to plug-type spoiler	6.1.1.1 6.2.1.1
α_v	angle of attack where onset of vortex lift begins	4.2.1.2
α_δ	control- or flap-effectiveness derivative, $\frac{\partial \alpha}{\partial \delta}$	Several
$(\alpha_\delta)_{C_L}$	value of α_δ for a wing	6.1.4.1 6.1.5.1 6.1.7
$(\alpha_\delta)_{c_\ell}$	value of α_δ for an airfoil section	6.1.4.1 6.1.5.1 6.1.7
α_0	angle of attack at zero lift	Several
$\Delta\alpha_0$	change in wing zero-lift angle of attack due to linear wing twist	4.1.3.1
$(\alpha_0)_B$	body zero-lift angle of attack	4.3.2.1
$(\alpha_0)_W$	wing zero-lift angle of attack	4.3.2.1
$(\alpha_0)_{WB}$	wing-body zero-lift angle of attack	4.3.2.1
$(\alpha_0)_{\theta=0}$	angle of attack for zero lift of untwisted, constant-section wing	4.1.3.1 4.1.4.3
α_∞	free-stream angle of attack	6.3.2
$\alpha_\perp$	effective angle of attack perpendicular to the wing leading edge, $\tan^{-1}\frac{\tan\alpha}{\cos\Lambda_{LE}}$	4.1.3.1 4.1.3.3
$\frac{d\alpha_{in}}{d\alpha}$	propeller inflow angle of attack gradient	9.1.3
$\dot{\alpha}$	rate of change of angle of attack	7.4.4.1 7.4.4.2
β	1. Mach number parameter, $\sqrt{M^2-1}$ or $\sqrt{1-M^2}$	Several
	2. propeller blade angle at .75 R blade station	Several
	3. angle of sideslip, positive nose left	Several
	4. boattail angle	4.6.4
	5. control-tab gear ratio	6.3.4

SYMBOL	DEFINITION	SECTIONS
$\frac{\beta C_{l_\beta}}{\kappa\Gamma}$	(listed under C_{l_β})	
Γ	dihedral angle, positive wing tips up	Several
Γ', Γ''	dihedral angles of forward and aft surfaces, respectively, positive for wing tips up	4.5.1.1 7.4.1.1
Γ_y	value of circulation at any spanwise station	4.4.1
Γ_o	circulation at zero spanwise station	4.4.1
$\frac{\Gamma}{2\pi\ Vr\alpha}$	nondimensional vortex strength	4.3.1.3 4.3.1.4 4.5.1.2 6.2.1.2
$\frac{\Gamma}{2\pi\ \alpha' Vr}$	nondimensional vortex strength from Figure 4.3.1.3-15 with α replaced by α'	5.3.1.2 5.6.1.2
$\left[\frac{\Gamma_B}{2\pi\ Vr\alpha}\right]'$, $\left[\frac{\Gamma_B}{2\pi\ Vr\alpha}\right]''$	nondimensional vortex strengths for the forward and aft panels, respectively	4.5.1.2
$\frac{\Gamma_{yi}}{V\alpha\ b/2}$	circulation strength at $y_{i,o}$	4.4.1
$\frac{\Gamma_{yi+1} - \Gamma_{yi-1}}{V\alpha\ b/2}$	incremental circulation strength	4.4.1
γ	1. ratio of specific heats	Several
	2. angle with origin at wing trailing edge, measured between the zero-angle-of-attack line and the point under consideration	4.4.1 7.4.1.1
	3. dihedral angle of tail	4.5.1.1
	4. jet spreading angle (see Sketch (i), Section 6.1.5.1)	6.1.5.1
Δ_r	ratio of maximum deflections of control tab to main control surface	6.3.4
δ	1. semiwedge nose angle of sharp airfoils or cones	4.1.3.2 4.4.1 6.3.2
	2. flap or control deflection angle (also δ_f), elevators and flaps, positive trailing edge down; ailerons, positive such as to give positive rolling moment; rudder, positive trailing edge left	Several
	3. local slope of the surface of the vertical panel	5.3.1.1
	4. boundary-layer thickness	6.3.1
δ'	1. slope of airfoil surface with respect to free-stream velocity	4.4.1 5.3.1.2 5.6.1.2
	2. flap deflection in plane normal to constant-percent-chord line through $x_{c.p._h}$	6.1.5.1

SYMBOL	DEFINITION	SECTIONS
δ_L	deflection of left-hand control surface	6.2.1.1 6.2.2.1
δ_{LE}	slope of airfoil surface at leading edge	4.4.1
δ_R	deflection of right-hand control surface	6.2.1.1 6.2.2.1
δ_{a_L} or δ_{a_R}	deflection of left or right aileron	6.2.2.1
δ_c	deflection of main control surface	6.3.4
$\delta_{c_{max}}$	maximum deflection of main control surface	6.3.4
δ_d	distance of deflector lip below lower surface of airfoil	6.2.1.1 6.2.2.1
δ_e	1. elevator deflection	6.3.4
	2. equivalent flap deflection due to wing camber and incidence	9.2 9.2.1 9.2.3
$\delta_{e_{max}}$	maximum elevator deflection	6.3.4
δ_{eff}	effective nose wedge angle for sharp-nosed airfoil (see Figure 4.1.3.3-61b)	4.1.3.3
δ_{eff_l}	effective nose semiwedge angle for sharp-leading-edge wing, perpendicular to leading edge (see Figure 4.1.3.3-61b)	4.1.3.3
δ_f	1. deflection of flap or control surface (see δ)	Several
	2. force phase angle	9.1 9.1.3
δ_{f_i}	deflection of the i^{th} segment of trailing-edge flap	6.1.2.1 6.1.5.1
$\delta_{f_{LE}}$	deflection of leading-edge device	6.1.2.1
$\delta_{f_1}, \delta_{f_2}$	deflections of forward and aft flaps, respectively, (see Figures 6.1.1.1-45, -46)	Several
$\delta_{f_1}, \delta_{f_2}, \delta_{f_3}$	deflection of first, second, and third segments, respectively, of trailing-edge flaps (see Sketch (f), Section 6.1.2.1)	6.1.2.1
$\delta_{f_{\perp LE}}$	deflection of leading-edge flap, measured perpendicular to airfoil leading edge	6.1.5.1
δ_{i_f}	net turning angle of internal flow including power effects	9.3 9.3.1 9.3.2 9.3.3
δ_{i_o}	turning angle of internal flow with power off	9.3 9.3.1
δ_j	trailing-edge jet momentum angle, with respect to trailing-edge camber line	Several
$\delta_{j_{eff}}$	effective jet deflection angle with respect to airfoil chord	Several
δ_ℓ	deflection of aft flap segment, measured between trailing edge of lower surface of flap segment and line parallel to wing chord	6.1.2.1 6.1.4.1 6.1.4.2 6.1.4.3
δ_{max}	maximum plain-flap deflection for linear aerodynamic characteristics	6.1.3

SYMBOL	DEFINITION	SECTIONS
δ_n	slope of airfoil surface with respect to chord plane	4.4.1
δ_o	boundary-layer thickness at point where interaction begins	6.3.1
δ_s	height of spoiler lip above upper surface of airfoil	6.2.1.1 6.2.2.1
δ_{tc}	deflection of control tab	6.3.4
$\delta_{tc_{max}}$	maximum deflection of control tab	6.3.4
δ_{tt}	deflection of trim tab	6.3.4
δ_u	deflection of primary flap segment, measured between trailing edge of upper surface of flap segment and line parallel to wing chord	6.1.2.1 6.1.4.1 6.1.4.2 6.1.4.3
δ_{vn}	parameter in span-loading calculation	6.1.7
$\delta_\perp$	semiwedge angle measured perpendicular to wing leading edge	Several
$\delta_{\perp HL}$	control deflection measured perpendicular to hinge line	6.1.5.1 6.2.1.1
ϵ	downwash angle in plane of symmetry	Several
$\Delta\epsilon$	1. downwash increment due to flaps 2. downwash increment due to subsonic jet in a subsonic stream	4.4.1 4.6 4.6.1
$\bar{\epsilon}$	1. average downwash over aft surface	4.4.1 6.2.1.2
	2. effective downwash over the wing span	4.6 4.6.4
$\Delta\bar{\epsilon}$	mean-effective-downwash increment	4.6 4.6.1
$(\Delta\epsilon)_G$	increment in downwash due to ground effect in the linear-lift range	4.7 4.7.1
ϵ_H	average downwash angle at the tail	4.4.1 4.5.3.2 4.6.3
$(\Delta\epsilon)_H$	increment in downwash at the tail	4.6.3
ϵ_p	downwash due to propeller power effects	4.6 4.6.1 4.6.3 4.6.4
$\epsilon_{power\ off}$	power-off downwash angle	4.6.3
ϵ_u	upwash angle ahead of the wing	4.6 4.6.1 4.6.3
ϵ_v	downwash at plane of symmetry at height of vortex core	4.4.1
$\epsilon_{z_{slip}}$	upwash induced by propeller slipstream, positive down	9.1 9.1.3

SYMBOL	DEFINITION	SECTIONS
η	1. dimensionless span station, $\frac{y}{b/2}$	Several
	2. ratio of the drag on a finite cylinder to the drag of a cylinder of infinite length	4..2.1.2 4.2.2.2 4.2.3.2 4.3.3.2
	3. angle of sweep of the line intersecting conical-flow regions of wing at angle of attack	6.1.6.1
	4. dimensionless span station, $\cos \frac{v\pi}{m+1}$, $\cos \frac{n\pi}{m+1}$	6.1.7
	5. control-surface efficiency	6.3.4
$\Delta\eta$	increment in dimensionless lateral direction, $\frac{\Delta y}{b/2}$	6.1.4.1 6.1.5.1
$\overline{\eta}$	lateral distance of wing MAC from body center line in semispans	6.1.5.1
η_B	1. dimensionless distance from plane of symmetry to break span station	Several
	2. Mach-number correction to the interference force	5.2.1.2 5.3.1.2
η_W	tail-effectiveness parameter	5.6.1.2
$\eta_{W(U)}$	lower-vertical-stabilizer effectiveness factor	5.6.1.2
$\eta_{W(V)}$	upper-vertical-stabilizer effectiveness factor	5.6.1.2
$\eta'_{\bar{c}}$	dimensionless span station of mean aerodynamic chord of wing segment affected by leading-edge device	6.1.5.1
$\eta_{c.p.}$	spanwise location of the center of pressure of the exposed horizontal tail	6.2.1.2
η_f	dimensionless distance from plane of symmetry to edge of flap or control surface, $\frac{y}{b/2}$	6.1.5.1
η_i	dimensionless distance from plane of symmetry to inboard edge of flap or control surface, $\frac{y_i}{b/2}$	Several
$\Delta\eta_i, \Delta\eta_o$	effective increments in spoiler spanwise inboard and outboard locations, respectively, due to spanwise flow of spoiler wake for partial-span spoilers	6.2.1.1
$\eta_{i_{eff}}, \eta_{o_{eff}}$	effective locations of inboard and outboard ends, respectively, of spoilers	6.2.1.1
η_k, η_{k-1}	dimensionless span stations denoting outboard and inboard ends, respectively, of the kth wing section	6.1.5.1
η_{max}	empirical factor accounting for maximum lifting efficiency	6.1.1.3
η_o	dimensionless distance from plane of symmetry to outboard edge of flap or control surface, $\frac{y_o}{b/2}$	Several
η_t	1. turning-efficiency factor of the aft flap segment	6.1.1.1
	2. static turning efficiency defined as resultant force divided by gross thrust	6.1.4.3 6.1.5.1

SYMBOL	DEFINITION	SECTIONS
η_α	lumped parameter containing the effects of downwash, dynamic-pressure ratio, and Mach number	4.5.1.2
η_δ	empirical factor accounting for changes in flap deflection from the optimum deflection	6.1.1.3
$\eta_0, \eta_1, \eta_2, \eta_3$	dimensionless span stations, from center line outboard on wing	6.1.5.1
η_1	empirical lift-efficiency factor of a single-slotted flap, a vane, or forward-flap segment of double-slotted flap	6.1.1.1
η_2	empirical lift-efficiency factor of the aft-flap segment of a double-slotted flap	6.1.1.1
$\eta\left(\frac{q_H}{q}\right)$	tail-effectiveness factor for configurations with body-mounted horizontal tails	6.2.1.2
θ	1. slope of airfoil mean line at leading edge	2.2.1
	2. linear angle of twist of wing tip with respect to root, negative for washout	Several
	3. ratio of ambient static temperature to jet-exit static temperature	4.6.1
	4. surface slope of cone frustum	Several
	5. shock-wave angle	4.4.1 6.3.1
	6. leading-edge shock angle	5.3.1.2 5.6.1.2
	7. angular pitching velocity	7.1.1.2
	8. slipstream turning angle measured from thrust axis	9.2 9.2.1 9.2.3
	9. spoiler deflection angle	6.2.1.1
	10. body surface slope	4.2.1.2 4.2.2.2
	11. angle of conical divergence	4.6.4
	12. angle of secondary shock	6.3.2
$\Delta\theta$	increment of slipstream turning angle due to wing camber and incidence	9.2 9.2.1
$\bar{\theta}$	angle between airfoil chord line and line connecting airfoil trailing edge with maximum airfoil upper-surface ordinate (see Sketch (a), Section 4.1.4.3)	4.1.4.3
θ_F	surface slope of flared afterbody	4.2.1.1 4.2.1.2 4.2.2.1
θ_N	1. surface slope of conical body section having a blunted nose	4.2.1.2
	2. surface slope of nose	4.2.3.1 4.3.3.1 5.3.3.1
θ_c	cone angle	4.2.2.1

SYMBOL	DEFINITION	SECTIONS
θ_f	slipstream turning angle adjusted to the condition of zero camber and zero incidence	9.2 9.2.1
θ_1	trailing-edge shock angle	5.3.1.2 5.6.1.2
$\theta_1, \theta_2, \theta_3, \ldots$	local surface slope of body segments	4.2.2.1
κ	ratio of two-dimensional lift-curve slope at appropriate Mach number to $2\pi/\beta$; or, ratio of incompressible two-dimensional lift-curve slope to 2π	Several
Λ_{HL}	sweepback angle of hinge line of flap or control surface	Several
$\Lambda_{H_{c/4}}$	sweep angle of horizontal-tail quarter-chord	4.6 4.6.3
$\Lambda_{LE}, \Lambda_{LE_W}, \Lambda$	sweepback angle of wing leading edge	Several
$\Lambda'_{LE}, \Lambda''_{LE}$	sweepback angles of leading edges of forward and aft surfaces, respectively	4.5.1.1 4.5.1.2 7.4.1.1
$\Lambda_{LE_{bw}}$	sweepback angle of leading edge of basic wing	4.1.3.2 4.1.5.1 4.3.3.1 5.1.2.1
Λ_{LE_e}	sweepback angle of leading edge of exposed wing	4.3.2.2
$(\Lambda_{LE_e})_i$	sweepback angle of leading edge of inboard panel of exposed wing	4.3.2.2
Λ_{LE_g}	sweepback angle of leading edge of glove of double-delta and cranked wings	4.1.3.2 5.1.2.1
Λ_{LE_H}	sweepback angle of horizontal-stabilizer leading edge	4.5.3.1 8.1
$\Lambda_{LE_i}, \Lambda_{LE_o}$	sweepback angles of leading edge of wing inboard and outboard panels, respectively	Several
Λ'_{LE_o}	sweepback angle of leading edge of constructed outboard panels of wing	4.1.4.2 4.3.2.2
Λ_{LE_U}	sweepback angle of lower-vertical-stabilizer leading edge	Several
Λ_{LE_V}	sweepback angle of upper-vertical-stabilizer leading edge	Several
$\Lambda_{LE_1}, \Lambda_{LE_2}$	sweepback angles of leading edge of constructed panels of non-straight-tapered wings	4.1.3.2
Λ_{TE}	sweepback angle of wing trailing edge	Several
$\Lambda_{TE_{bw}}$	sweepback angle of trailing edge of basic wing	4.1.3.2 4.1.5.1 4.3.3.1
Λ_{TE_E}	sweepback angle of trailing edge of extension of double-delta and cranked wings	4.1.3.2

SYMBOL	DEFINITION	SECTIONS
$\Lambda_{TE_i}, \Lambda_{TE_o}$	sweepback angles of trailing edge of wing inboard and outboard panels, respectively	4.1.3.2 4.1.4.2 4.1.5.1
Λ_b	sweepback of constant-percent-chord line through center of pressure of basic loading (see Equation 6.1.5.1-g)	6.1.5.1
Λ_c	complement of leading-edge sweep angle; $\Lambda_c = 90^o - \Lambda_{LE}$	4.1.3.2 4.1.4.1
$\Lambda_{c/(\ )}$	sweepback angle of a constant-percent-chord line	Several
$\Lambda_{c/2}, \Lambda_{c/2_W}$	sweepback angle of wing 50-percent-chord line	Several
$\Lambda'_{c/2}, \Lambda''_{c/2}$	sweepback angles of 50-percent-chord line of forward and aft surfaces, respectively	4.5.1.1 7.4.1.1
$\Lambda_{3c/4}$	sweepback angle of the three-quarter-chord point of the wing	4.4.1
$\Lambda_{c/2_e}$	sweepback angle of midchord line of exposed wing	4.3.2.2
$\Lambda_{c/2_{eff}}$	effective sweepback angle of midchord line of exposed wing	4.1.3.2 4.1.3.3
$\Lambda_{c/2_i}, \Lambda_{c/2_o}$	sweepback angles of midchord line of wing inboard and outboard panels, respectively	4.1.3.2 4.1.3.3 4.1.4.2 5.1.2.1
$\Lambda_{c/2_j}$	sweepback angle of midchord line of one section of n sections	4.1.3.2 4.1.3.3
$\Lambda'_{c/2_o}$	sweepback angle of midchord line of constructed outboard panel of wing	5.1.2.1
$\Lambda_{c/2_U}$	sweepback angle of the midchord line of the lower vertical stabilizer	5.3.1.1 5.6.1.1
$\Lambda_{c/2_V}$	sweepback angle of the midchord line of the upper vertical stabilizer	5.3.1.1
$\Lambda_{c/4_W}, \Lambda_{c/4}$	sweepback angle of the quarter-chord line of the wing	Several
$\Lambda'_{c/4}, \Lambda''_{c/4}$	sweepback angles of quarter-chord line of forward and aft surfaces, respectively	4.5.1.1 7.4.4.1
Λ_m, Λ_n	sweepback angles of arbitrary chordwise locations	2.2.2
Λ_s	sweepback angle of spoiler hinge line	6.2.1.1
$\Lambda_{(t/c)_{max}}$	sweepback angle of airfoil maximum-thickness line of wing	4.1.5.1 4.3.3.1 4.5.3.1
$\Lambda_{(t/c)_{max_i}}, \Lambda_{(t/c)_{max_o}}$	sweepback angles of airfoil maximum-thickness line of wing inboard and outboard panels, respectively	4.1.5.1 4.3.3.1

SYMBOL	DEFINITION	SECTIONS
Λ_β	compressible sweep parameter, $\tan^{-1}\left(\frac{\tan \Lambda_{c/4}}{\beta}\right)$	Several
λ	1. taper ratio, $\frac{\text{tip chord}}{\text{root chord}}$	Several
	2. mean free path (average distance traveled between molecular collisions)	6.3.2
λ', λ''	taper ratios of forward and aft surfaces, respectively	4.5.1.1 7.4.1.1 7.4.4.1
λ_H	taper ratio of horizontal tail or canard surface	Several
λ_{H_e}	taper ratio of exposed horizontal tail	6.2.1.2
λ_U	taper ratio of lower vertical stabilizer, measured from fuselage center line	Several
λ_{U_e}	taper ratio of exposed lower vertical stabilizer	Several
λ_V	taper ratio of upper vertical stabilizer, measured from fuselage center line	Several
λ_{V_e}	taper ratio of exposed upper vertical stabilizer	Several
λ_W	wing taper ratio	Several
λ_{bw}	taper ratio of basic wing	4.1.3.2 4.1.5.1 4.3.3.1 5.1.2.1
λ_e	taper ratio of exposed wing panel	Several
λ_e', λ_e''	taper ratios of forward and aft exposed surfaces, respectively	4.4.1 4.5.1.1 7.4.1.1
$(\lambda_e)_i$ or $(\lambda_i)_e$	taper ratio of inboard panel of exposed wing	4.3.2.2 4.3.3.1
λ_f	taper ratio of flap or control surface	6.1.4.1 6.1.5.1
λ_g	taper ratio of glove of double-delta and cranked wings	4.1.3.2 5.1.2.1
λ_i, λ_o	taper ratios of wing inboard and outboard panels, respectively	Several
λ_o'	taper ratio of constructed outboard panel of wing	4.1.4.2 4.3.2.2 5.1.2.1
λ_1, λ_2	taper ratios of constructed panels of non-straight-tapered wings	4.1.3.2

SYMBOL	DEFINITION	SECTIONS
μ	Mach angle, $\sin^{-1}\frac{1}{M}$	Several
ν	Prandtl-Meyer angle	4.4.1 5.3.1.2 5.6.1.2
$\Delta\nu$	increment in flow angle between two points on the body surface	4.4.1
ξ	1. any station along body	4.3.3.1
	2. pressure ratio along secondary shock	6.3.2
ξ_{ru}	distance required for complete rollup of wing-tip vortices, measured parallel to the wing root chord from the tip quarter-chord point, in semispans	4.4.1 7.4.4.1
ρ	1. ratio of weight to chord for wing	8.1
	2. air density	4.6 6.3.2
ρ_P	pitch radius of gyration	8.2
ρ_R	roll radius of gyration	8.2
$\rho_{x_o}, \rho_{y_o}, \rho_{z_o}$	radii of gyration at the c.g. of the component	8.2
σ	1. geometric planform parameter, $\frac{A}{4}(1+\lambda)\tan\Lambda_{LE}$	2.2.2 4.1.3.2 4.1.4.3
	2. Prandtl interference coefficient	4.7 4.7.1 4.7.4
	3. sidewash, positive out the left wing	5.4.1
	4. boundary-layer separation angle	6.3.2
	5. air density ratio, ρ/ρ_o	6.3.4
	6. propeller solidity, ratio of blade element area to annular area at 0.75R	9.1 9.1.1 9.1.3
σ_e	effective propeller solidity	9.1 9.1.1 9.1.3
τ	1. one-half the thickness ratio of the forward-facing surface of a wedge airfoil	4.1.5.1
	2. angle denoting an arbitrary position of the ray in the conical-flow field	6.1.6.1
$\tau_{c.p.}$	angle of a ray in the conical-flow field which passes through the center of pressure	6.1.6.1
Φ	effective turning angle	6.1.1.1

SYMBOL	DEFINITION	SECTIONS
ϕ	1. angle of bank of elliptical-cross-section body about its longitudinal axis, measured from the major axis	4.2.1.2 4.2.2.2 4.2.3.2
	2. roll angle	4.3.3.1 6.1.7
	3. angle of inclination normal to body center line, $\tan^{-1}\frac{\beta}{\alpha}$	5.3.1.2 5.6.1.2
	4. angle associated with geometry of separation	6.3.1
	5. inclination of nozzle center line relative to an axis normal to surface	6.3.2
ϕ_{TE}	1. streamwise trailing-edge angle	Several
	2. trailing-edge angle measured normal to control hinge line	6.1.4.1 6.1.5.1 6.1.6.1 6.2.1.1
ϕ'_{TE}	trailing-edge angle based on airfoil ordinates at 90- and 99-percent chord	Several
ϕ''_{TE}	trailing-edge angle based on airfoil ordinates at 95- and 99-percent chord	6.1.3.1 6.1.3.2 6.1.6.1 6.1.6.2
$\phi_{TE_{upper}}$	$\tan^{-1}\frac{Y_{90} - Y_{100}}{0.10}$	6.1.1.1
ϕ_n	span-loading angle calculated at spanwise station n, $\frac{n\pi}{m+1}$	6.1.7
ϕ_v	span loading angle calculated at spanwise station v, $\frac{v\pi}{m+1}$	6.1.7
ϕ_β	lift-efficiency factor for a geared tab system, $1 + \beta C_2/C_1$	6.3.4
Ω	angle used in determination of trim drag (see Figure 4.5.3.2-4)	4.5.3.2

C. CAPITAL-LETTER COEFFICIENTS AND DERIVATIVES

SYMBOL	DEFINITION	SECTIONS
ΔC_A	increment in axial-force coefficient	6.3.1
C_D	drag coefficient, $\frac{\text{drag}}{qS}$	Several
$(C_D)'$	total drag coefficient of the forward panel and body, including wing-body interference	4.5.2.1
$(C_D)''$	total drag coefficient of the aft panel, including wing-body interferences	4.5.2.1
ΔC_D	zero-lift drag coefficient due to flap deflection based on free-stream velocity	9.2 9.2.3
$C_D(\alpha)$	drag due to angle of attack	4.2.3.2 4.3.3.2
$[C_D(\alpha)]_B$	body drag due to angle of attack	4.3.3.2
$[C_D(\alpha)]_{a/b}$	drag due to angle of attack of a body having an elliptical cross section	4.2.3.2
C_{D_A}	wave-drag coefficient based on maximum frontal area of afterbody	Several
ΔC_{D_A}	reduction in afterbody wave-drag coefficient of a body of revolution with elliptic cross section	4.2.3.1
$C_{D_{A(NC)}}$	coefficient of interference drag acting on the afterbody due to the nose and cylindrical section	4.2.3.1 4.2.3.2 4.3.3.1 4.5.3.1
C_{D_b}	base drag coefficient	Several
$\left(C_{D_b}\right)_B$	base-pressure drag coefficient for the body	4.3.3.1
C_{D_e}	external duct drag coefficient, $\frac{-F_{x_e}}{q_\infty S_D}$	9.3 9.3.1
C_{D_f}	1. skin-friction drag coefficient	Several
	2. power-off zero-lift drag coefficient	9.2 9.2.3
$\Delta\left(C_{D_f}\right)$	increment of skin-friction drag due to control-surface or flap deflection	6.1.7
$\left(C_{D_f}\right)_B$	body skin-friction drag coefficient	4.2.3.1 4.3.3.1

SYMBOL	DEFINITION	SECTIONS
$\left(C_{D_f}\right)_b$	zero-lift drag of body exclusive of the base drag, based on body base area	4.2.3.1 4.2.3.2 4.3.3.1 4.5.3.1
$\left(C_{D_f}\right)_H$	compressible skin-friction drag coefficient of horizontal stabilizer, based on total horizontal stabilizer area	4.5.3.1
$\left(C_{D_f}\right)_V$	compressible skin-friction drag coefficient of vertical stabilizer, based on vertical stabilizer area to body center line	4.5.3.1
$\left(C_{D_f}\right)_W$	compressible skin-friction drag coefficient of wing, based on total wing area	4.3.3.1 4.5.3.1
C_{D_H}	drag coefficient of horizontal stabilizer, $\frac{\text{horizontal-tail drag}}{qS_H}$	4.5.3.2 4.6.2
$\left(C_{D_H}\right)_{\alpha_{C_{L_{max}}}}$	horizontal-tail-body drag at stall angle of attack	4.5.1.3
C_{D_i}	induced-drag coefficient	6.1.7
C_{D_L}	drag coefficient due to lift	Several
ΔC_{D_L}	increment in drag due to lift resulting from a breakdown in leading-edge suction at lift coefficients above parabolic-drag-polar region	4.1.5.2
$C_{D_{LE}}$	pressure-drag coefficient of a swept, cylindrical leading edge	4.1.5.1 4.3.3.1
$\left(\Delta C_{D_L}\right)_G$	change in drag due to lift caused by ground effect	4.7 4.7.4
$\left(C_{D_L}\right)_W$	drag due to lift of the wing, based on total wing area	4.3.3.2
$\left(C_{D_L}\right)_{WB}$	drag due to lift of a wing-body configuration	4.3.3.2
$(C_D)_{min}$	minimum drag coefficient	6.1.7
$\Delta C_{D_{min}}$	increment in minimum drag coefficient due to control-surface or flap deflection	6.1.7
$\left(C_{D_{min}}\right)_{flaps\ up}$ or $\left(C_{D_{min}}\right)_{\delta = 0}$	minimum drag coefficient for undeflected control or flap	6.1.7
$C_{D_{N_I}}$	wave-drag coefficient of spherically blunted noses	4.2.3.1 4.3.3.1 4.5.3.1

SYMBOL	DEFINITION	SECTIONS
$\Delta C_{D_{N_1}}$	reduction in forebody wave-drag coefficient of a body of revolution with an elliptic cross section	4.2.3.1
$C_{D_{N_2}}$	wave-drag coefficient of conical or ogive-profile nose, based on maximum frontal area of nose	4.2.3.1 4.3.3.1 4.5.3.1
C_{D_o}	power-off drag coefficient based on free-stream velocity and wing area, $\frac{\text{drag}}{q_\infty S}$	9.2 9.2.3
C_{D_P}	subsonic pressure-drag coefficient	4.2.3.1 4.3.3.1 4.5.3.1
$C_{D_{P_n}}$	pressure-drag coefficient of any of n segments of a body	4.2.3.1
$C_{D_{P_1}}, C_{D_{P_2}}, C_{D_{P_3}}, \ldots$	pressure-drag coefficient of given body segments	4.2.3.1
$\Delta C_{D_{Trim}}$	incremental drag coefficient of horizontal stabilizer including both zero-lift and induced drag	4.5.3.2
C_{D_v}	viscous drag coefficient due to lift	4.1.5.2
C_{D_w}	supersonic wave-drag coefficient of the body	Several
$C_{D_{wave}}$	wave-drag coefficient	6.1.7
$\Delta\left(C_{D_{wave}}\right)$	increment in wave-drag coefficient due to control deflection	6.1.7
$\left(C_{D_{wave}}\right)_{\delta = 0}$ or $\left(\Delta C_{D_0}\right)_{\delta = 0}$	zero-lift wave-drag increment at transonic speeds for undeflected control or flap	6.1.7
$\left(C_{D_w}\right)_B$	wave-drag coefficient of the body	4.3.3.1
$C_{D_{WB}}$	wing-body drag coefficient in absence of ground plane	4.7 4.7.4

SYMBOL	DEFINITION	SECTIONS
$(C_D)_{WB}$	drag coefficient of a wing-body combination at angle of attack	4.3.3.2
$(C_{D_{WB}})_G$	wing-body drag coefficient in the presence of the ground	4.7 4.7.4
$(C_{D_w})_H$	supersonic wave-drag coefficient of the horizontal-tail panel	4.5.3.1
$C_{D_{w_{peak}}}{}_{\Lambda_{c/4} = n}$	maximum wave-drag-coefficient increment for swept wing with $\Lambda_{c/4} = n$	4.1.5.1 4.3.3.1
$C_{D_{w_{peak}}}{}_{\Lambda_{c/4} = 0}$	maximum wave-drag-coefficient increment for an unswept wing	4.1.5.1
$(C_{D_w})_V$	supersonic wave-drag coefficient of the vertical-tail panel	4.5.3.1
$(C_{D_w})_W$	supersonic wave-drag coefficient of the wing	4.3.3.1 4.5.3.1
$(C_{D_\alpha})'$	total drag-curve slope of the forward panel and body, including interferences	4.5.2.1
$(C_{D_\alpha})''$	total drag-curve slope of the aft panel and body, including interferences	4.5.2.1
$(C_D)_\delta$	drag coefficient for control surface or flap deflection	6.1.7
$(C_D)_{\delta = 0}$	drag coefficient for zero control surface or flap deflection	6.1.7
C_{D_0}	1. zero-lift drag coefficient	Several
	2. profile-drag coefficient of the wing at any given lift coefficient	7.1.3.2 7.1.3.3 7.3.2.2
ΔC_{D_0}	increment of zero-lift wave-drag coefficient at transonic speeds	4.1.5.1 4.3.3.1 4.5.3.1
$(C_{D_0})_B'$	total zero-lift drag coefficient of body	4.3.3.1 4.5.3.1
$(\Delta C_{D_0})_{flap}$	increment of zero-lift drag coefficient due to flap deflection	4.6.4
$(\Delta C_{D_0})_{\substack{flaps \\ power\ on}}$	increment of zero-lift drag coefficient for the flap extended and immersed in the propeller slipstream	4.6.4

SYMBOL	DEFINITION	SECTIONS
$(C_{D_0})_H$	zero-lift drag coefficient of horizontal stabilizer, based on total horizontal-stabilizer area	4.5.3.1 4.5.3.2
$(C_{D_0})_i, (C_{D_0})_o$	zero-lift drag coefficients of wing inboard and outboard panels, respectively	4.1.5.1 4.3.3.1
$(C_{D_0})_{\text{lifting surface}}$	zero-lift drag coefficient of lifting surface	4.5.3.1
$(C_{D_0})_{M_D}$	zero-lift drag coefficient at drag-divergence Mach number	4.5.3.1
$(C_{D_0})_{M_I}$	zero-lift drag coefficient at initial drag-rise Mach number	4.5.3.1
$(\Delta C_{D_0})_{\text{power on}}$	increment of zero-lift drag for propeller power	4.6.4
$(\Delta C_{D_0})_s$	increment of skin-friction zero-lift drag coefficient due to propeller slipstream	4.6.4
$(C_{D_0})_V$	zero-lift drag coefficient of vertical stabilizer, based on vertical-stabilizer area to body center line	4.5.3.1 4.5.3.2
$(C_{D_0})_W$	zero-lift drag coefficient of wing, based on total wing area	4.3.3.1 4.5.3.1
$(C_{D_0})_{WB}$	zero-lift drag coefficient of wing-body combination	4.3.3.1 4.3.3.2 4.5.3.1 4.5.3.2
$C_{D_1}, C_{D_2}, C_{D_3}, \cdots$	drag coefficients of various components of body	4.2.3.1
C_{F_c}	control-force coefficient	6.3.2
$(C_{F_c})_{cr}$	corrected control-force coefficient	6.3.2
C_{F_x}	1. negative-drag coefficient based on free-stream velocity and wing area, $\frac{F_x}{q_\infty S}$	9.2
	2. duct negative-drag coefficient based on free-stream velocity and duct planform area, $\frac{F_x}{q_\infty S_D}$	9.3 9.3.2 9.3.3

SYMBOL	DEFINITION	SECTIONS
C_{F_x}''	negative-drag coefficient based on slipstream velocity and wing area, $\frac{F_x}{q''S}$	9.2 9.2.3
$C_{F_{x_e}}$	external duct negative-drag coefficient based on free-stream velocity and duct planform area, $\frac{F_{x_e}}{q_\infty S_D}$	9.3 9.3.1 9.3.3
C_J	three-dimensional trailing-edge jet momentum coefficient for jet-flap configurations	6.1.4.1 6.1.4.2 6.1.4.3 6.1.5.1
C_J'	three-dimensional trailing-edge jet momentum coefficient, based on blown-flap affected area	6.1.4.1 6.1.4.2
C_L	1. lift coefficient, $\frac{\text{lift}}{qS}$	Several
	2. duct lift contribution, $\frac{\text{lift}}{q_\infty S_D}$	9.3 9.3.1 9.3.2
ΔC_L	1. increment in lift due to leading-edge vortex at particular angle of attack (see Sketch (b), Section 4.1.3.2)	4.1.3.2 4.1.4.3
	2. increment in lift beyond the lift coefficient at α_{break}	4.1.3.3
	3. increment of wing lift coefficient due to flap or control-surface deflection	6.1.4.1 6.1.5.1
$(C_L)'$	total lift coefficient of the forward panel and body, including wing-body interference	4.5.2.1 7.4.1.1
C_L''	lift coefficient based on slipstream velocity, $\frac{\text{lift}}{q''S}$	9.2 9.2.1
$(C_L)''$	total lift coefficient of the aft panel, including wing-body interferences	4.5.2.1
$(C_L)_{a/b}$	lift coefficient of a body with elliptical cross section	4.2.1.2
$C_{L_{basic}}$	basic wing lift coefficient excluding leading-edge vortex-induced effects	4.1.4.3
$C_{L_{break}}$	lift coefficient where lift curve becomes nonlinear	4.1.3.3
C_{L_c}	"critical" lift coefficient, where drag-due-to-lift factor is no longer a constant	4.1.5.2
ΔC_{L_c}	lift increment due to control surface	6.3.4
C_{L_d}	conical-camber design lift coefficient for a M = 1.0 design with the designated camber ray line intersecting the wing trailing edge at 0.8 b/2	4.3.2.1
C_{L_e}	lift coefficient resulting from external mass flow	9.3 9.3.1 9.3.2
$(C_L)_e'$	lift coefficient of the exposed forward panel	4.5.1.2

SYMBOL	DEFINITION	SECTIONS
ΔC_{L_f}	increment in wing lift coefficient due to symmetric flap deflection in absence of ground plane	4.7 4.7.1 6.1.7
$\left(C_{L_f}\right)_{WB}$	wing-body lift coefficient including flap effects in absence of ground plane	4.7.1
$\Delta\left(\Delta C_L\right)_{flap}$	empirical factor accounting for flap effects in the presence of the ground	4.7 4.7.1
$C_L(g)$	lift-coefficient correction term	7.1.4.1 7.3.4.1
$\left(\Delta C_L\right)_G$	increment in wing or horizontal tail lift due to the presence of the ground plane	4.7
C_{L_H}	lift coefficient of horizontal tail, $\frac{\text{horizontal-tail lift}}{qS_H}$	4.5.3.2 4.6.3 4.7.1 6.3.4
$\left(\Delta C_L\right)_H$	increment in lift coefficient due to horizontal tail	4.6 4.6.1
$\left(\Delta C_{L_H}\right)_G$	increment in horizontal-tail lift in the presence of the ground	4.7 4.7.3
$C_{L_{H(WBV)}}$	horizontal-tail-body lift in presence of the wing, body, and vertical tail	4.5.1.3
C_{L_i}	lift coefficient resulting from internal mass flow	9.3 9.3.1 9.3.2
$\left(C_{L_i}\right)_{WB}$	rate of change of lift coefficient with wing incidence (fuselage angle of attack held constant)	4.3.1.2
$C_{L_{max}}$	maximum lift coefficient, $\frac{\text{maximum lift}}{qS}$	Several
$\Delta C_{L_{max}}$	1. increment in wing maximum lift coefficient accounting for Mach-number effects	4.1.3.3 4.1.3.4
	2. increment in wing maximum lift coefficient due to propeller power	4.6 4.6.2
	3. increment in wing maximum lift coefficient due to flap deflection	6.1.4.3
$C_{L^*_{max}}$	maximum lift coefficient of a wing as determined by the low-aspect-ratio method	4.1.3.3
$\left(C_{L_{max}}\right)_{base}$	base value of parameter	4.1.3.3 4.1.3.4
$\left[\left(C_{L_{max}}\right)_{base}\right]''_e$	subsonic maximum lift coefficient of exposed aft panel	4.5.1.2
$\left(C_{L_{max}}\right)_e$	maximum lift coefficient for exposed wing	4.1.3.4

SYMBOL	DEFINITION	SECTIONS
$\left(C_{L_{max}}\right)_e'$, $\left(C_{L_{max}}\right)_e''$	maximum lift coefficients of exposed forward and aft panels, respectively	4.1.5.2
$\left(\Delta C_{L_{max}}\right)_e'$, $\left(\Delta C_{L_{max}}\right)_e''$	increments in wing maximum lift coefficients accounting for Mach number effects on the forward and aft panels, respectively	4.1.5.2
$\left(C_{L_{max}}\right)_W$	value of parameter for wing	4.3.1.4
$\left(C_{L_{max}}\right)_{WB}$	maximum lift coefficient for wing-body	4.3.1.4 4.5.1.3
$\left(\Delta C_L\right)_{N_j}$	increment in lift coefficient acting at jet-engine inlet due to inclination of thrust axis to oncoming flow	4.6 4.6.1 4.6.4
$\left(\Delta C_L\right)_{N_p}$	increment in lift coefficient due to inclination of propeller plane to oncoming flow	4.6 4.6.1 4.6.3
$C_{L_{nonlinear}}$	lift coefficient above point where the lift curve ceases to be linear	4.1.3.3
C_{L_o}	power-off lift coefficient based on free-stream velocity and wing area, $\frac{L}{q_\infty S}$	9.2 9.2.1 9.2.3
C_{L_p}	lift coefficient due to propeller effects	4.6 4.6.4
$\left(C_L\right)_{\substack{power \\ off}}$	lift coefficient of configuration, power off	4.6.1
$\left(\Delta C_L\right)_{\substack{power \\ on}}$	increment in lift coefficient due to propeller power	4.6.1 4.6.2
C_{L_q}	pitching derivative, $\frac{\partial C_L}{\partial\left(\frac{q\bar{c}}{2V_\infty}\right)}$	Several
$\left(\Delta C_L\right)_q$	increment in lift coefficient due to change in dynamic pressure behind propeller	4.6 4.6.1 4.6.3
C_{L_q}'	value of pitching derivative referred to body axes with origin at wing aerodynamic center	7.1.1.1 7.1.1.2 7.3.1.1
C_{L_q}''	value of pitching derivative referred to body axes with origin at wing leading-edge vertex	7.1.1.1 7.1.1.2
$\left(C_{L_q}\right)_B$	contribution of the body to pitching derivative C_{L_q}	7.3.1.1 7.4.1.1

SYMBOL	DEFINITION	SECTIONS
$\left(C_{L_q}\right)_c$	contribution of the exposed wing to the pitching derivative C_{L_q}	7.3.1.1 7.3.1.2
$\left(C_{L_q}\right)_e'$, $\left(C_{L_q}\right)_e''$	contributions of exposed forward and aft panels, respectively, to the pitching derivative C_{L_q}	7.4.1.1
$\left(C_{L_q}\right)_W$	contribution of the wing to the pitching derivative C_{L_q}	7.3.1.1
$\left(C_{L_q}\right)_{WB}$	contribution of the wing-body combination to the pitching derivative C_{L_q}	7.3.1.1 7.4.1.1
C_{L_s}	lift coefficient of surface to which the main control surface is attached	6.3.4
$\left(\Delta C_L\right)_{SE}$	increment in lift coefficient, accounting for the direct influence of the wing shock-expansion field	4.4.1
$\left(\Delta C_L\right)_T$	increment in lift coefficient due to angle of attack of thrust axis	4.6 4.6.1 4.6.4
$\Delta C_{L_{tc}}$	lift loss due to tab	6.3.4
$\Delta C_{L_{trim}}$	incremental lift coefficient required for trim	4.5.3.2
C_{L_V}	vertical-tail lift coefficient	6.3.4
C_{L_W}	1. wing lift coefficient with power effects	4.6 4.6.4
	2. wing lift coefficient, including tab and control deflections	6.3.4
$C_{L_{WB}}$	wing-body lift coefficient in absence of ground plane	4.5.3.2 4.7 4.7.3
$\left(\Delta C_{L_{WB}}\right)_G$	increment in wing-body lift coefficient in the presence of the ground	4.7 4.7.3
$C_{L_{W''(v)}}$	contribution to the lift coefficient due to the effect of the forward-surface vortices on the aft surface	4.5.1.2
C_{L_α}	lift-curve slope, rate of change of lift coefficient with angle of attack, $\frac{dC_L}{d\alpha}$	Several
ΔC_{L_α}	increment in lift-curve slope	4.3.1.2
$\left(\Delta C_L\right)_{\Delta \alpha_W}$	increment in wing lift coefficient due to change in angle of attack induced by propeller flow field	4.6 4.6.1 4.6.3
$C_{L_{\alpha=0}}$	lift coefficient where $\alpha = 0$	4.1.3.3
$\left(C_{L_\alpha}\right)'$	1. complete lift-curve slope of forward panel and body, including interferences	4.5.2.1
	2. lift-curve slope of forward panel	4.5.1.2 7.4.4.1
$\left(C_{L_\alpha}\right)''$	1. lift-curve slope of aft panel, including wing-body interference effects	4.5.2.1
	2. lift-curve slope of aft panel	4.5.1.2

SYMBOL	DEFINITION	SECTIONS
$\left(C_{L_\alpha}\right)_a$	value of the derivative at M_a	4.1.3.2
$\left(C_{L_\alpha}\right)_B$	lift-curve slope of body	7.3.1.1 7.3.4.1
$\left(C_{L_\alpha}\right)_b$	value of the derivative at M_b	4.1.3.2
$\left(C_{L_\alpha}\right)_{basic}$	low-lift-region lift-curve slope, including thickness effects	4.1.3.2 4.1.4.3
$\left(C_{L_\alpha}\right)_{B(W)}$ or $C_{L_{\alpha_{B(W)}}}$	lift-curve slope of body in presence of wing	4.3.2.2 4.5.2.1 4.5.3.2
$\left(C_{L_\alpha}\right)_{C_L}$	value of the derivative at a given lift coefficient	5.1.2.2 7.1.2.2 7.3.2.2
$\left(C_{L_\alpha}\right)_e$	lift-curve slope of the exposed wing	Several
$\left(C_{L_\alpha}\right)'_e, \left(C_{L_\alpha}\right)''_e$	lift-curve slopes of the exposed forward and aft panels, respectively	Several
$\left(C_{L_\alpha}\right)_{fb}$	value of derivative at M_{fb}	4.1.3.2
$C_{L_{\alpha_H}}$	lift-curve slope of the horizontal surface	Several
$\left(C_{L_{\alpha_H}}\right)_e$	lift-curve slope of the exposed horizontal surface	6.2.1.2
$\left(C_{L_{\alpha_H}}\right)_{M_H}$	lift-curve slope of the horizontal tail operating at the local Mach number of the flow in the vicinity of the horizontal tail	4.5.1.2
$\left(C_{L_{\alpha_H}}\right)_{M_\infty}$	lift-curve slope of the isolated horizontal tail at the free-stream Mach number	4.5.1.2
$\left(C_{L_\alpha}\right)_i$	lift-curve slope of the inboard panel of wing	4.1.4.2 5.1.2.1
$\left(C_{L_\alpha}\right)_{limit}$	limiting value of lift-curve slope	4.1.3.2
$\left(C_{L_\alpha}\right)_{low\ speed}$ or $\left(\frac{dC_L}{d\alpha}\right)_{low\ speed}$	lift-curve slope at low speeds	4.4.1
$\left(C_{L_\alpha}\right)_M$	value of derivative at a given Mach number	Several

SYMBOL	DEFINITION	SECTIONS
$\left(C_{L_\alpha}\right)_M$ or $\left(\frac{dC_L}{d\alpha}\right)_M$	lift-curve slope at high subsonic Mach numbers	4.4.1
$\left(C_{L_\alpha}\right)_{M_{cr}}$	value of derivative at the critical Mach number	7.1.1.2
$\left(C_{L_\alpha}\right)_N$	value of derivative for nose of body	Several
$C_{L_{\alpha_o}}$	power-off lift-curve slope	9.2.1
$\left(C_{L_\alpha}\right)_o'$	lift-curve slope of the constructed outboard panel of wing	4.1.4.2 5.1.2.1
$\left(C_{L_\alpha}\right)_p$	lift-curve slope of isolated vertical panel mounted on a reflection plane	5.3.1.1
$\left(C_{L_\alpha}\right)_{pred}$	lift-curve slope of cranked wing, predicted by double-delta-wing method	4.1.3.2
$\left(C_{L_\alpha}\right)_{theory}$	value of derivative derived from theory	4.1.3.2
$\left(C_{L_\alpha}\right)_U$	lift-curve slope of isolated lower vertical panel mounted on a reflection plane (the aspect ratio is taken as twice the aspect ratio defined by the average exposed span and exposed area)	Several
$\left(C_{L_\alpha}\right)_V$	1. lift-curve slope of isolated upper vertical panel with effective aspect ratio defined by Equation 5.3.1.1-a	5.3.1.1 5.6.1.1
	2. lift-curve slope of isolated upper vertical panel mounted on a reflection plane (the aspect ratio is taken as twice the aspect ratio defined by the average exposed span and exposed area)	Several
$\left(C_{L_\alpha}\right)_W$	lift-curve slope of the wing	4.3.1.2 4.3.1.3 4.3.3.2
$\left(C_{L_\alpha}\right)_{WB}$	lift-curve slope of the wing-body combination	4.2.2.1 4.3.1.2 4.7 4.7.1
$\left(C_{L_\alpha}\right)_{W\,(B)}$	lift-curve slope of wing in presence of body	4.3.2.2 4.5.2.1
$\left(C_{L_\alpha}\right)_{W_e\,(B)}$	lift-curve slope of the exposed wing in presence of body	4.3.1.2
$\left(C_{L_\alpha}\right)_{W''\,(v)}$	contribution to the lift-curve slope due to the effect of the forward-surface vortices on the aft surface	Several
$\left(C_{L_\alpha}\right)_\delta$	lift-curve slope of flap-deflected wing	6.1.4.2

SYMBOL	DEFINITION	SECTIONS
$\left(C_{L_\alpha}\right)_{\delta=0}$	lift-curve slope of flap-retracted wing	6.1.4.2
$\left(C_{L_\alpha}\right)_{II}, \left(C_{L_\alpha}\right)_{III}$	total lift-curve slopes between $C_{L_{II}}$ and $C_{L_{III}}$, and beyond $C_{L_{III}}$, respectively, (see Sketch (b), Section 4.1.3.2)	4.1.3.2 4.1.4.3
$\delta C_{L_{\alpha_{II}}}, \delta C_{L_{\alpha_{III}}}$	incremental increase in lift-curve slopes starting at $C_{L_{II}}$ and $C_{L_{III}}$, respectively, (see Sketch (b), Section 4.1.3.2)	4.1.3.2
$\frac{\left(C_{L_\alpha}\right)_{test}}{\left(C_{L_\alpha}\right)_{pred}}$	correction factor for subsonic lift-curve slope of cranked wings	4.1.3.2
$C_{L_{\dot\alpha}}$	change in lift coefficient with variation in rate of change of angle of attack, $\frac{\partial C_L}{\partial\left(\frac{\dot\alpha\,\bar c}{2V_\infty}\right)}$	Several
$\left(C_{L_{\dot\alpha}}\right)_B$	value of derivative for body	7.3.4.1 7.4.4.1
$\left(C_{L_{\dot\alpha}}\right)_e$	value of derivative for exposed wing	7.3.4.1 7.3.4.2
$\left(C_{L_{\dot\alpha}}\right)_e''$	contribution of exposed aft panel to acceleration derivative $C_{L_{\dot\alpha}}$	7.4.4.1
$\left(C_{L_{\dot\alpha}}\right)_W$	value of derivative for wing	7.3.4.1
$\left(C_{L_{\dot\alpha}}\right)_{WB}$	value of derivative for wing-body combination	7.3.4.1 7.4.4.1
$\left(C_{L_{\dot\alpha}}\right)_1, \left(C_{L_{\dot\alpha}}\right)_2$	components of the wing contribution to $C_{L_{\dot\alpha}}$	7.1.4.1
C_{L_δ}	rate of change of lift coefficient with wing flap deflection at constant angle of attack, $\frac{d C_L}{d\delta}$	6.1.4.1 6.1.5.1
C_{L_δ}'	lift-effectiveness of one symmetric, straight-sided flap, based on flap area	6.1.4.1 6.1.5.1 6.2.1.1
$\left(\Delta C_L\right)_\epsilon$	increment in lift due to inflow velocity of the flow surrounding the jet	4.6 4.6.1 4.6.3
$C_{L_{II}}, C_{L_{III}}$	breaks in lift-curve slope (see Sketch (b), Section 4.1.3.2)	4.1.3.2 4.1.4.3
C_N	1. normal-force coefficient, $\frac{N}{qS}$	Several
	2. normal-force coefficient, $\frac{N}{\rho n^2 D^4}$	9.1

SYMBOL	DEFINITION	SECTIONS
ΔC_N	1. increment in normal-force coefficient	6.3.1
	2. increment in coefficient due to jet-pressure interference on vehicle surfaces	4.6.1
C_N'	1. pseudonormal-force coefficient defined by the equation $C_N' = \frac{C_L}{\cos \alpha}$	4.1.3 4.1.3.3 4.1.3.4 7.4.1.1 9.1
	2. normal-force coefficient based on free-stream velocity and propeller disk area, $\frac{N}{q_\infty S_p}$	
$\left[C_N' @ C_{L_{max}}\right]_e'$, $\left[C_N' @ C_{L_{max}}\right]_e''$	pseudonormal-force coefficients at $C_{L_{max}}$ for exposed forward and aft panels, respectively	4.5.1.2
$\left(\frac{C_N}{C_{N_{cir}}}\right)_{NT}$	ratio of normal-force coefficient for body of noncircular cross section to that for an equivalent body of circular cross section (same cross-sectional area) as determined by Newtonian impact theory	4.2.1.2 4.2.2.2
$\left(\frac{C_N}{C_{N_{cir}}}\right)_{SB}$	ratio of normal-force coefficient for body of noncircular cross section to that for an equivalent body of circular cross section (same cross-sectional area) as determined by slender-body theory	4.2.1.2 4.2.2.2
$(C_N)_{\substack{cone \\ cyl}}$	coefficient for cone-cylinder	4.2.1.2 4.2.3.2
$(C_N)_e$	coefficient for exposed wing	4.3.1.3 4.3.1.4
$(\Delta C_N)_F$	increment in coefficient due to body flare	4.2.1.2 4.2.3.2
$(C_N)_N$	coefficient for nose	4.3.1.3 4.3.1.4
$(\Delta C_N)_N$	increment in coefficient due to body nose	4.2.1.2
C_{N_p}	propeller normal-force coefficient	4.6 4.6.4
C_{N_q}	pitching derivative, $\frac{\partial C_N}{\partial\left(\frac{q\bar{c}}{2V_\infty}\right)}$	7.2.1.1
C_{N_q}'	value of derivative for forward panel	7.2.1.1 7.2.1.2
$(C_N)_W$	coefficient for wing	4.3.1.3
$C_{N_{W''(v)}}$	contribution to the normal-force coefficient due to the effect of the forward-surface vortices on the aft surface	4.5.1.2
C_{N_α}	1. rate of change of normal-force coefficient with angle of attack, $\frac{d C_N}{d \alpha}$	Several
	2. value of derivative for forward panel	Several
	3. value of derivative for propeller	9.1.3

SYMBOL	DEFINITION	SECTIONS
ΔC_{N_α}	increment in normal-force-curve slope of a boattail following a semi-infinite cylinder	4.2.2.1
$\left(C_{N_\alpha}\right)_B$	1. value of derivative for the body	5.2.1.1 7.3.1.1 7.3.1.2 7.3.4.1
	2. value of derivative for the body nose, based on nose frontal area	4.3.2.2
$C_{N_{\alpha_{B\,(W)}}}$	value of derivative for the body in presence of the wing	4.3.2.2
$\left(C_{N_\alpha}\right)_{bw}$	normal-force-curve slope of the basic wing	4.1.3.2 5.1.2.1
$\left(C_{N_\alpha}\right)_E$	value of derivative for trailing-edge extension of double-delta and cranked wings	4.1.3.2
$\left(C_{N_\alpha}\right)_e$	value of derivative for exposed wing	4.3.1.3 4.3.1.4 4.3.2.2 7.3.1.1
$\left(C_{N_\alpha}\right)_e', \left(C_{N_\alpha}\right)_e''$	normal-force-curve slopes of the exposed forward and aft panels, respectively	Several
$\left[\left(C_{N_\alpha}\right)_e\right]_i$	normal-force-curve slope of exposed inboard panel of wing	4.3.2.2
$\left[\left(C_{N_\alpha}\right)_e\right]_{theory}$	theoretical value of derivative for exposed wing	4.3.1.2
$\left[\left(C_{N_\alpha}\right)_{e\ theory}\right]_i$	theoretical value of normal-force-curve slope of exposed inboard panel of wing	4.3.2.2
$\left(\Delta C_{N_\alpha}\right)_F$	increment in normal-force-curve slope of a flared body of revolution following a semi-infinite cylinder	4.2.1.1 4.2.2.1
$\left(C_{N_\alpha}\right)_g$	normal-force-curve slope of glove of double-delta and cranked wings	4.1.3.2 5.1.2.1
$\left(C_{N_{\alpha_H}}\right)_e$	normal-force-curve slope of the exposed horizontal surface	6.2.1.2
$\left(C_{N_\alpha}\right)_i$	normal-force-curve slope of inboard panel of wing	4.1.4.2
$C_{N_{\alpha\ in}}'$	propeller normal-force-curve slope with respect to inflow angle of attack at propeller disk	9.1.3
$\left(C_{N_\alpha}\right)_N$	normal-force-curve slope of nose of body based on total wing area	4.3.1.2 4.3.2.2
$\left(C_{N_\alpha}\right)_o'$	normal-force-curve slope of constructed outboard panel of wing	4.1.4.2
$\left(C_{N_\alpha}\right)_p$	1. propeller normal-force derivative	4.6 4.6.1 4.6.4
	2. normal-force-curve slope of isolated vertical panel mounted on a reflection plane	5.3.1.1

SYMBOL	DEFINITION	SECTIONS
$\left[\left(C_{N_\alpha}\right)_p\right]_{K_N=80.7}$	propeller normal-force derivative for K_N=80.7	4.6 4.6.1
$\left(C_{N_\alpha}\right)_{theory}$	theoretical value of derivative	Several
$\left[\left(C_{N_\alpha}\right)_{theory}\right]_e$	theoretical value of normal-force-curve slope of exposed wing	4.3.2.2
$\left[\left(C_{N_\alpha}\right)_{theory}\right]_i$	theoretical value of normal-force-curve slope of inboard panel of wing	4.1.4.2
$\left[\left(C_{N_\alpha}\right)_{theory}\right]'_o$	theoretical value of normal-force-curve slope of constructed outboard panel of wing	4.1.4.2 4.3.2.2
$\left(C_{N_\alpha}\right)'_U$	normal-force-curve slope of isolated lower vertical panel mounted on a reflection plane (the aspect ratio is taken as twice the aspect ratio determined by the average exposed span and exposed area)	Several
$\left(C_{N_\alpha}\right)_V$	normal-force-curve slope of isolated upper vertical panel mounted on a reflection plane (the aspect ratio is taken as twice the aspect ratio detrmined by the average exposed span and exposed area)	Several
$C_{N_{\alpha_{W(B)}}}$	normal-force-curve slope of exposed wing in presence of the body	4.3.2.2
$\left(C_{N_\alpha}\right)_1, \left(C_{N_\alpha}\right)_2$	normal-force-curve slopes for constructed panels of non-straight-tapered wings	4.1.3.2 5.1.2.1
$\left(\frac{dC_N}{d\alpha}\right)_{\alpha=0}$	linear normal-force-curve slope for propeller	9.1.3
$C_{N_{\alpha\alpha}}$	nonlinear increment in normal-force coefficient	4.1.3.3 4.1.3.4
$\Delta C_{N_{\alpha\alpha}}$	incremental value of coefficient	4.3.1.3 4.1.3.3
$C_{N'_{\alpha\alpha}}$	value of coefficient at end of shock-detachment transition region	4.1.3.3
$C^*_{N_{\alpha\alpha}}$	value of coefficient at incipient shock separation	4.1.3.3
$\left(C_{N_{\alpha\alpha}}\right)'_e$, $\left(C_{N_{\alpha\alpha}}\right)''_e$	increments in coefficient at $C_{L_{max}}$ for exposed forward and aft surface, respectively	4.5.1.2
$\left(\Delta C_{N_{\alpha\alpha}}\right)'_e$, $\left(\Delta C_{N_{\alpha\alpha}}\right)''_e$	incremental values of coefficient for exposed forward and aft panels, respectively	4.5.1.2

SYMBOL	DEFINITION	SECTIONS
$\left(C_{N_{\alpha\alpha}}\right)_{ref}$	increment in coefficient at $C_{L_{max}}$	4.1.3.3
$\left[\left(C_{N_{\alpha\alpha}}\right)_{ref}\right]_e'$, $\left[\left(C_{N_{\alpha\alpha}}\right)_{ref}\right]_e''$	values of derivatives at $C_{L_{max}}$ for exposed forward and aft panels, respectively	4.5.1.2
$\left[\left(C_{N_{\alpha\alpha}}\right)_{ref}\right]_{WB}$	value of derivative for wing-body combination	4.3.1.3
$\left(C_{N_{\alpha\alpha}}\right)_{theory}$	theoretical value of coefficient	4.1.3.3
$\left(\Delta C_{N_{\alpha\alpha}}\right)_{WB}$	value of increment for wing-body combination	4.3.1.3
$\left(C_{N_{\alpha\alpha}}\right)_{90}$	value of coefficient $\alpha = 90^o$	4.1.3.3
$C_{N_{\dot{\alpha}}}$	rate of change of normal-force coefficient with rate of change in angle of attack	7.2.2.1
$\left(C_{N_{\dot{\alpha}}}\right)_B$	value of derivative for body	7.3.4.1
$\left(C_{N_{\dot{\alpha}}}\right)_e$	value of derivative for exposed wing	7.3.4.1
$\left(C_{N_{\dot{\alpha}}}\right)_{WB}$	value of derivative for wing-body combination	7.3.4.1 7.4.4.1
$\left[\left(C_{N_{\dot{\alpha}}}\right)_1\right]_e$, $\left[\left(C_{N_{\dot{\alpha}}}\right)_2\right]_e$	components to the exposed-wing contribution $C_{N_{\dot{\alpha}}}$	7.3.4.1
$\left(C_{N_1'}\right)_e'$, $\left(C_{N_2'}\right)_e'$	pseudonormal-force coefficients of the exposed forward panel	4.5.1.2
$\left(C_{N_1'}\right)_e''$, $\left(C_{N_2'}\right)_e''$	pseudonormal-force coefficients of the exposed aft panel	4.5.1.2
C_T	thrust coefficient, $\frac{T}{\rho n^2 D^4}$	9.1 9.1.1 9.1.3

SYMBOL	DEFINITION	SECTIONS
C_X	axial-force coefficient	4.2.3.2
$(C_X)_{\alpha = 0}$	axial-force coefficient at zero angle of attack	4.2.3.2
$(C_X)_{\alpha = 180^\circ}$	axial-force coefficient at $\alpha = 180^\circ$	4.2.3.2
C_Y	total side-force coefficient	Several
C_{Y_B}	side-force coefficient of body	5.2.1.2 5.2.3.2
$C_{Y_{H(B)}}$	side-force coefficient of horizontal tail in the presence of the body	5.3.1.2 5.3.3.2 5.6.1.2 5.6.3.2
$C_{Y_{HVU(B)}}$	side-force coefficient of empennage on tail-body configuration	5.3.1.2
$C_{Y_{HVU(WB)}}$	side-force coefficient of empennage on wing-body-tail configuration	5.6.1.2
C_{Y_p}	rotary derivative, $\frac{dC_Y}{d\left(\frac{pb}{2V_\infty}\right)}$	Several
$(C_{Y_p})_{WB}$	wing-body contribution to the derivative	7.4.2.1
$(\Delta C_{Y_p})_\Gamma$	increment in derivative due to geometric dihedral	7.1.2.1
C_{Y_r}	rotary derivative, $\frac{dC_Y}{d\left(\frac{rb}{2V_\infty}\right)}$	7.1.3.1 7.1.3.2 7.3.3.1 7.4.3.1
$(C_{Y_r})_{WB}$	wing-body contribution to the derivative	7.4.3.1
C_{Y_U}	side-force coefficient of ventral fin on tail-body configuration	5.3.1.2 5.3.3.2 5.6.1.2
$C_{Y_{U(K,\phi)}}$	side-force coefficient of ventral fin due to interference and cross-coupling of α and β	5.3.1.2 5.6.1.2
$C_{Y_{U(\eta)}}$	side-force coefficient of ventral fin on wing-body-tail configuration	5.6.1.2 5.6.3.2
C_{Y_V}	side-force coefficient of upper vertical tail on tail-body configuration	5.3.1.2 5.3.3.2

SYMBOL	DEFINITION	SECTIONS
$C_{Y_{V(K,\phi)}}$	side-force coefficient of upper vertical tail due to interference and cross-coupling of α and β	5.3.1.2 5.6.1.2
$C_{Y_{V(\Gamma_B)}}$	side-force coefficient of upper vertical tail due to body vortices	5.3.1.2 5.6.1.2
$C_{Y_{V(\eta)}}$	side-force coefficient of upper vertical tail on wing-body-tail configuration	5.6.1.2 5.6.3.2
$C_{Y_{WB}}$	side-force coefficient of wing-body configuration	5.2.1.2 5.6.1.2
$C_{Y_{W(B)}}$	side-force coefficient of the wing in the presence of the body	5.2.1.2 5.2.3.2
$C_{Y_{WBHVU}}$	side-force coefficient of wing-body-tail configuration	5.6.1.2
C_{Y_β}	rate of change of side force with sideslip angle, $\frac{dC_Y}{d\beta}$	Several
$\left(C_{Y_\beta}\right)_B$	value of derivative for body	5.2.1.1 5.3.1.1 5.6.1.1
$\left(\Delta C_{Y_\beta}\right)_{H(BW)}$	increment in C_{Y_β} due to the horizontal tail in the presence of the wing and body	5.3.1.1 5.6.1.1
$\left(\Delta C_{Y_\beta}\right)_{H(BWU)}$	increment in C_{Y_β} due to the horizontal tail in the presence of the wing, body, and lower vertical tail	5.3.1.1
$\left(\Delta C_{Y_\beta}\right)_{HV(BWU)}$	increment in C_{Y_β} due to the horizontal tail and upper vertical tail in the presence of the wing, body, and lower vertical tail	5.3.1.1
$\left(\Delta C_{Y_\beta}\right)_p$	increment in C_{Y_β} due to panel in empennage	Several
$\left(C_{Y_\beta}\right)_U$	value of derivative for lower vertical panel	Several
$\left(\Delta C_{Y_\beta}\right)_{U(WBHV)}$	increment in C_{Y_β} due to lower vertical stabilizer in presence of wing, body, horizontal tail, and upper vertical stabilizer	Several
$\left(C_{Y_\beta}\right)_V$	value of derivative for upper vertical panel	Several
$\left(\Delta C_{Y_\beta}\right)_{V(BWUH)}$	increment in C_{Y_β} due to the upper vertical tail in the presence of the wing, body, lower vertical tail, and horizontal tail	Several
$\left(C_{Y_\beta}\right)_{V_{eff}}$	lift-curve slope of equivalent rectangular vertical panel	5.3.1.1 5.6.1.1

SYMBOL	DEFINITION	SECTIONS
$\left(\Delta C_{Y_\beta}\right)_{V(WBH)}$	increment in C_{Y_β} due to upper vertical stabilizer in presence of wing, body, and horizontal tail	Several
$\left(C_{Y_\beta}\right)_W$	value of derivative for wing	5.2.1.1
$\left(C_{Y_\beta}\right)_{WB}$	value of derivative for wing-body combination	5.2.1.1 5.2.1.2 5.6.1.1
$\left(\Delta C_{Y_\beta}\right)_\Gamma$	increment in C_{Y_β} due to geometric dihedral	5.2.1.1 5.6.1.1
C_f	skin-friction coefficient for incompressible flow	Several
$\left(C_f\right)_B$	turbulent flat-plate skin-friction coefficient of the body including roughness effects	4.3.3.1 4.5.3.1
C_{f_c}	skin-friction coefficient for compressible flow	4.2.3.1 7.4.1.1
$\left(C_f\right)_H$	turbulent flat-plate skin-friction coefficient of the horizontal-tail panel	4.5.3.1
$\left(C_f\right)_i, \left(C_f\right)_o$	skin-friction coefficients for incompressible flow of wing inboard and outboard panels, respectively	4.1.5.1
$\left(C_f\right)_{inc}$	incompressible, turbulent, flat-plate skin-friction coefficient, including roughness effects, as a function of Reynolds number based on total body length	4.2.3.1
$\left(C_f\right)_p$	turbulent flat-plate skin-friction coefficient based on the MAC of the exposed tail panel	4.5.3.1
$\left(C_f\right)_V$	turbulent flat-plate skin-friction coefficient of the vertical-tail panel	4.5.3.1
$\left(C_f\right)_W$	turbulent flat-plate skin-friction coefficient of the wing including roughness effects	4.3.3.1 4.5.3.1
$\left(C_{f_W}\right)_i, \left(C_{f_W}\right)_o$	turbulent flat-plate skin-friction coefficients of the wing inboard and outboard panels, respectively, including roughness effects	4.3.3.1
C_{f_0}	vacuum-thrust coefficient	6.3.2
C_h	hinge-moment coefficient, $\frac{\text{hinge moment}}{qS_f c_f}$	6.1.3.2
C_{h_c}	hinge-moment coefficient of control surface	6.3.4
$C_{h_{tc}}$	hinge-moment coefficient of control tab	6.3.4
C_{h_α}	rate of change of hinge moment with angle of attack at constant flap or control deflection, $\frac{d C_h}{d\alpha}$	6.1.6 6.1.6.1

SYMBOL	DEFINITION	SECTIONS
ΔC_{h_α}	increment in derivative accounting for induced-camber effects	6.1.6.1
$\left(C_{h_\alpha}\right)_{t/c}$	hinge-moment derivative for a symmetric, straight-sided control, based on twice the area-moment of the control about its hinge line	6.1.6.1
$\left(C_{h_\alpha}\right)_{t/c\,=\,0}$	supersonic flat-plate hinge-moment derivative	6.1.6.1
C_{h_δ}	rate of change of hinge moment with control-surface deflection at constant angle of attack, $\frac{dC_h}{d\delta}$	6.1.6 6.1.6.2
ΔC_{h_δ}	increment in derivative due to induced-camber effects	6.1.6.2
C'_{h_δ}	value of derivative for zero-thickness control surface	6.1.6.2
C_l	rolling-moment coefficient, $\frac{\text{rolling moment}}{qSb}$	Several
C_{l_p}	rotary derivative $\frac{dC_l}{d\left(\frac{pb}{2V_\infty}\right)}$	Several
$\left(C_{l_p}\right)_{C_L}$	value of derivative at a given lift coefficient	7.1.2.2 7.3.2.1 7.3.2.2 7.4.2.2
$\left(\Delta C_{l_p}\right)_{drag}$	increment in derivative due to drag	7.1.2.2 7.4.2.2
$\left(C_{l_p}\right)_H$	horizontal-tail contribution to the derivative	7.4.2.2
$\left(C_{l_p}\right)_{WB}$	wing-body contribution to the derivative	7.4.2.2
$\left(C_{l_p}\right)_\Gamma$	contribution to derivative due to geometric dihedral	7.1.2.2 7.3.2.1 7.3.2.2 7.4.2.2
$\left(C_{l_p}\right)_{\substack{\Gamma\,=\,0 \\ C_L\,=\,0}}$	derivative at zero lift of wing without dihedral	7.1.2.1 7.1.2.2 7.4.2.2
$\frac{\left(C_{l_p}\right)_{C_{D_L}}}{C_L{}^2}$	drag-due-to-lift roll-damping parameter	7.1.2.2 7.4.2.2

SYMBOL	DEFINITION	SECTIONS
$\left(\frac{\beta C_{l_p}}{\kappa}\right)_{C_L = 0}$	roll-damping parameter at zero lift	7.1.2.2
C_{l_r}	rotary derivative, $\frac{dC_l}{d\left(\frac{rb}{2V_\infty}\right)}$	7.1.3.2 7.3.3.2 7.4.3.2
ΔC_{l_r}	increment in derivative due to geometric dihedral	7.1.3.2
$\left(\Delta C_{l_r}\right)_{C_L}$	semiempirical correction factor used to extrapolate potential-flow values of C_{l_r} to higher lift coefficients	7.1.3.2
$\left(\Delta C_{l_r}\right)_{\substack{\text{side} \\ \text{force}}}$	increment in derivative due to wing side force	7.1.3.2
$\left(C_{l_r}\right)_{WB}$	wing-body contribution to the derivative	7.4.3.2
$\frac{\Delta C_{l_r}}{\Gamma}$	increment in C_{l_r} due to dihedral	7.1.3.2
$\frac{\Delta C_{l_r}}{\theta}$	increment in C_{l_r} due to wing twist	7.1.3.2
C_{l_β}	rate of change of rolling moment with sideslip angle, $\frac{dC_l}{d\beta}$	Several
ΔC_{l_β}	difference between calculated and test values of the derivative	5.1.2.1
$\left(\Delta C_{l_\beta}\right)_P$	increment in C_{l_β} due to panel present in empennage	5.3.2.1 7.4.3.2
$\left(\Delta C_{l_\beta}\right)_U$	increment in C_{l_β} for lower vertical panel	5.3.2.1
$\left(C_{l_\beta}\right)_V$	value of derivative for upper vertical panel	5.3.2.1
$\left(C_{l_\beta}\right)_{WB}$	value of derivative for wing-body combination	5.2.2.1 5.6.2.1
$\left(\Delta C_{l_\beta}\right)_{z_W}$	increment in derivative due to wing height	5.2.2.1 5.6.2.1

SYMBOL	DEFINITION	SECTIONS
$\left(\frac{C_{l_\beta}}{C_L}\right)_A$	contribution of wing aspect ratio to C_{l_β}	5.1.2.1 5.2.2.1 5.6.2.1
$\left(\frac{C_{l_\beta}}{C_L}\right)_{\Lambda_c/2}$	contribution of wing sweep to C_{l_β}	5.1.2.1 5.2.2.1
$\left(\frac{C_{l_\beta}}{C_L}\right)_{\Lambda_i}$	contribution of sweep of inboard panel of wing to C_{l_β}	5.1.2.1
$\left(\frac{C_{l_\beta}}{C_L}\right)_{\Lambda_o'}$	contribution of sweep of constructed outboard panel of wing to C_{l_β}	5.1.2.1
$\frac{C_{l_\beta}}{\Gamma}$	dihedral effect on C_{l_β} for uniform geometric dihedral	5.1.2.1
$\left(\frac{C_{l_\beta}}{\Gamma}\right)_{C_L}$	value of parameter at a given lift coefficient	5.1.2.2 5.6.1.2
$\frac{\Delta C_{l_\beta}}{\theta \tan \Lambda_{c/4}}$	wing-twist correction factor	5.1.2.1
$\frac{\beta C_{l_\beta}}{\kappa\Gamma}$	rolling-moment-due-to-sideslip parameter for any symmetric, spanwise distribution of dihedral angle	5.1.2.1
C_{l_δ}	rate of change of rolling moment with control deflection, $\frac{dC_l}{d\delta}$	Several
C_{l_δ}	rolling-moment effectiveness of one symmetric, straight-sided control about its root-chord line	6.1.5.1 6.2.1.1
$C_{l_{\delta_{\perp HL}}}$	value of derivative for control deflection perpendicular to the hinge line	6.2.1.1
C_m	1. pitching-moment coefficient, $\frac{\text{pitching moment}}{qS\bar{c}}$	Several
	2. duct pitching-moment coefficient, $\frac{M}{q_\infty S_D c}$	9.3

SYMBOL	DEFINITION	SECTIONS
ΔC_m	1. increment in pitching-moment coefficient about root-chord midpoint due to leading-edge vortex	4.1.4.3
	2. increment in pitching-moment coefficient	6.1.5.1 6.3.1
$C_{m_{a/b}}$	pitching-moment coefficient of body having elliptical cross sections	4.2.2.2
$C_{m_{C_L}}$	pitching-moment derivative, $\frac{dC_m}{dC_L}$	4.1.4 4.1.4.2 4.3.2.2
$\frac{\Delta C'_m}{C_L}$	ratio of pitching-moment increment to lift increment for a full-span flap on a rectangular wing	6.1.5.1
$\left(\frac{dC_m}{dC_L}\right)_{theory}$	wing pitching-moment-curve slope uncorrected for thickness effects	4.1.4.2
ΔC_{m_f}	increment in coefficient due to flaps at constant angle of attack	6.1.5.1
$(\Delta C_m)_G$	increment in pitching-moment coefficient in the presence of the ground	4.7 4.7.3 4.7.4
$(\Delta C_m)_H$	total change in pitching-moment coefficient of horizontal tail	4.6 4.6.1
$(\Delta C_{m_H})_G$	increment in horizontal-tail pitching moment in the presence of the ground	4.7 4.7.3
$[(\Delta C_m)_{HL}]_{\Delta C_A}$	increment in pitching moment about the hinge line due to axial-force increment	6.3.1
$[(\Delta C_m)_{HL}]_{\Delta C_N}$	increment in pitching moment about the hinge line due to normal-force increment	6.3.1
$(\Delta C_{m_H})_q$	increment in coefficient due to change in dynamic pressure at horizontal tail due to propeller-power effects	4.6 4.6.1 4.6.3
$[C_{m_{H(WBV)}}]_{\alpha_{C_{L_{max}}}}$	horizontal-tail pitching moment at stall angle of attack	4.5.1.3
$(\Delta C_{m_H})_e$	increment in coefficient due to change in downwash at horizontal tail due to propeller-power effects	4.6 4.6.1 4.6.3
$(\Delta C_m)_L$	increment in coefficient due to change in wing lift caused by propeller power	4.6 4.6.3
C_{m_m}	sum of wing section pitching-moment increments	6.1.5.1

SYMBOL	DEFINITION	SECTIONS
$(\Delta C_{m}{}_{MRP}$	increment in pitching moment about vehicle moment reference point	6.3.1
$(\Delta C_m)_{N_j}$	increment in coefficient due to normal force acting at jet inlet due to inclination of oncoming flow to thrust axis	4.6.3
$(\Delta C_m)_{N_p}$	increment in coefficient due to propeller normal force	4.6 4.6.3
$C_{m_o}(g)$	pitching-moment coefficient correction term	7.1.4.2 7.3.4.2
$(\Delta C_m)_{\substack{power \\ on}}$	total increment in vehicle pitching-moment coefficient at a given angle of attack due to propeller power effects	4.6.3
$(\Delta C_m)_q$	increment in coefficient due to change in propeller-slipstream dynamic pressure	4.6 4.6.3
C_{m_q}	rotary derivative, $\dfrac{\partial C_m}{\partial\left(\dfrac{q\bar{c}}{2V_\infty}\right)}$	Several
$C_{m_q}{}'$	1. value of derivative referred to body axis with origin at wing aerodynamic center	7.1.1.2
	2. pitching derivative of body segment based on base area and base diameter and referred to moment center at forward face of segment	7.2.1.2
$C_{m_q}{}''$	value of derivative referred to body axis with origin at wing leading-edge vertex	7.1.1.2
$(C_{m_q})_B$	value of derivative for body	7.3.1.2 7.4.1.2
$(C_{m_q})_e$	value of derivative for exposed wing	7.3.1.2
$(C_{m_q})_e'$	value of derivative for exposed forward panel	7.3.1.2 7.4.1.2
$(C_{m_q})_M$	value of derivative at given Mach number	7.1.1.2 7.3.1.2
$(C_{m_q})_{M_{cr}}$	value of derivative at the critical Mach number	7.1.1.2
$(C_{m_q})_W$	value of derivative for wing	7.3.1.2
$(C_{m_q})_{WB}$	value of derivative for wing-body combination	7.3.1.2 7.4.1.2
$(\Delta C_m)_T$	increment in coefficient due to direct thrust force	4.6 4.6.3
$\Delta C_{m\ trim}$	incremental pitching-moment coefficient required for trim	4.5.3.2
$C_{m_{WB}}$	wing-body pitching-moment coefficient, $\dfrac{\text{pitching moment}}{qS\bar{c}}$	4.5.3.2

SYMBOL	DEFINITION	SECTIONS
$\left(\Delta C_{m_{WB}}\right)_G$	increment in wing-body pitching moment in the presence of the ground	4.7 4.7.3
$\left(C_{m_{WB}}\right)_{\alpha_{C_{L_{max}}}}$	wing-body pitching moment at stall angle of attack	4.5.1.3.
C_{m_α}	rate of change of pitching-moment coefficient with angle of attack at constant flap deflection, $\frac{d C_m}{d \alpha}$	Several
C'_{m_α}	pitching-moment-curve slope for body segment	4.2.2.1 7.2.1.2
$\left(C_{m_\alpha}\right)_B$	value of derivative for body	4.3.2.1 7.3.1.2 7.3.4.2
$C_{m_{\dot\alpha}}$	rate of change of pitching-moment coefficient with rate of change of angle of attack, $\frac{\partial C_m}{\partial\left(\frac{\dot\alpha\,\bar c}{2 V_\infty}\right)}$	Several
$C''_{m_{\dot\alpha}}$	value of pitching derivative referred to body axis with origin at wing leading-edge vertex	7.1.4.2
$\left(C_{m_{\dot\alpha}}\right)_B$	contribution of body to acceleration derivative $C_{m_{\dot\alpha}}$	7.3.4.2 7.4.4.2
$\left(C_{m_{\dot\alpha}}\right)_e$	contribution of exposed wing to acceleration derivative $C_{m_{\dot\alpha}}$	7.3.4.2
$\left(C_{m_{\dot\alpha}}\right)'_e$	contribution of exposed forward panel to the acceleration derivative $C_{m_{\dot\alpha}}$	7.4.4.2
$\left(C_{m_{\dot\alpha}}\right)''_e$	contribution of exposed aft panel to the acceleration derivative $C_{m_{\dot\alpha}}$	7.3.4.2
$\left(C_{m_{\dot\alpha}}\right)_W$	contribution of wing to acceleration derivative $C_{m_{\dot\alpha}}$	7.3.4.2
$\left(C_{m_{\dot\alpha}}\right)_{WB}$	contribution of wing-body combination to acceleration derivative $C_{m_{\dot\alpha}}$	7.3.4.2 7.4.4.2
$\left(C_{m_{\dot\alpha}}\right)_1, \left(C_{m_{\dot\alpha}}\right)_2$	components of the wing contribution to $C_{m_{\dot\alpha}}$	7.1.4.2 7.3.4.2
$\left[\left(C_{m_{\dot\alpha}}\right)_1\right]_e,$ $\left[\left(C_{m_{\dot\alpha}}\right)_2\right]_e$	components of the exposed wing contribution to $C_{m_{\dot\alpha}}$	7.3.4.2
C_{m_δ}	rate of change of pitching-moment coefficient with control or flap deflection at constant angle of attack, $\frac{d C_m}{d \delta}$	6.1.5.1
C'_{m_δ}	pitching-moment effectiveness for one symmetric, straight-sided control, based on twice its moment-area about the hinge line	6.1.5.1

SYMBOL	DEFINITION	SECTIONS
$(\Delta C_m)_\epsilon$	increment in coefficient due to jet interference effects at the horizontal tail	4.6.3
C_{m_0}	pitching-moment coefficient at zero lift	4.1.4.1 4.1.4.3 4.6.3
ΔC_{m_0}	increment in pitching-moment coefficient at zero lift due to linear twist	4.1.4.1
$C_{m_0}(g)$	pitching-moment-coefficient correction term	7.1.4.2 7.3.4.2
$(C_{m_0})_{\text{area not immersed}}$	pitching-moment coefficient at zero lift for portion of vehicle not immersed in propeller slipstream	4.6 4.6.3
$(C_{m_0})_B$	body zero-lift pitching-moment coefficient without Mach-number effects	4.3.2.1
$(C_{m_0})_i$	pitching-moment coefficient at zero lift of portion of vehicle immersed in propeller slipstream	4.6 4.6.3
$(C_{m_0})_{\text{theory}}$	zero-lift pitching-moment coefficient uncorrected for thickness effects	4.1.4.1
$(C_{m_0})_W$	wing zero-lift pitching-moment coefficient	4.3.2.1
$(C_{m_0})_{WB}$	zero-lift pitching-moment coefficient of the wing-body combination	Several
$(C_{m_0})_{\text{wing-body}}$		
$(C_{m_0})_{\theta=0}$	pitching-moment coefficient at zero lift of untwisted, constant-section wing	4.1.4.1
$\frac{(C_{m_0})_M}{(C_{m_0})_{M=0}}$	Mach-number correction factor	4.3.2.1
C_n	yawing-moment coefficient, $\frac{N_z}{qSb}$	Several
ΔC_n	yawing moment due to aileron deflection	6.2.2.1
C_{n_B}	yawing-moment coefficient of body	5.2.3.2
$C_{n_{HVU(B)}}$	yawing-moment coefficient of empennage on tail-body configuration	5.3.3.2
$C_{n_{HVU(WB)}}$	yawing-moment coefficient of empennage on wing-body-tail configuration	5.6.3.2
C_{n_p}	rotary derivative, $\frac{dC_n}{d\left(\frac{pb}{2V_\infty}\right)}$	7.1.2.1 7.3.2.1 7.3.2.2 7.4.2.3

SYMBOL	DEFINITION	SECTIONS
$\left(C_{n_p}\right)_M$	value of derivative for a given Mach number	7.3.2.3
$\left(C_{n_p}\right)_{WB}$	wing-body contribution to the derivative	7.4.2.3
$\frac{C_{n_p}}{\alpha}$	supersonic yawing moment due to rolling referred to stability axes with origin at the center of gravity	7.1.2.3
$\left(\frac{C_{n_p}}{\alpha}\right)_{\substack{\text{body}\\\text{axis}}}$	supersonic yawing moment due to rolling referred to body axes with origin at the wing apex	7.1.2.3
$\left(\frac{C_{n_p}}{\alpha}\right)_{1,2,3}$	supersonic yawing moment due to rolling components – body axes	7.1.2.3
C_{n_r}	rotary derivative, $\frac{dC_n}{d\left(\frac{rb}{2V_\infty}\right)}$	7.1.3.3. 7.3.3.3 7.4.3.3
$\left(C_{n_r}\right)_{WB}$	wing-body contribution to the derivative	7.4.3.3
$\frac{C_{n_r}}{C_{D_0}}$	low-speed profile-drag yaw-damping parameter	7.1.3.3
$\frac{C_{n_r}}{C_L{}^2}$	low-speed drag-due-to-lift yaw-damping parameter	7.1.3.3
$C_{n_{VU(B)}}$	yawing-moment coefficient of vertical tail and ventral fin on tail-body configuration	5.3.3.2
$C_{n_{WB}}$	yawing-moment coefficient of wing-body combination	5.2.3.2 5.6.3.2
$C_{n_{WBHVU}}$	yawing-moment coefficient of wing-body-tail configuration	5.6.3.2
C_{n_β}	rate of change of yawing moment with sideslip angle, $\frac{dC_n}{d\beta}$	Several
$\left(\Delta C_{n_\beta}\right)_p$	increment in C_{n_β} due to panel in empennage	Several
$\left(\Delta C_{n_\beta}\right)_V$	increment in C_{n_β} for vertical panel	5.3.3.1
$\left(C_{n_\beta}\right)_W$	value of derivative for wing alone	5.2.3.1
$\left(C_{n_\beta}\right)_{WB}$	value of derivative for wing-body combination	5.2.3.1 5.2.3.2 5.6.3.1

SYMBOL	DEFINITION	SECTIONS
C_{n_δ}	rate of change of yawing moment with control deflection, $\frac{dC_n}{d\delta}$	6.2.2.2
C_p	pressure coefficient $\frac{p - p_\infty}{q_\infty}$	Several
$\Delta C_p, \Delta C_{p_1}$ ...	sums of the pressure coefficients acting on the two sides of a given surface	5.3.1.1
C_{p_b}	base pressure coefficient	4.2.3.1 4.5.3.1 4.6.4
$C_{p_{inc}}$	incipient pressure-rise coefficient	6.3.1
C_{p_o}	two-dimensional pressure coefficient	6.1.6.1
$C_{p_{stag}}$	stagnation-pressure coefficient	4.2.1.2 4.2.2.2
$\left(C_{p_\alpha}\right)_p$	plateau-pressure coefficient referred to local pressure upstream of interaction	6.3.1
$\left(C_{p_\alpha}\right)_{inc}$	incipient pressure-rise coefficient referred to local pressure upstream of interaction	6.3.1
$\left(C_{p_\alpha}\right)_2$	peak value of pressure coefficient referred to local pressure upstream of interaction	6.3.1
C_{p_u}	maximum negative upper-surface section pressure coefficient	4.1.3.2
C_{p_2}	plateau-pressure coefficient	6.3.2
C_{p_∞}	free-stream pressure coefficient	6.3.1
$\left(C_{p_\infty}\right)_p$	plateau-pressure coefficient referred to free-stream pressure	6.3.1
$\left(C_{p_\infty}\right)_\alpha$	local pressure coefficient upstream of interaction referred to free-stream pressure	6.3.1
$\left(C_{p_\infty}\right)_2$	peak value of pressure coefficient referred to free-stream pressure	6.3.1
C_x	drag coefficient	6.3.2
C_{λ_k}	lift contribution to wing section pitching-moment coefficient	6.1.5.1
C_μ	section nondimensional trailing-edge jet momentum coefficient	Several
C'_μ	section nondimensional trailing-edge jet momentum coefficient based on extended airfoil chord	Several

D. LOWER-CASE COEFFICIENTS AND DERIVATIVES

SYMBOL	DEFINITION	SECTIONS
c_d	section drag coefficient, $\frac{\text{drag}}{qc}$	Several
c_{d_c}	cross-flow drag coefficient of circular cylinder of infinite length normal to flow direction	Several
Δc_{d_f}	airfoil-section drag coefficient with flap deflected	6.1.7
c_h	section hinge moment	6.1.3.2
$c_{h_{f_\alpha}}$	flap section hinge moment due to change in angle of attack	6.1.3.1
$\left(c_{h_f}\right)_{\delta_f}$	flap section hinge moment due to flap deflection	6.1.3.2
$\left(c_{h_f}\right)_{\delta_t}$	section hinge-moment derivative of control surface due to tab deflection	6.1.3.3
$c_{h_{t_\alpha}}$	tab section hinge moment due to change in angle of attack	6.1.3.1
$\left(c_{h_t}\right)_{\delta_f}$	section hinge moment derivative of a tab due to control-surface deflection	6.1.3.4
$\left(c_{h_t}\right)_{\delta_t}$	tab section hinge moment due to tab deflection	6.1.3.2
c_{h_α}	rate of change of control section hinge-moment coefficient with angle of attack at control deflection, $\frac{dc_h}{d\alpha}$	6.1.3.1 6.1.3.2 6.1.6.1 6.1.6.2
Δc_{h_α}	increment in derivative accounting for finite control thickness at supersonic speeds	6.1.3.1
c'_{h_α}	hinge-moment derivative (see Page 6.1.3.1-3, Step 1)	6.1.3.1 6.1.6.1 6.1.6.2
c''_{h_α}	hinge-moment derivative (see Page 6.1.3.1-3, Step 2)	6.1.3.1 6.1.6.1
$\left(c_{h_\alpha}\right)_{\text{balance}}$	value of derivative for aerodynamically balanced control surface	6.1.3.1 6.1.6.1
$\left(c_{h_\alpha}\right)_{\text{low speed}}$	value of derivative uncorrected for compressibility	6.1.3.1
$\left(c_{h_\alpha}\right)_M$	value of derivative corrected for compressibility	6.1.3.1
$\left(c_{h_\alpha}\right)_{\text{theory}}$	theoretical value of derivative	6.1.3.1 6.1.6.1

SYMBOL	DEFINITION	SECTIONS
$\frac{\Delta c_{h_\alpha}}{t/c}$	thickness-correction factor for symmetric, circular-arc airfoils	6.1.3.1
c_{h_δ}	rate of change of hinge-moment coefficient with control deflection, $\frac{dc_h}{d\delta}$	6.1.3.2 6.1.6.2
Δc_{h_δ}	increment in derivative accounting for thickness effects at supersonic speeds	6.1.3.1 6.1.3.2
c'_{h_δ}	hinge-moment derivative (see Page 6.1.3.2-3, Step 1)	6.1.3.2 6.1.6.2
c''_{h_δ}	hinge-moment derivative (see Page 6.1.3.2-4, Step 2)	6.1.3.2 6.1.6.2
$(c_{h_\delta})_{balance}$	value of derivative for an aerodynamically balanced control	6.1.3.2 6.1.6.2
$(c_{h_\delta})_{low\ speed}$	value of derivative uncorrected for compressibility	6.1.3.2
$(c_{h_\delta})_M$	value of derivative corrected for compressibility	6.1.3.2
$(c_{h_\delta})_{theory}$	theoretical value of derivative	6.1.3.2 6.1.6.2
$\frac{\Delta c_{h_\delta}}{t/c}$	thickness-correction factor for symmetric, circular-arc airfoils	6.1.3.1
c_ℓ	section lift coefficient, $\frac{lift}{qc}$	Several
Δc_ℓ	increment in section lift coefficient due to flap or control deflection	Several
c_{ℓ_i}	design lift coefficient	Several
$c_{\ell_{max}}$	section maximum lift coefficient	Several
$\Delta c_{\ell_{max}}$	increment in section maximum lift coefficient due to flap deflection	6.1.1 6.1.1.3 6.1.4.3
$\Delta_1 c_{\ell_{max}}$	increment in coefficient accounting for effect of camber for airfoils with maximum thickness at 30% chord	4.1.1.4 4.1.3.3
$\Delta_2 c_{\ell_{max}}$	increment in coefficient accounting for effect of camber for airfoils with maximum thickness at positions other than 30% chord	4.1.1.4 4.1.3.3
$\Delta_3 c_{\ell_{max}}$	increment in coefficient accounting for Reynolds-number effects	4.1.1.4 4.1.3.3
$\Delta_4 c_{\ell_{max}}$	increment in coefficient accounting for airfoil-roughness effects	4.1.1.4
$\Delta_5 c_{\ell_{max}}$	increment in coefficient accounting for Mach-number effects	4.1.1.4

SYMBOL	DEFINITION	SECTIONS
$(c_{\ell_{max}})_{base}$	base or reference value of coefficient	4.1.1.4 4.1.3.3
$(\Delta c_{\ell_{max}})_{base}$	base or reference value of coefficient	6.1.1.3 6.1.4.3
$(c_{\ell_{max}})'_e$	section maximum lift coefficient of exposed forward panel	4.1.5.2
c_{ℓ_α}	1. section lift-curve slope, rate of change of section lift coefficient with angle of attack at constant flap deflection, $\frac{dc_\ell}{d\alpha}$	Several
	2. lift-curve slope for wing of infinite span	Several
	3. section lift-curve slope for propeller blade	9.1.3
Δc_{ℓ_α}	increment in section lift-curve slope due to NACA roughness	4.1.1.2
c'_{ℓ_α}	jet-flap section lift-curve slope uncorrected for thickness effects	Several
$(c_{\ell_\alpha})_M$	lift-curve slope corrected for compressibility effects	Several
$(c_{\ell_\alpha})_{theory}$	theoretical value of derivative	Several
$(c_{\ell_\alpha})_\delta$	value of derivative for deflected control or flap conditions	6.1.1.1 6.1.1.2 6.1.5.1
$(c_{\ell_\alpha})_{\delta=0}$	value of derivative for unflapped airfoil, including compressibility effects	6.1.1.2
c_{ℓ_δ}	rate of change of section lift with flap or control deflection at constant angle of attack, $\frac{dc_\ell}{d\delta}$	Several
$c_{\ell_{\delta_a}}$	section lift effectiveness due to deflection of a hypothetical flap	6.1.2.1 6.1.5.1
$c_{\ell_{\delta_f}}$	rate of change of section lift coefficient due to flap deflection	6.1.1.1 6.1.2.1 6.1.4.1
$c_{\ell_{\delta_{f_1}}}, c_{\ell_{\delta_{f_2}}}, c_{\ell_{\delta_{f_i}}}$	theoretical lifting-efficiency factors for first, second, and i^{th} segments, respectively, of trailing-edge flaps	6.1.1.1 6.1.2.1
$c_{\ell_{\delta_j}}$	rate of change of section lift coefficient due to jet deflection	6.1.1.1 6.1.2.1 6.1.4.1 6.1.5.1
$c_{\ell_{\delta_{max}}}$	theoretical maximum lifting effectiveness	6.1.1.3

SYMBOL	DEFINITION	SECTIONS
$(c_{\ell_\delta})_{theory}$	theoretical value of derivative	Several
$(c_{\ell_\delta})_\alpha$	value of derivative at a given angle of attack	6.1.1.1 6.1.5.1
$c_{\ell_{\delta_\perp}}$	value of derivative for control or flap deflection measured perpendicular to hinge line	6.1.6.2
c_{ℓ_Λ}	incremental section lift coefficient due to control deflections	6.1.5.1
$c_{\ell_{\Lambda=0}}$	incremental section lift coefficient as function of span station, referred to basic load line	6.1.5.1
c_m	section pitching-moment coefficient with flaps retracted	6.1.2.1
Δc_m	increment in section pitching-moment coefficient near maximum lift due to flaps and controls	6.1.2.1 6.1.2.2 6.1.2.3 6.1.5.1
dc_m/dc_ℓ	wing section pitching-moment-curve slope	6.1.2.2
$c_{m_{c/4}}$	section pitching-moment coefficient measured about the quarter-chord point	4.1.1 6.1.2.2
Δc_{m_f}	increment in section pitching-moment coefficient at low angles of attack due to flaps and controls	6.1.5.1
c_{m_α}	rate of change of section pitching-moment coefficient with angle of attack, $\frac{dc_m}{d\alpha}$	6.1.2.1 6.1.2.2
Δc_{m_α}	pitching-moment increment due to airfoil angle of attack	6.1.2.1 6.1.5.1
c_{m_δ}	rate of change of section pitching-moment coefficient with flap deflection at constant angle of attack, $\frac{dc_m}{d\delta}$	6.1.2.1
c'_{m_δ}	theoretical flap pitching-moment effectiveness (about the leading edge)	6.1.2.1
$c_{m_{\delta_f}}$	flap pitching-moment effectiveness measured about the leading edge	6.1.2.1
$(\Delta c_m)_{\delta_f}$	pitching-moment increment due to trailing-edge flaps	6.1.2.1 6.1.5.1
$(\Delta c_m)_{\delta_{f_{LE}}}$	pitching-moment increment due to deflection of a leading-edge device	6.1.2.1 6.1.5.1
$c_{m_{\delta_j}}$	rate of change of pitching-moment coefficient measured about the leading edge with respect to the jet deflection	6.1.2.1
$(\Delta c_m)_{\delta_j}$	pitching-moment increment due to jet sheet acting at an angle to trailing-edge camber line	6.1.2.1 6.1.5.1
$c'_{m_{\delta_{LE}}}$	theoretical two-dimensional flap pitching-moment effectiveness about the leading edge	6.1.5.1

SYMBOL	DEFINITION	SECTIONS
$c_{m_0}, (c_{m_0})_W$	section pitching-moment coefficient for zero lift	4.1.1 4.1.2.1 4.1.4.1 4.3.2.1
$(c_{m_0})_{\text{area not immersed}}$	section pitching-moment coefficient for zero lift of the area not immersed in propeller slipstream	4.6.3
$(c_{m_0})_{root}$	section pitching-moment coefficient at zero lift of root section	4.1.4.1
$(c_{m_0})_{tip}$	section pitching-moment coefficient at zero lift of tip section	4.1.4.1
$\Delta c_{m_3}, \Delta c_{m_4}$	intermediate terms in determining pitching-moment increments due to leading-edge devices and angle of attack, respectively	6.1.2.1 6.1.5.1

E. PARTIAL DERIVATIVES

SYMBOL	DEFINITION	SECTIONS
$\frac{\partial C_D}{\partial M}$	slope of curve of C_D vs M	4.3.3.1 4.5.3.1
$\frac{\partial \alpha}{\partial \delta}$	rate of change of zero-lift angle of attack with flap deflection	Several
$\frac{\partial \epsilon}{\partial \alpha}$	downwash gradient acting on the aft surface	Several
$\frac{\partial \bar{\epsilon}}{\partial \alpha}$	average downwash gradient acting on the aft surface	4.2.2.1 4.5.1.1
$\left(\frac{\partial \bar{\epsilon}}{\partial \alpha}\right)_{\text{low speed}}$	average downwash gradient acting on the tail at low speeds	4.4.1
$\left(\frac{\partial \epsilon}{\partial \alpha}\right)_M$	downwash gradient acting on the tail at high subsonic Mach numbers	4.4.1
$\left(\frac{\partial \epsilon}{\partial \alpha}\right)_v$	downwash gradient in the plane of symmetry at the height of the vortex core	4.4.1 4.5.1.1 7.4.4.1

SYMBOL	DEFINITION	SECTIONS
$\left(\frac{\partial \epsilon}{\partial \alpha}\right)_{\infty}$	downwash gradient at infinity	4.4.1 4.5.1.1 7.4.4.1
$\frac{\partial \epsilon_p}{\partial \alpha_p}$	downwash parameter due to propeller	4.6 4.6.1 4.6.4
$\frac{\partial \epsilon_u}{\partial \alpha}$	upwash gradient in the plane of symmetry of an unswept wing	Several
$\frac{d\epsilon_{z_{slip}}}{\partial \alpha_{in}}$	induced upwash gradient due to propeller slipstream	9.1.3
$\frac{\partial \sigma}{\partial \beta}$	sidewash parameter	Several
$\left(\frac{\partial c_{h_f}}{\partial c_\ell}\right)_{\delta_t, \delta_f}$	change in section hinge-moment coefficient of a control surface due to lift variation, measured at constant values of tab and flap deflections	6.1.3.3
$\left(\frac{\partial c_{h_f}}{\partial \delta_t}\right)_{c_\ell, \delta_f}$	change in section hinge-moment coefficient of a control surface due to tab deflection, measured at constant values of lift and flap deflection	6.1.3.3
$\left(\frac{\partial c_{h_f}}{\partial \delta_t}\right)_{\alpha, \delta_f}$	change in section hinge-moment coefficient of a control surface due to tab deflection, measured at constant values of angle of attack and flap deflection	6.1.3.3
$\left(\frac{\partial c_{h_t}}{\partial c_\ell}\right)_{\delta_f, \delta_t}$	change in section hinge-moment coefficient of a tab due to lift variation, measured at constant values of flap and tab deflections	6.1.3.4
$\left(\frac{\partial c_{h_t}}{\partial \delta_f}\right)_{c_\ell, \delta_t}$	change in section hinge-moment coefficient of a tab due to control-surface deflection, measured at constant values of lift and tab deflection	6.1.3.4
$\left(\frac{\partial c_{h_t}}{\partial \delta_f}\right)_{\alpha, \delta_t}$	change in section hinge-moment coefficient of a tab due to control-surface deflection, measured at constant values of angle of attack and tab deflection	6.1.3.4

SYMBOL	DEFINITION	SECTIONS
$\left(\frac{\partial c_\ell}{\partial \alpha}\right)_{\delta_f, \delta_t}$	section lift-curve slope of a control surface at constant values of flap and tab deflections	6.1.3.3 6.1.3.4
$\left(\frac{\partial \alpha}{\partial \delta_f}\right)_{c_\ell, \delta_t}$	rate of change of angle of attack due to change in flap deflection at constant values of lift and tab deflection	6.1.3.4
$\left(\frac{\partial \alpha}{\partial \delta_t}\right)_{c_\ell, \delta_f}$	rate of change of angle of attack due to change in tab deflection at constant values of lift and flap deflection	6.1.3.3

F. ABBREVIATIONS

SYMBOL	DEFINITION	SECTIONS
a.c.	aerodynamic center	Several
av	average	Several
c.g.	center of gravity	Several
c.p.	center of pressure	Several
EBF	externally blown flap	Several
FRP	fuselage reference plane	4.5.2.1
fus	fuselage	9.1 9.1.3
HL	hinge line	Several
HM	hinge moment	6.3.1
IBF	internally blown flap	Several
inc	incipient	6.3.1
LE	leading edge	Several
LER	leading-edge radius	Several
MAC	mean aerodynamic chord	Several
max	maximum	Several
MRP	moment reference point	6.1.5.1 6.3.1
ref	reference	Several
SF	safety factor	6.3.2
slip	propeller slipstream	9.1 9.1.3
STOL	short take-off and landing	Several
TE	trailing edge	Several
U	lower vertical stabilizer	Several
V	upper vertical stabilizer	Several
VTOL	vertical take-off and landing	4.6 9 9.1 9.2

2.2 WING PARAMETERS
2.2.1 SECTION PARAMETERS

Airfoil section parameters that are useful in estimating aerodynamic data are presented in this Section. An airfoil-designation summary that has general utility throughout the Handbook is given. Figure 2.2.1-6 gives the trailing-edge angle for standard airfoils. This parameter is used in estimating section lift-curve slopes and control derivatives. Figure 2.2.1-7 gives the leading-edge radius of standard airfoils. This parameter is not used in this Handbook but is used extensively as a correlation parameter in the literature. It is presented for convenience only. The parameter that is used in place of leading-edge radius in the Handbook is the $\triangle y$ parameter (see definition on figure 2.2.1-8). This parameter has been found to be highly successful in correlating data, e.g., see Section 4.1.3.4. It is presented for standard airfoils in figure 2.2.1-8 .

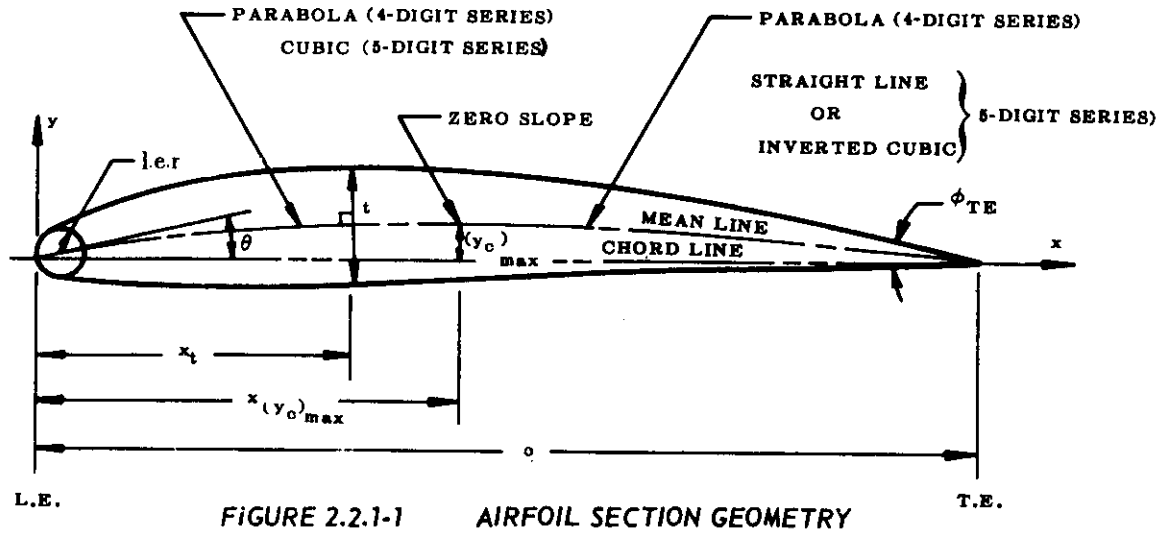

FIGURE 2.2.1-1 AIRFOIL SECTION GEOMETRY

BASIC SYMMETRIC AIRFOIL

- c = chord of airfoil section
- x = distance along chord measured from l.e.
- y = ordinate at some value of x (measured normal to and from the chord line for symmetric airfoils, measured normal to and from the mean line for cambered airfoils)
- y(x) = thickness distribution of airfoil
- $t = 2y_{max}$ = maximum thickness of airfoil
- x_t = position of maximum thickness
- l.e.r. = leading-edge radius
- ϕ_{TE} = trailing-edge angle (included angle between the tangents to the upper and lower surfaces at the trailing edge)

CAMBER MEAN LINE

- $(y_c)_{max}$ = maximum ordinate of mean line
- $y_c(x)$ = shape of mean line
- $x_{(y_c)_{max}}$ = position of maximum camber
- θ = slope of l.e.r. through l.e. equals the slope of the mean line at the l.e.
- c_ℓ = section lift coefficient
- c_{ℓ_i} = design section lift coefficient

AIRFOIL SECTION DESIGNATION

"CLARK Y" AIRFOIL

x_t = 80% CHORD FOR ANY THICKNESS

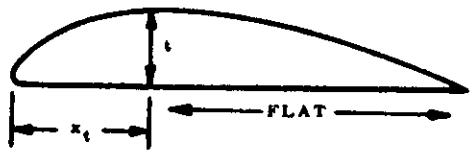

NACA 4-DIGIT SERIES AIRFOILS

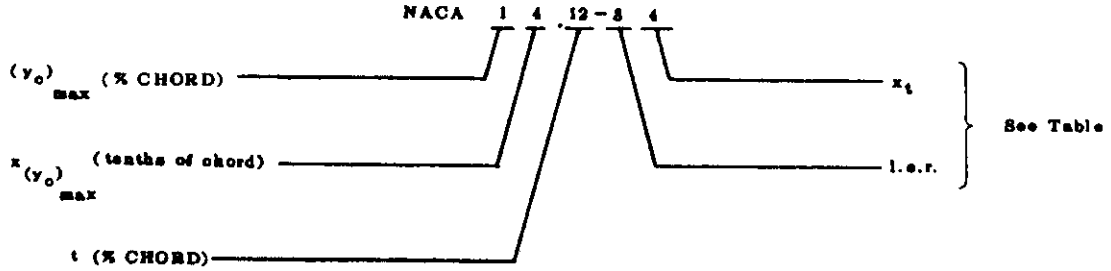

"Dash" numbers (numbers following a dash placed after the standard notation) are expressed only when l.e.r. and/or x_t are different from normal.

FIRST DASH NO.	l.e.r.	SECOND DASH NO.	x_t (% CHORD)
0	Sharp	2	20
3	½ Normal	3	30 (Normal)
6	Normal	4	40
9	3 × Normal	5	50

GERMAN NOTATION OF NACA 4-DIGIT AND 5-DIGIT SERIES AIRFOILS

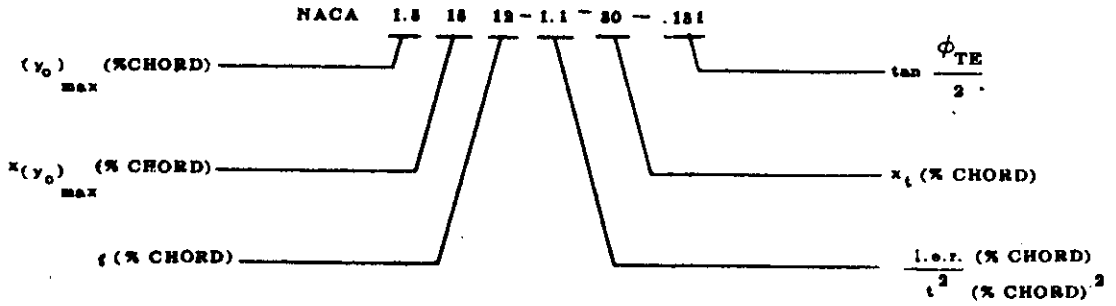

NACA 5-DIGIT SERIES AIRFOIL

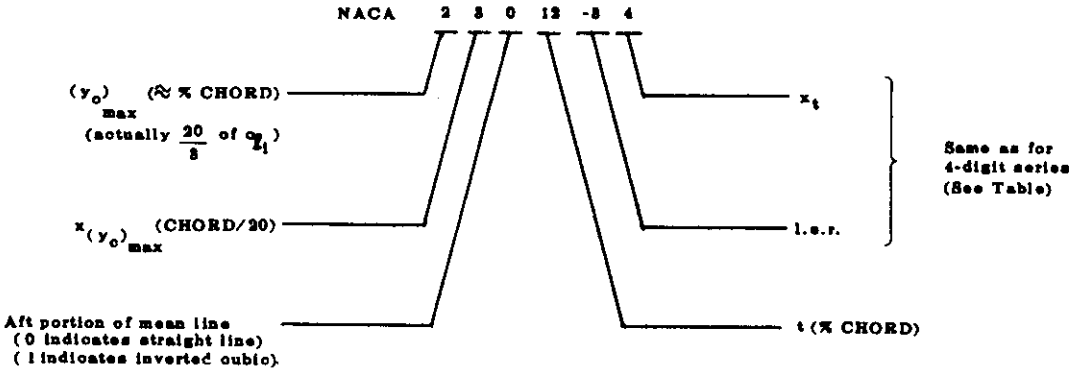

NACA 1- SERIES AIRFOILS

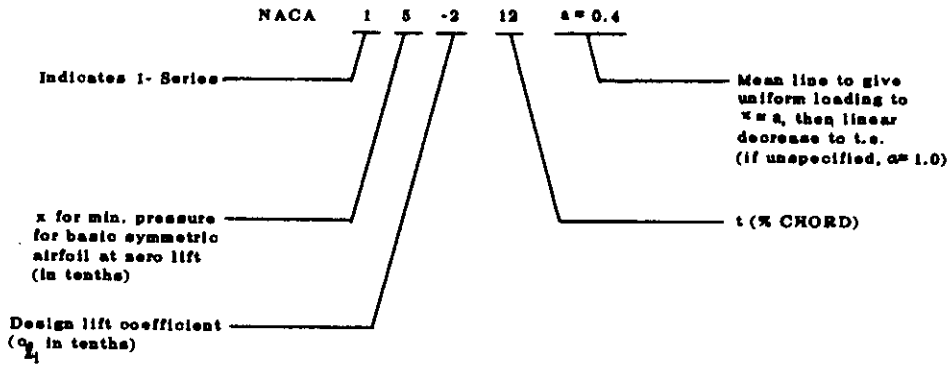

NACA 6- SERIES AIRFOILS

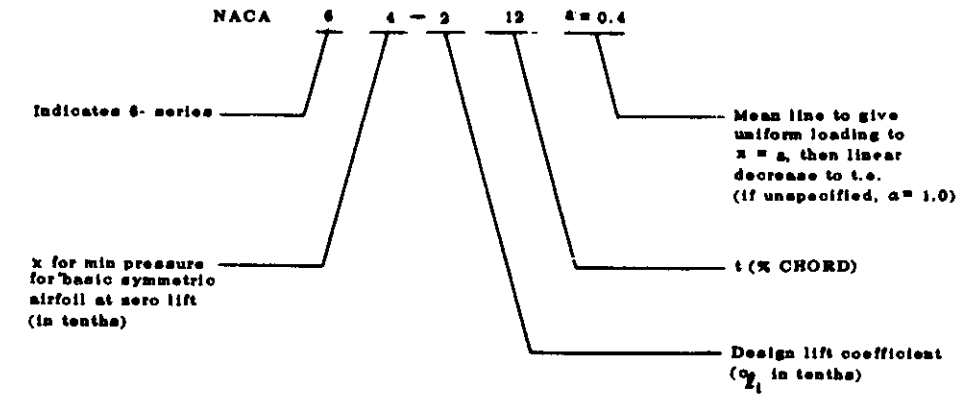

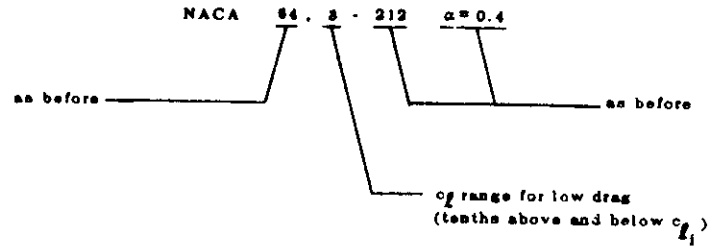

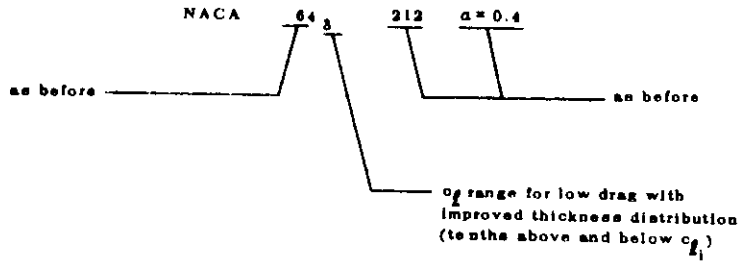

To increase or decrease the airfoil thickness

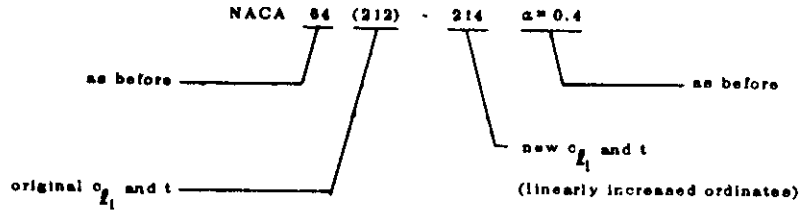

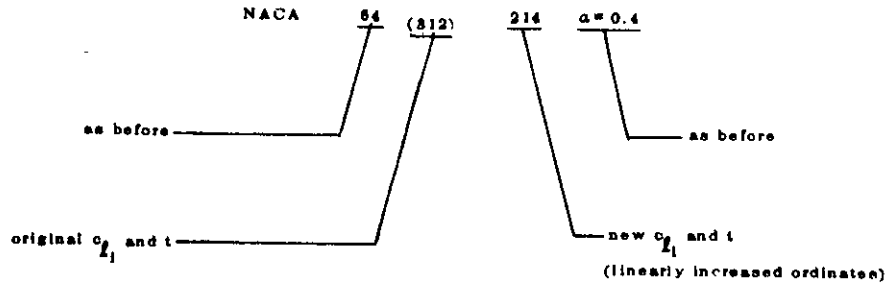

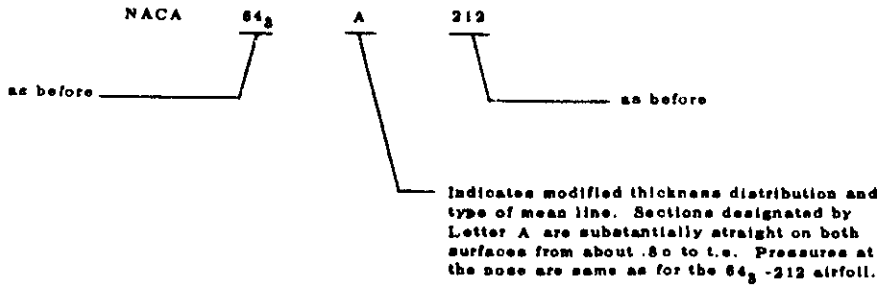

NACA 7- SERIES AIRFOILS

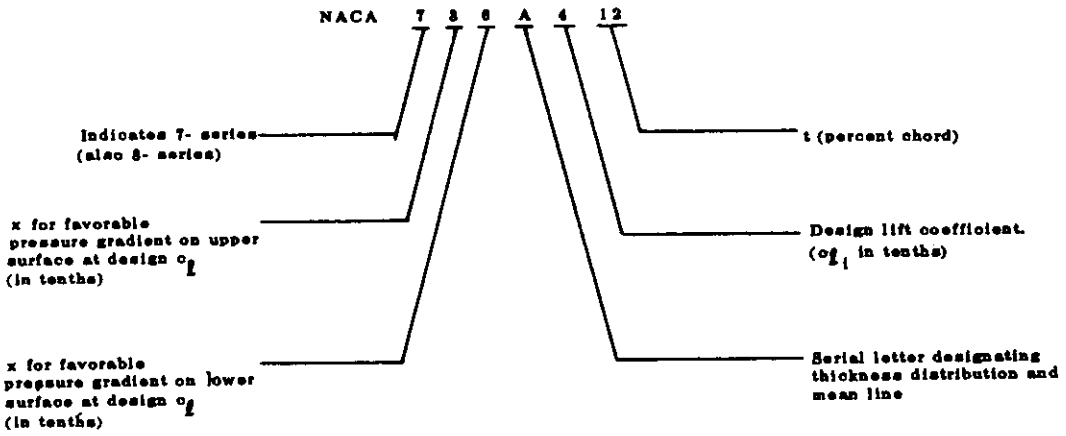

SUPERSONIC AIRFOILS (WEDGE AND CIRCULAR ARC)

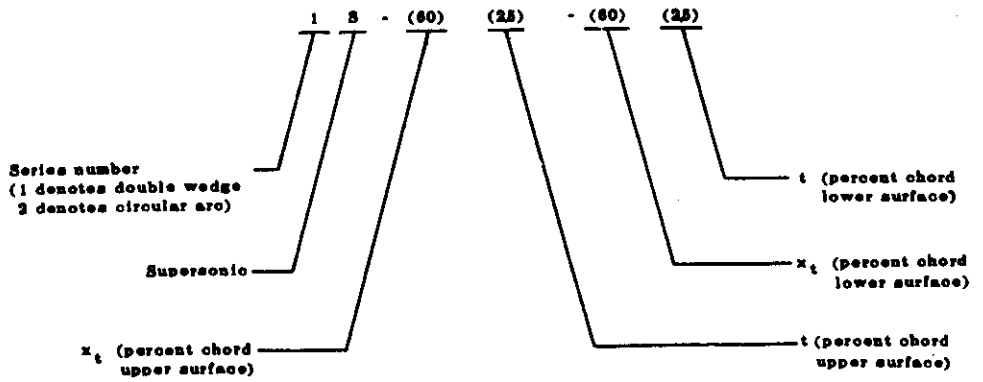

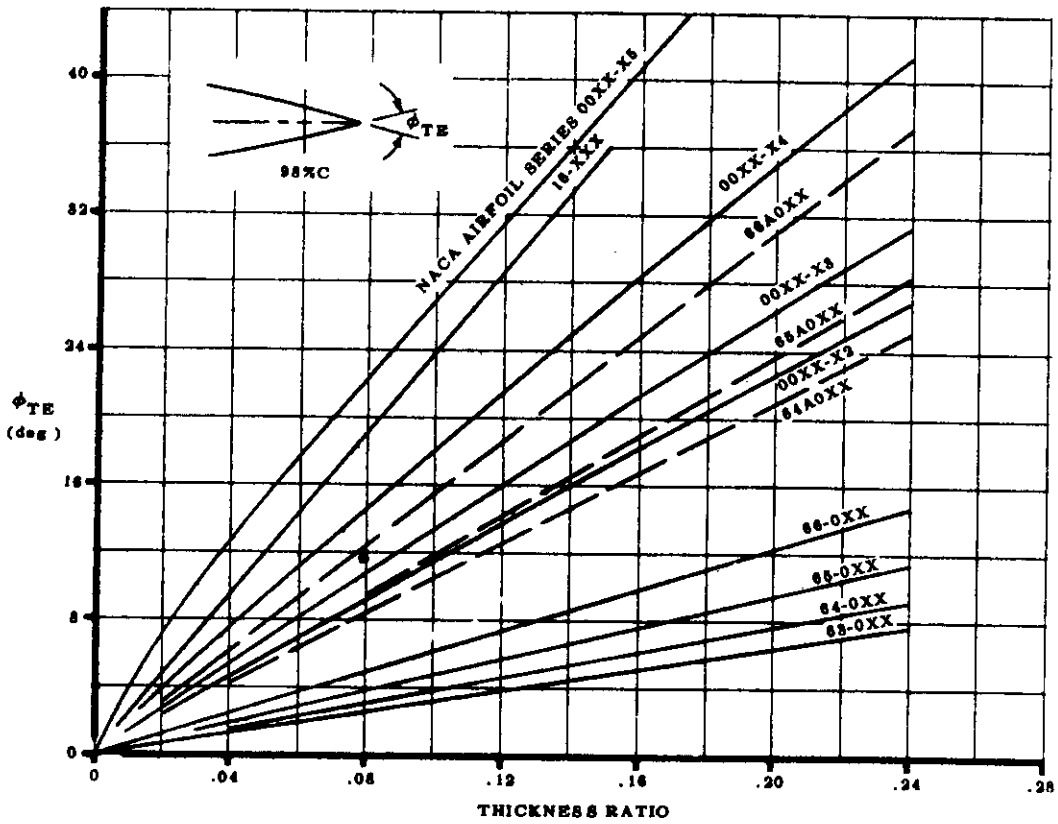

FIGURE 2.2.1-6 VARIATION OF TRAILING-EDGE ANGLE WITH AIRFOIL THICKNESS RATIO

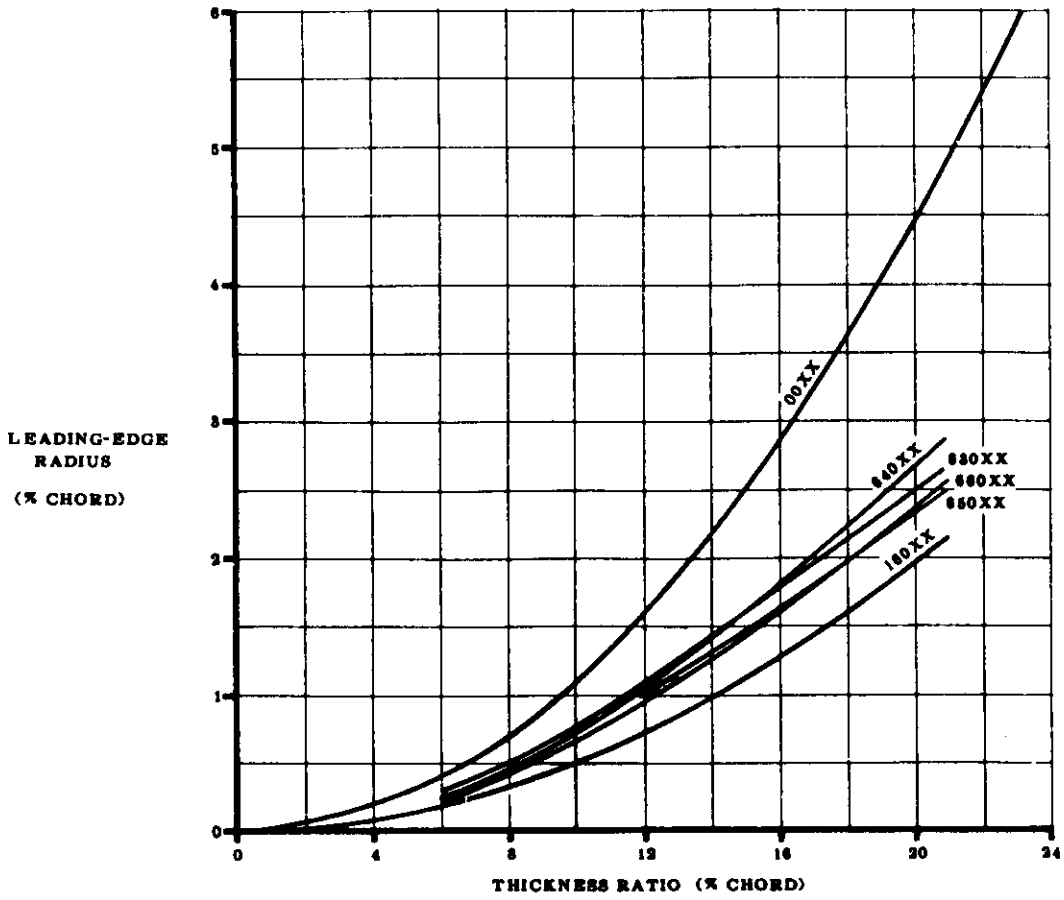

FIGURE 2.2.1-7 VARIATION OF LEADING-EDGE RADIUS WITH THICKNESS RATIO OF AIRFOILS

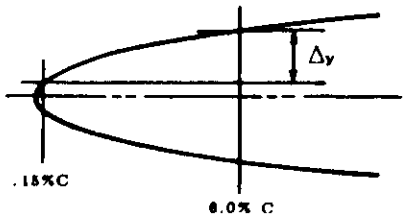

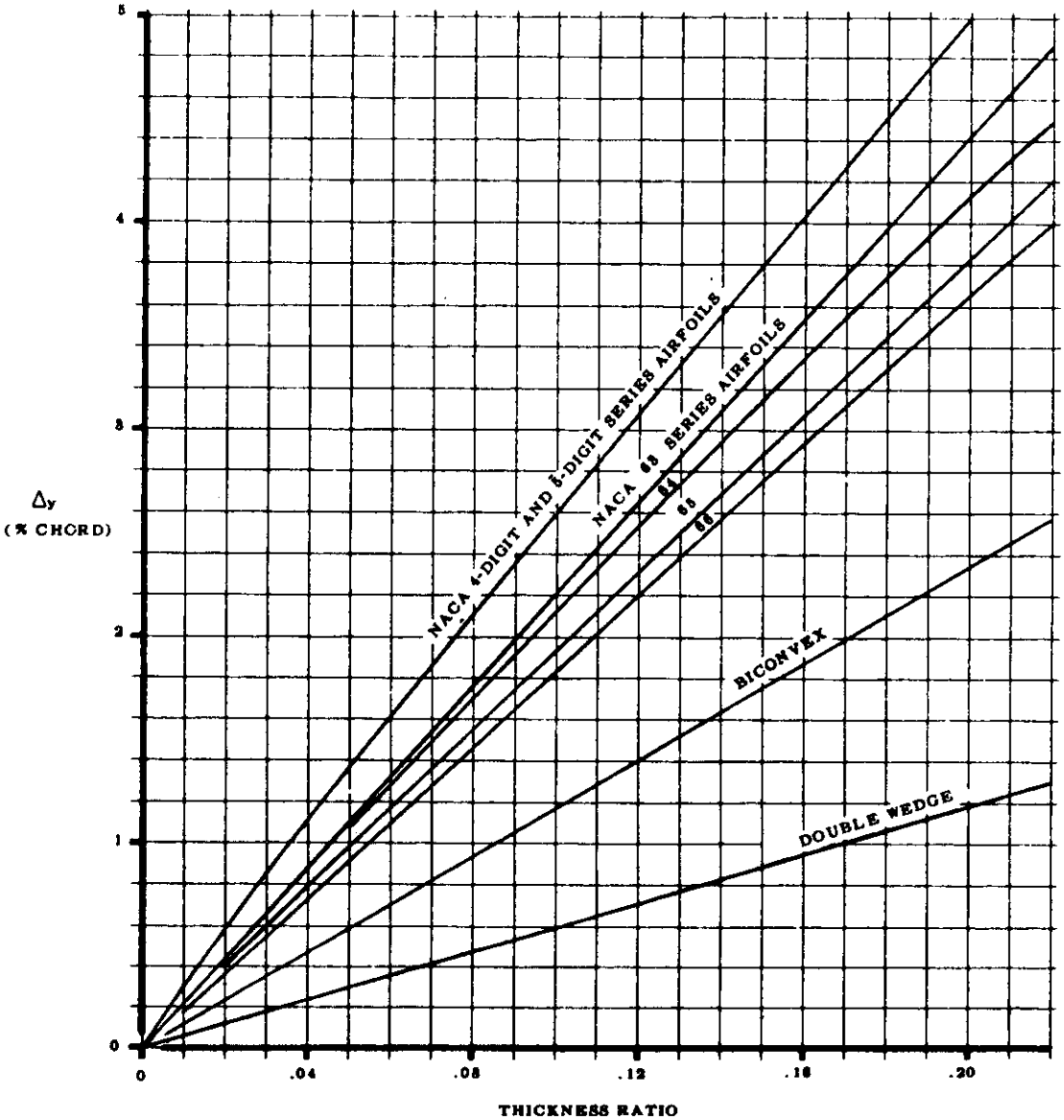

FIGURE .2.2.1-8 VARIATION OF LEADING-EDGE SHARPNESS PARAMETER WITH AIRFOIL THICKNESS RATIO

2.2.2 PLANFORM PARAMETERS

General planform parameters that are useful in estimating aerodynamic data are presented in this section. These parameters are given in equation form for conventional, straight-tapered wings and non-straight-tapered wings.

1. GENERAL PLANFORM PARAMETERS

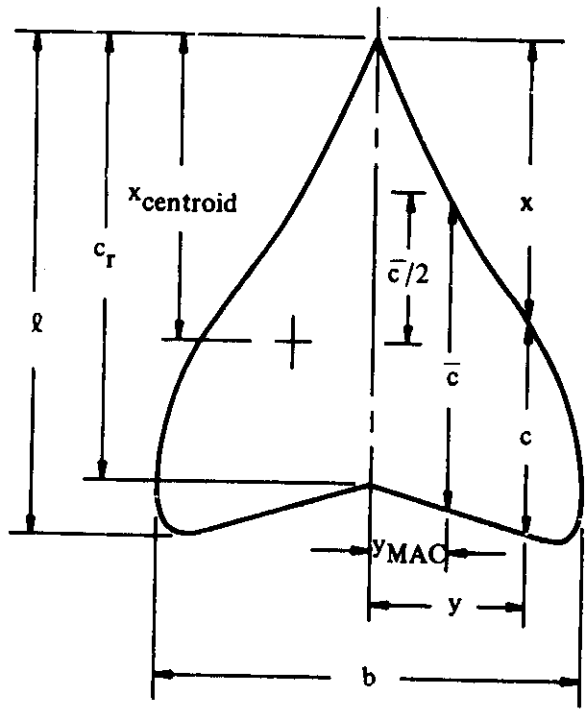

Definitions

A	aspect ratio = b^2/S
b	wing span
$b/(2\ell)$	wing-slenderness parameter
c	chord (parallel to axis of symmetry) at any given span station y
$\bar{c}$	mean aerodynamic chord (MAC)

$$\bar{c} = \frac{2}{S} \int_0^{b/2} c^2 \, dy$$

c_r	root chord
ℓ	over-all length from wing apex to most aft point on trailing edge

p planform-shape parameter = $S/(b\ell)$

S wing area = $2\int_0^{b/2} c\,dy$

x chordwise location of leading edge at span station y

$x_{centroid}$ chordwise location of centroid of area (chordwise distance from apex to $\bar{c}/2$)

$$x_{centroid} = \frac{2}{S}\int_0^{b/2} c\left(x + \frac{c}{2}\right)dy$$

y general span station measured perpendicular to plane of symmetry

y_{MAC} spanwise location of MAC (equivalent to spanwise location of centroid of area)

$$y_{MAC} = \frac{2}{S}\int_0^{b/2} cy\,dy$$

2. CONVENTIONAL, STRAIGHT-TAPERED PLANFORM PARAMETERS

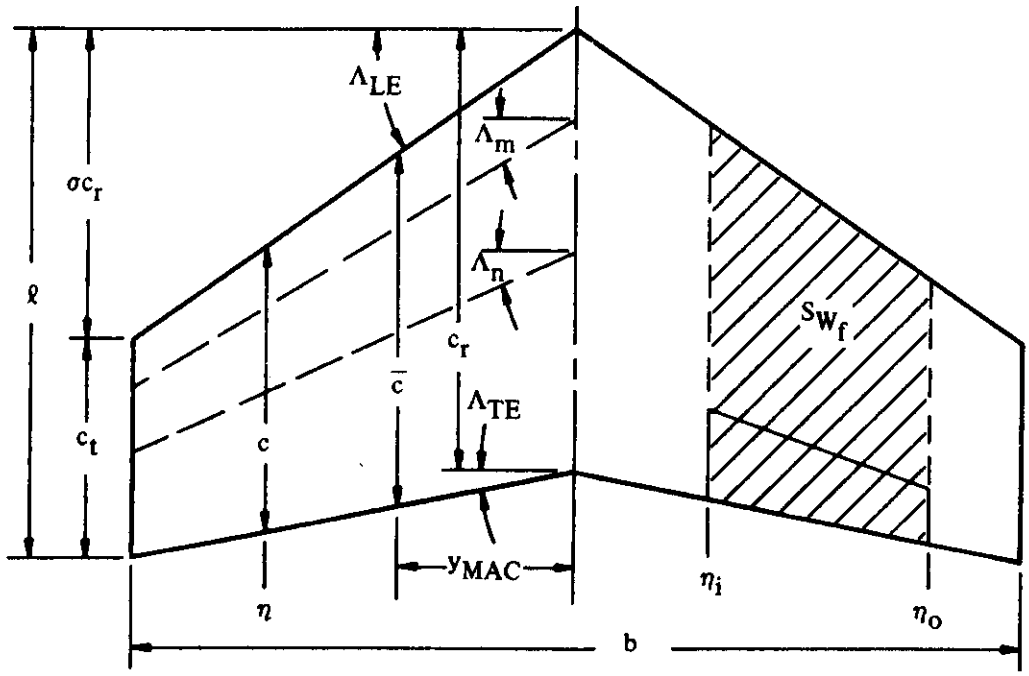

Definitions

b wing span

c chord of wing (parallel to axis of symmetry) at any given span station y

$\bar{c}$	mean aerodynamic chord (MAC)
c_r	root chord
c_t	tip chord
m, n	nondimensional chordwise stations in terms of c
S_{W_f}	wing area affected by trailing-edge deflection
y_{MAC}	spanwise location of MAC
η	nondimensional span station = y/(b/2)
η_i, η_o	nondimensional span stations at inboard and outboard edges of control, respectively.
λ	taper ratio = c_t/c_r
Λ_{LE}	sweep angle of leading edge
Λ_{TE}	sweep angle of trailing edge
Λ_m, Λ_n	sweep angles of arbitrary chordwise locations
σ	ratio of chordwise position of leading edge at tip to root chord length = $(b/2)\tan\Lambda_{LE}/c_r$

Equations

$$A = \frac{b^2}{S} = \frac{2b}{c_r(1+\lambda)}$$

$$\bar{c} = \frac{2}{3} c_r \frac{1+\lambda+\lambda^2}{1+\lambda}$$

$$S = (b/2)c_r(1+\lambda)$$

$$S_{W_f} = \frac{b}{2}(\eta_o - \eta_i)\, c_r\, [2 - (1-\lambda)(\eta_i + \eta_o)]$$

$$\frac{x_{centroid}}{c_r} = \frac{1}{3}\left(\lambda + \sigma + \frac{1+\lambda\sigma}{1+\lambda}\right)$$

$$\frac{y_{MAC}}{b/2} = \frac{1 - \frac{\bar{c}}{c_r}}{1-\lambda} = \frac{1}{3}\left(\frac{1+2\lambda}{1+\lambda}\right)$$

$$\tan\Lambda_n = \tan\Lambda_m - \frac{4}{A}\left[(n-m)\frac{1-\lambda}{1+\lambda}\right]$$

$$\tan \Lambda_{LE} = \frac{4}{A} \quad (\lambda = 0)$$

$$\sigma = \frac{A}{4}(1 + \lambda) \tan \Lambda_{LE}$$

3. DOUBLE-DELTA AND CRANKED WING PLANFORM PARAMETERS

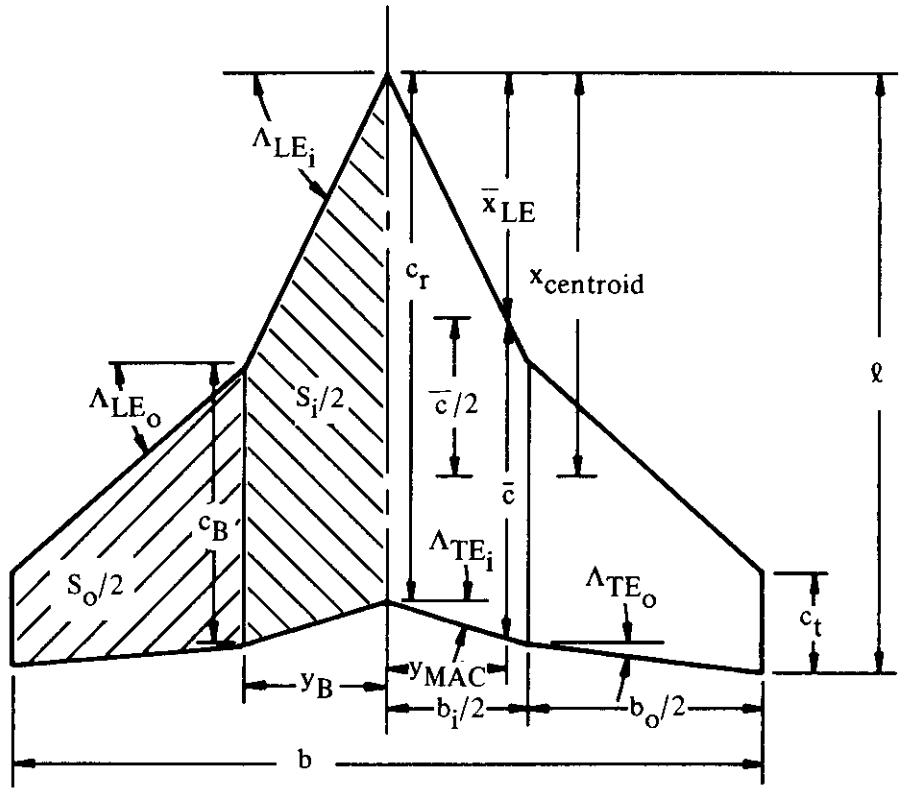

Definitions

b	wing span
b_i	span of planform formed by two inboard panels
b_o	span of planform formed by joining two outboard panels as an isolated wing
$\bar{c}$	mean aerodynamic chord (MAC)
c_B	chord at break span station
c_r	root chord
c_t	tip chord
S_i	total area of inboard panels
S_o	total area of outboard panels

$x_{centroid}$ chordwise location of centroid of area (chordwise distance from apex to $\bar{c}/2$)

$\bar{x}_{LE}$ chordwise distance from apex to leading edge of MAC

y_B spanwise location of break span station

y_{MAC} spanwise location of MAC

$\eta_B = y_B/(b/2)$

$\lambda = c_t/c_r$

$\lambda_i = c_B/c_r$

$\lambda_o = c_t/c_B$

Subscripts

B refers to span station where leading edges and/or trailing edges change sweep angles

i, o refer to inboard and outboard panels, respectively

Equations

$$A = \frac{b^2}{S} = \frac{2b}{c_r\left[(1-\lambda)\eta_B + \lambda_i + \lambda\right]}$$

$$\bar{c} = \frac{2}{S}\int_0^{b/2} c^2\,dy = \frac{\bar{c}_i S_i + \bar{c}_o S_o}{S_i + S_o}$$

$$S = S_i + S_o = \frac{b^2}{A} = (b/2)c_r\left[(1-\lambda)\eta_B + \lambda_i + \lambda\right]$$

$$\frac{x_{centroid}}{c_r} = \frac{\bar{x}_{LE} + \bar{c}/2}{c_r}$$

$$\bar{x}_{LE} = \frac{\left(y_{MAC_i}\tan\Lambda_{LE_i}\right)S_i + \left(y_B\tan\Lambda_{LE_i} + y_{MAC_o}\tan\Lambda_{LE_o}\right)S_o}{S_i + S_o}$$

$$y_{MAC} = \frac{2}{S}\int_0^{b/2} cy\,dy = \frac{y_{MAC_i}S_i + \left(y_B + y_{MAC_o}\right)S_o}{S_i + S_o}$$

$$\eta_B = \frac{b_i}{b} = \frac{1}{1-\lambda}\left(\frac{2b}{Ac_r} - \lambda_i - \lambda\right) = \frac{1}{1-\lambda}\left(\frac{2S}{bc_r} - \lambda_i - \lambda\right)$$

2.3 BODY PARAMETERS

Charts for estimating body volumes and surface areas for various families of profiles are presented in this Section.

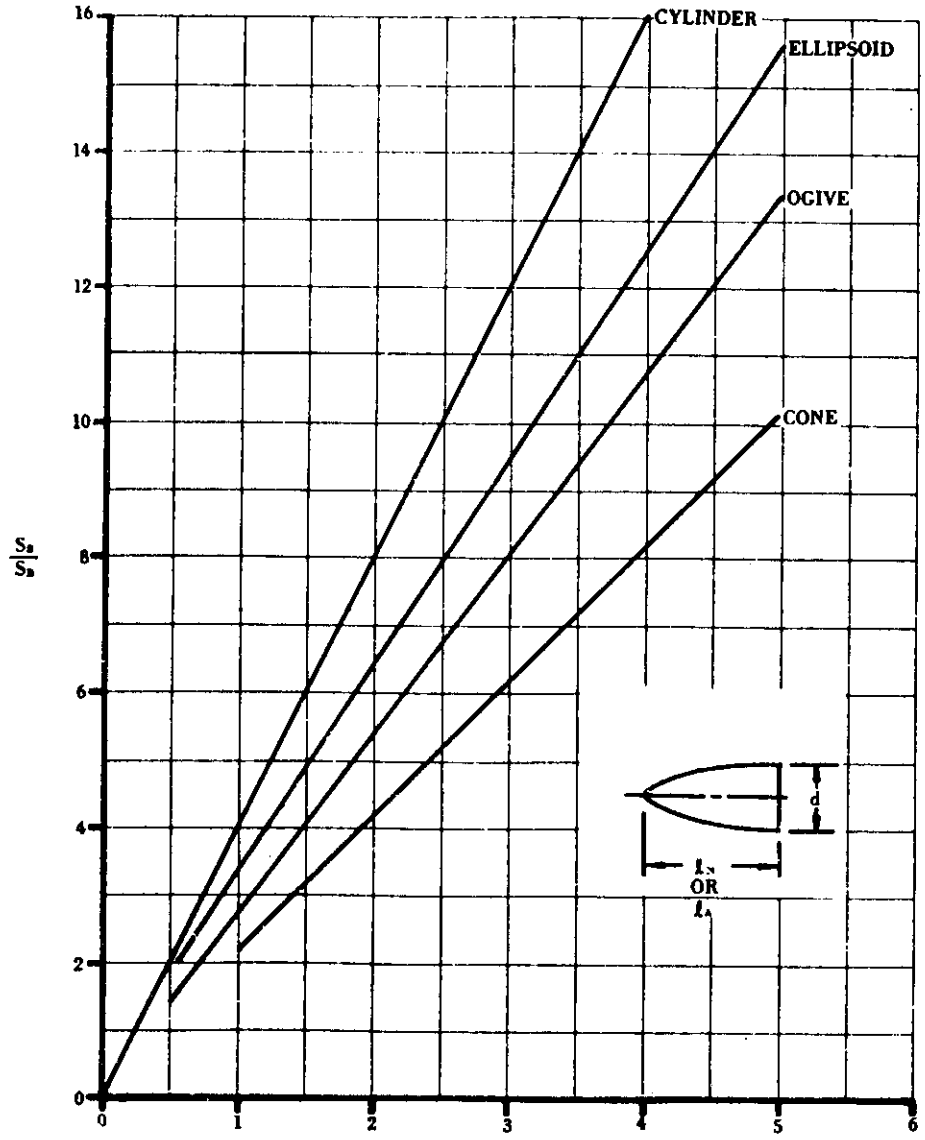

FIGURE 2.3-2 FOREBODY OR AFTERBODY WETTED AREA

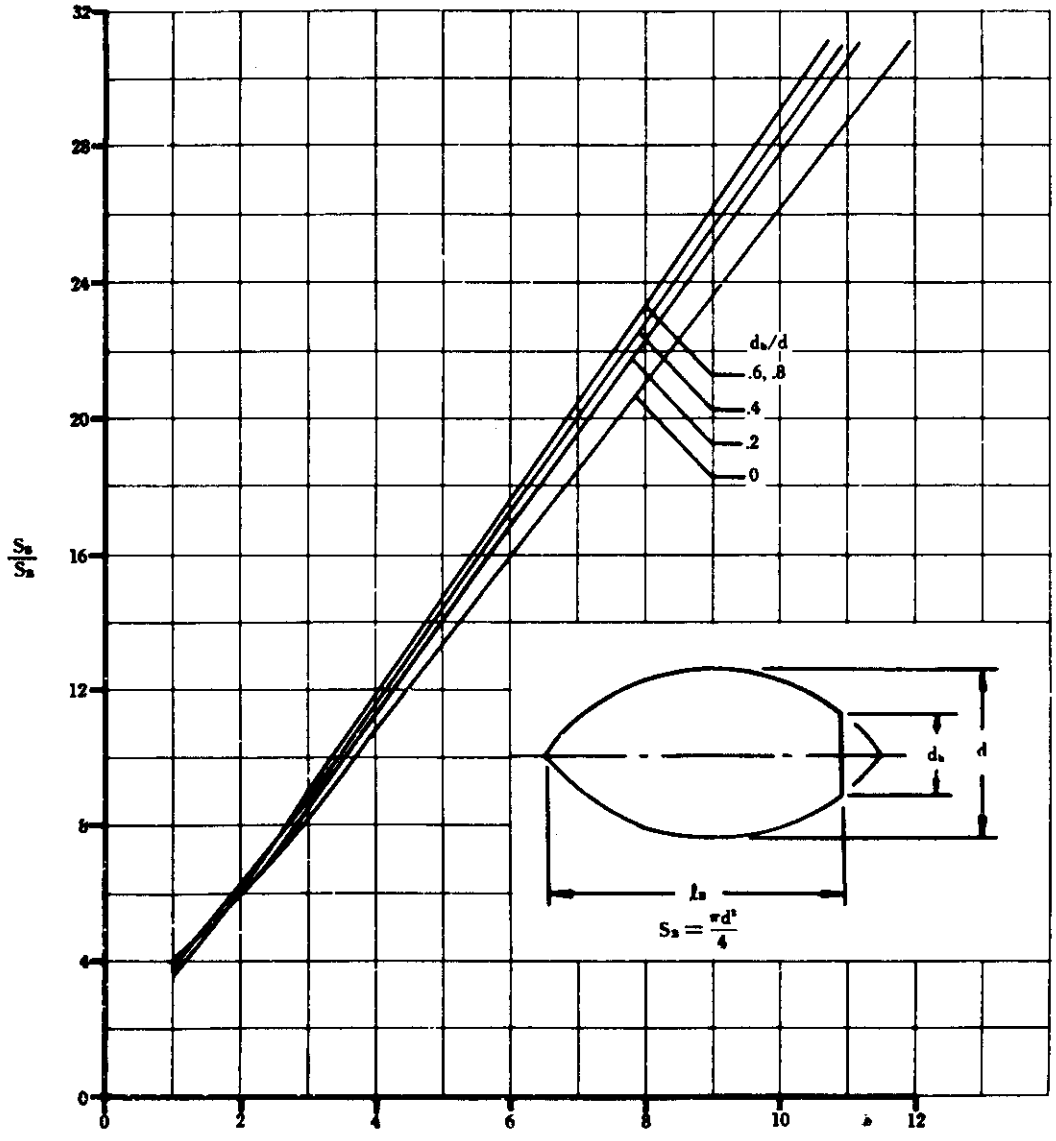

FINENESS RATIO , l_a/d

FIGURE 2.3-3 WETTED AREA OF BLUNT-BASE OGIVE BODIES

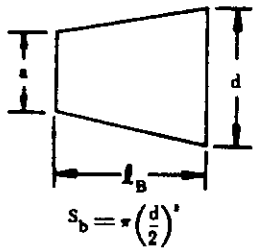

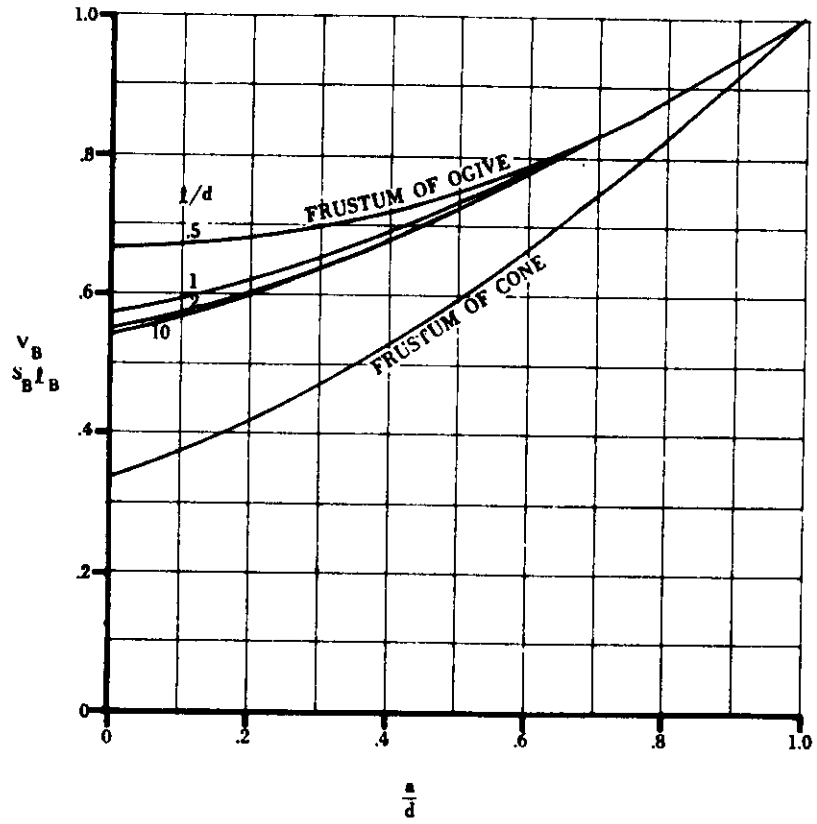

FIGURE 2.3-4 VOLUME OF BODY FRUSTUMS

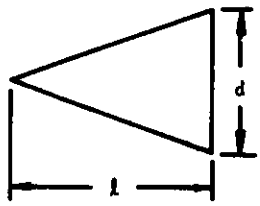

$$S_b = \pi\left(\frac{d}{2}\right)^2$$

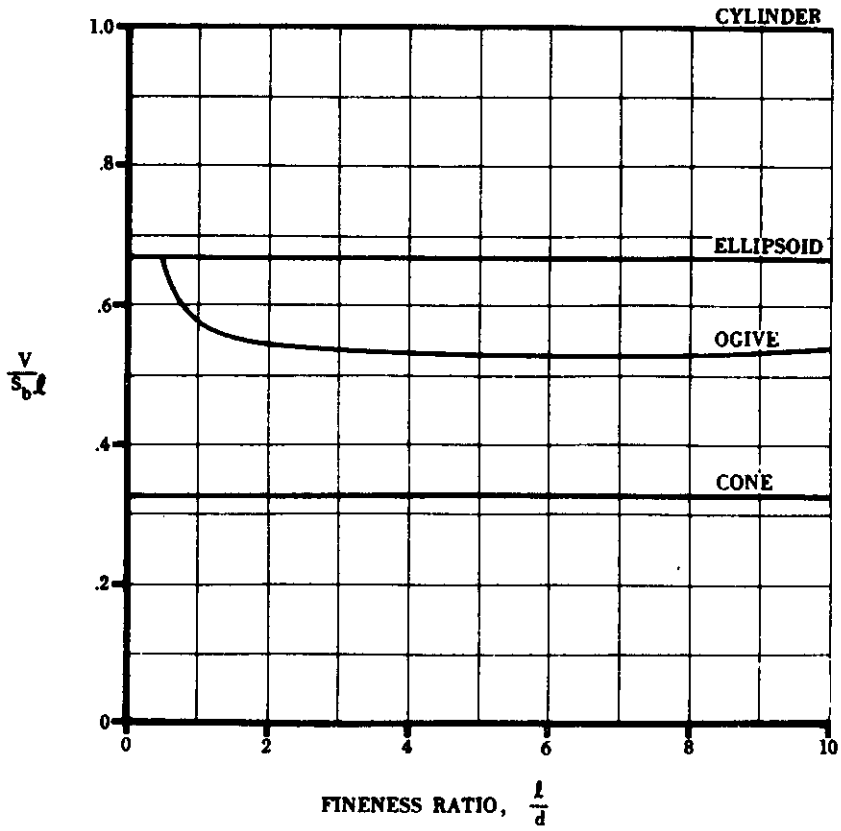

FIGURE 2.3-5 BODY VOLUME